

Hydrogen Effects on Carbon Steel Used Fuel Containers

NWMO TR-2009-29

December 2009

Fraser King

Integrity Corrosion Consulting Ltd.

nwmo

NUCLEAR WASTE
MANAGEMENT
ORGANIZATION

SOCIÉTÉ DE GESTION
DES DÉCHETS
NUCLÉAIRES



Nuclear Waste Management Organization
22 St. Clair Avenue East, 6th Floor
Toronto, Ontario
M4T 2S3
Canada

Tel: 416-934-9814
Web: www.nwmo.ca

Hydrogen Effects on Carbon Steel Used Fuel Containers

NWMO TR-2009-29

December 2009

Fraser King
Integrity Corrosion Consulting Ltd.

Disclaimer:

This report does not necessarily reflect the views or position of the Nuclear Waste Management Organization, its directors, officers, employees and agents (the "NWMO") and unless otherwise specifically stated, is made available to the public by the NWMO for information only. The contents of this report reflect the views of the author(s) who are solely responsible for the text and its conclusions as well as the accuracy of any data used in its creation. The NWMO does not make any warranty, express or implied, or assume any legal liability or responsibility for the accuracy, completeness, or usefulness of any information disclosed, or represent that the use of any information would not infringe privately owned rights. Any reference to a specific commercial product, process or service by trade name, trademark, manufacturer, or otherwise, does not constitute or imply its endorsement, recommendation, or preference by NWMO.

ABSTRACT

Title: Hydrogen Effects on Carbon Steel Used Fuel Containers
Report No.: NWMO TR-2009-29
Author(s): Fraser King
Company: Integrity Corrosion Consulting Ltd.
Date: December 2009

Abstract

Hydrogen affects the properties of many structural materials including steels and, more particularly, the general class of carbon steels from which a used fuel container would likely be fabricated. Degradation of the mechanical and corrosion properties of steels can take many forms but, in general, the severity of damage increases with increasing absorbed hydrogen concentration, increasing stress, and increasing strength of the material.

Various aspects of the possible hydrogen-related damage of used fuel containers (UFC) are reviewed, including (i) the generation and absorption of hydrogen due to aqueous corrosion and from the gaseous H₂ phase that will form in the repository, (ii) the diffusion of hydrogen through the container wall and the interaction of H with various kinds of trap sites, (iii) the resultant forms of damage and the mechanisms proposed to account for this damage, (iv) threshold conditions that can be used to predict the susceptibility of UFC in the repository environment, and (v) the implications for the containers, including an assessment of the most likely forms of H-related damage, a prediction of the susceptibility of the containers, an assessment of the period during which H-related damage is possible, and possible mitigation strategies based on the container material and design.

Of the various forms of H damage, those deemed most likely to affect the containers are blister formation or hydrogen-induced cracking and cracking associated with the inner surface of the closure weld once gaseous hydrogen has entered the void space inside the container. Overall, however, the probability of H-related failure is considered small because of the benign nature of the environment, the low applied and residual stresses, and the low strength of the container material.

This low probability of failure due to H damage can be reduced even further through proper selection of the container material and of the design of the closure weld.

Although the susceptibility to H-related damage is judged to be minimal for a UFC, the period of greatest susceptibility extends throughout the long-term anaerobic period in the evolution of the repository environment. Therefore, unlike other forms of localized damage such as stress corrosion cracking and localized corrosion which are only possible during the initial short aerobic transient period, H-related damage is possible for the vast majority of the container design life.

TABLE OF CONTENTS

	<u>Page</u>
ABSTRACT	v
1. INTRODUCTION	1
2. HYDROGEN GENERATION AND PICK UP	3
2.1 HYDROGEN GENERATION.....	3
2.1.1 Mechanism of Hydrogen Evolution.....	3
2.1.2 Rate of Hydrogen Generation	4
2.1.3 Fate of Generated Hydrogen in the Repository	5
2.2 HYDROGEN ABSORPTION.....	6
2.2.1 Hydrogen Absorption from the Discharge of Protons or Water	6
2.2.1.1 Hydrogen absorption reaction	6
2.2.1.2 Promoters and inhibitors of hydrogen absorption	7
2.2.1.3 Effect of surface films.....	8
2.2.1.4 Hydrogen absorption and localized corrosion.....	9
2.2.2 Hydrogen Absorption from Molecular Hydrogen in Aqueous Solution	10
2.2.3 Hydrogen Absorption from the Gaseous Phase	10
3. HYDROGEN TRANSPORT AND TRAPPING	11
3.1 CONCENTRATION OF LATTICE HYDROGEN	12
3.1.1 Hydrogen Absorbed from the Aqueous Phase	12
3.1.2 Hydrogen Absorbed from the Gaseous Phase	15
3.2 HYDROGEN TRANSPORT	16
3.3 TRAPPING AND INTERACTIONS WITH THE MATERIAL	20
3.3.1 Types and Number of Traps	20
3.3.2 Interaction of Hydrogen with the Stress Field	23
4. HYDROGEN DEGRADATION MODES AND MECHANISMS	27
4.1 DEGRADATION MODES	27
4.1.1 Hydrogen Embrittlement	28
4.1.1.1 Delayed failure.....	28
4.1.1.2 Reduced plasticity.....	31
4.1.1.3 Brittleness	31
4.1.1.4 Hydrogen embrittlement of welds.....	32
4.1.2 Blister Formation.....	33
4.1.3 Hydrogen Attack	33
4.1.4 Miscellaneous Effects of Hydrogen on Steels and Their Oxides.....	34
4.2 DEGRADATION MECHANISMS	35
4.2.1 Internal Pressure.....	36
4.2.2 Decohesion.....	36
4.2.3 Hydrogen Enhanced Local Plasticity	37
4.2.4 Adsorption Induced Dislocation Emission	37
4.3 THRESHOLD OR CRITICAL CONDITIONS FOR HYDROGEN DAMAGE	37
4.3.1 Critical Hydrogen Concentration	38
4.3.2 Threshold Stress Intensity Factor.....	44
5. IMPLICATIONS FOR CARBON STEEL USED FUEL CONTAINERS.....	47

5.1	POSSIBLE DEGRADATION MODES FOR CARBON STEEL UFC	47
5.1.1	UFC Susceptibility to Hydrogen -related Damage	47
5.1.2	UFC Susceptibility to Specific Forms of H-related Damage.....	48
5.1.2.1	Hydrogen embrittlement.....	48
5.1.2.2	Blister formation.....	49
5.1.2.3	Hydrogen attack.....	49
5.1.2.4	Miscellaneous forms of hydrogen damage.....	49
5.1.3	Possible Forms of Hydrogen-related Damage for C-steel UFC	49
5.2	PREDICTIONS OF UFC SUSCEPTIBILITY TO HYDROGEN DEGRADATION	49
5.2.1	Prediction Based on Threshold Concentration	50
5.2.2	Prediction Based on the Threshold Stress Intensity Factor	52
5.2.3	Predicted Behaviour for UFC	55
5.3	PERIOD OF SUSCEPTIBILITY TO HYDROGEN EFFECTS	55
5.3.1	Time Dependence of Factors Related to Hydrogen Damage	55
5.3.1.1	Lattice H concentration	55
5.3.1.2	Critical conditions for damage.....	56
5.3.1.3	Applied and residual stress	56
5.3.2	Period of Susceptibility to Hydrogen Damage	57
5.4	MITIGATION OF HYDROGEN EFFECTS	57
5.4.1	Material Selection	57
5.4.2	Container Design and Manufacture.....	61
5.4.2.1	Closure weld design.....	61
5.4.2.2	Container wall thickness	62
5.4.2.3	Miscellaneous design issues.....	62
5.5	GAP ANALYSIS	62
6.	SUMMARY AND CONCLUSIONS	64
	REFERENCES	67

LIST OF TABLES

	<u>Page</u>
Table 1: Diagnostic Criteria for the Mechanism of the Hydrogen Evolution Reaction.....	4
Table 2: Characteristics of Trap Sites in Iron and Steel.....	21
Table 3: Forms of Delayed Cracking of Carbon Steels.....	30
Table 4: Critical Hydrogen Concentrations for Various Forms of Hydrogen Damage.....	40
Table 5: Critical Threshold Stress Intensity Factors for Hydrogen-assisted Cracking.	46

LIST OF FIGURES

	<u>Page</u>
Figure 1: Schematic of the Processes Involved in the Hydrogen Degradation of Steel.....	2
Figure 2: Steady-state Cathodic Polarization Curves for the Reduction of Water on Various Steel Surfaces in Dilute Synthetic Groundwater at ~pH 6.5.....	5
Figure 3: Mechanism of Possible Hydrogen Evolution Reaction Pathways and of the Hydrogen Absorption Reaction.	7
Figure 4: Processes Involved in the Absorption of Hydrogen from the Gas Phase and the Subsequent Embrittlement Reaction.	10
Figure 5: Dependence of the Lattice Hydrogen Concentration on Solution pH in the Presence of 0.01 MPa H ₂ S at 25°C.....	13
Figure 6: Dependence of the Lattice Hydrogen Concentration on pH and Dissolved Sulphide Concentration at 25°C.....	14
Figure 7: Temperature Dependence of the Solubility of Hydrogen in Iron as a Function of the Fugacity of Hydrogen Gas.....	16
Figure 8: Compilations of the Reported Diffusivity of Hydrogen in Iron and Steels.	18
Figure 9: Relationship Between Cold Work and the Apparent Diffusivity of Hydrogen in 1020 Carbon Steel at 25°C.....	19
Figure 10: Dependence of the Apparent Diffusivity on the Fraction of Particle Formers in the Steel.....	19
Figure 11: Effect of Stress Gradient on the Diffusivity of Hydrogen in a High-strength Low-alloy Steel.....	20
Figure 12: Effect of Cold Work on the Density of Trap Sites.....	22
Figure 13: Dependence of the Aspect Ratio of MnS Inclusions on Total Sulphur Content.....	23
Figure 14: Schematic Illustration of the Processes Occurring in the Fracture Process Zone.	24
Figure 15: Photoelectrochemical Image of Hydrogen Concentrating at the Locations of Highest Stress in the Fracture Process Zone Ahead of the Crack Tip.	25
Figure 16: Measured Accumulation of Hydrogen Ahead of a Notch in Carbon Steel as a Function of Stress Intensity Factor.	25
Figure 17: Predicted Hydrogen Repartition Probability for a Carbon Steel with a Yield Strength of 483 MPa as a Function of Trap Binding Energy.....	27
Figure 18: Dependence of the Fracture Toughness of Two Carbon Steels on the Hydrogen Gas pressure.	32
Figure 19: Nelson Curves for Carbon Steel as a Function of Exposure Time.....	34
Figure 20: Enhanced Anodic Dissolution of Carbon Steel in 0.005 mol·dm ⁻³ NaHCO ₃ Solution Following Hydrogen Cathodic Pre-charging for 24 Hours in 1 mol·dm ⁻³ H ₂ SO ₄ + 250 µg·g ⁻¹ As ₂ O ₃ Solution.....	35
Figure 21: Zones of Susceptibility and Immunity to Cracking and Blister Formation as a Function of the Steel Yield Strength and Diffusible (Lattice) Hydrogen Concentration.....	39

Figure 22: Temperature Dependence of the Critical Hydrogen Concentration (C_K) for Blister Formation on Armco Iron.....	43
Figure 23: Dependence of the Threshold Stress Intensity Factor for Hydrogen Embrittlement of Alloy and C-Mn Steels at 23°C.	44
Figure 24: Dependence of the Threshold Stress Intensity Factor for Crack Growth (K_{IH}) for ASTM A516 Carbon Steel and for Crack Arrest (K_{TH}) for Three Low-alloy Steels on Hydrogen Pressure.	45
Figure 25: Temperature Dependence of the Threshold Stress Intensity Factor for Crack Arrest for Various High-strength Steels in Gaseous Hydrogen.....	45
Figure 26: Compilation of Critical Lattice Hydrogen Concentrations for Various Forms of Hydrogen Damage as a Function of Yield Strength.	51
Figure 27: Schematics of Crack-like Defects Used for the Analysis of the Maximum Stress Intensity Factor on Carbon Steel Used Fuel Containers.	53
Figure 28: Predicted Dependence of the Stress Intensity Factor on the Depth of an Edge Crack Subject to Various Tensile Loads.	54
Figure 29: Predicted Dependence of the Stress Intensity Factor on the Combined Depth of a Crack in a Notch Subject to Various Tensile Loads.	54
Figure 30: Regions of Susceptibility to Sulphide Stress Cracking (SSC) as a Function of H_2S Partial Pressure (X in kPa) and pH (Y).	60

1. INTRODUCTION

The use of carbon steel (C-steel) as a container material for the long-term management of used fuel or high-level waste is being considered in a number of national nuclear waste management programs. Carbon steel offers a number of advantages as a used fuel container (UFC) material, including the ease of forming and welding, the generally good corrosion characteristics in the expected environment, the cost and availability of the material, and, above all, the extensive experience in the use of steel for industrial components. In Canada, the Nuclear Waste Management Organization (NWMO) is considering the use of C-steel as an alternate corrosion resistant material for a used fuel container in a deep geological repository (DGR) in sedimentary rock (King 2005, Mazurek 2004). A conceptual model for the corrosion behaviour of a C-steel UFC in a DGR in sedimentary host rock has been developed (King 2007).

A major issue with the use of C-steel UFC is the generation of hydrogen from the anaerobic corrosion of the container. The generation of H_2 affects both the container itself and, potentially, the other engineered and natural barriers. The impacts on the other barriers include (King 2007): two-phase flow of H_2 and the possibility of pathway dilation in the host rock and low-permeability buffer and backfill materials, alteration of bentonite clay by interaction with Fe(II) (produced along with the generation of H_2), and the suppression of used fuel dissolution. For the container itself, absorption of hydrogen generated by corrosion may impact the mechanical and physical properties of the UFC through processes such as the loss of ductility or the formation of discontinuities (cracks, blisters).

The focus of the current review is on the effects of hydrogen on low-carbon or mild steel. These are subsets of the wider class of carbon steels, the latter defined as alloys of iron and carbon with a C content of <2 wt.% (ASM 1987). Low-carbon and mild steels have C contents of 0.05-0.15 wt.% and 0.16-0.29 wt.%, respectively, and encompass the various grades of "carbon steel" considered as container materials worldwide. For the purposes of the review, it is assumed that the UFC are placed of in a backfilled DGR located in saturated rock. Therefore, the environment can be expected to become anaerobic once all of the initially trapped oxygen has been consumed. The low permeability of the repository sealing materials and host rock will result in the formation of a separate H_2 gas phase as the evolved hydrogen cannot be transported away from the container fast enough as dissolved H_2 (Nagra 2004).

Figure 1 illustrates schematically the various processes involved in the generation and absorption of hydrogen and the consequences for the container that are discussed in this report. Hydrogen is generated at a rate determined by the rate of anaerobic corrosion (Section 2.1) and can be absorbed from both the aqueous and, assuming that hydrogen gas accumulates at the container surface, gaseous phases (Section 2.2). Once absorbed, hydrogen can diffuse within the steel (Section 3.1) and interact with traps and other defects within the material (Section 3.2). There are a number of hydrogen damage mechanisms, with the consequences broadly classified as resulting in the formation of discontinuities (cracks and blisters), the loss of ductility or strength, or decarburisation of the material (Section 4.1). There is no universal agreement regarding the mechanism of hydrogen damage, and indeed more than one mechanism may apply (Section 4.2). Regardless of the lack of mechanistic consensus, many forms of hydrogen damage exhibit a threshold absorbed hydrogen concentration, the dependence of which on microstructure, strength and other alloy properties can be a useful predictor of the performance of the material in service (Section 4.3). The implications of these different aspects of the interaction of hydrogen on the performance of C-steel UFC are discussed in Section 5, with

specific reference to selection of the container material, mitigation of hydrogen effects, and prediction of the long-term performance of the container.

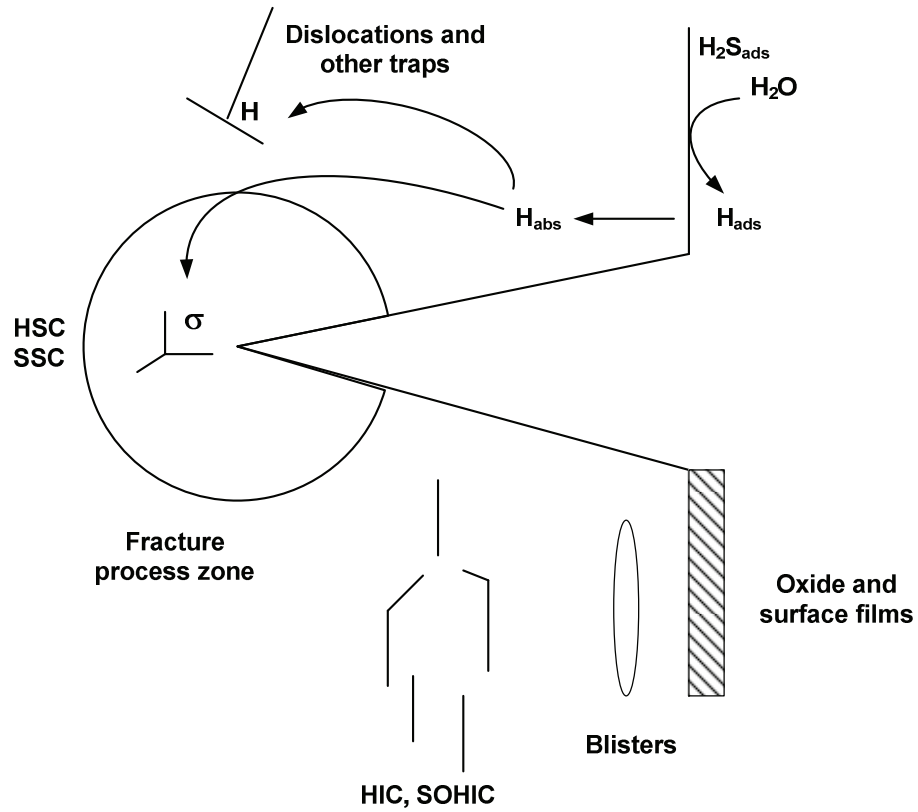


Figure 1: Schematic of the Processes Involved in the Hydrogen Degradation of Steel.

2. HYDROGEN GENERATION AND PICK UP

2.1 HYDROGEN GENERATION

2.1.1 Mechanism of Hydrogen Evolution

The cathodic reduction of H^+ (or H_2O in neutral and alkaline solutions) is one of the most extensively studied electrochemical processes (Bockris and Reddy 1970). Various pathways have been suggested for the two-stage reaction, but the generally accepted mechanism involves the initial discharge reaction



followed by either chemical desorption



or an electrochemical desorption process



Regardless, the overall reaction can be written as



Reactions (1) and (2) may either be fast (reversible) or slow (rate controlling). There are, therefore, six possible mechanisms involving different combinations of reversible and rate-determining reactions; two mechanisms involving a slow discharge reaction followed by fast chemical or electrochemical desorption, two mechanisms involving slow chemical or electrochemical desorption following a fast discharge reaction, and two mechanisms involving a coupled discharge-desorption control with either chemical or electrochemical desorption. These mechanisms can be distinguished from each other by the measured Tafel slopes and the reaction order with respect to $[H^+]$ (Table 1). (Different dependencies result from adsorption via a Langmuir or Temkin isotherm.)

The mechanism of the hydrogen evolution reaction (HER) is not just of academic interest, as it may impact the surface coverage by adsorbed hydrogen and, hence, the probability of hydrogen absorption. For Fe, the mechanism is thought to involve either slow discharge followed by fast electrochemical desorption or coupled discharge-desorption control with chemical desorption (Subramanyan 1981).

Table 1: Diagnostic Criteria for the Mechanism of the Hydrogen Evolution Reaction*

Mechanism	Tafel slope		Reaction order	
	Langmuir	Temkin	Langmuir	Temkin
Slow discharge, fast chemical desorption	2RT/F	2RT/F	1	1
Slow discharge, fast electrochemical desorption	2RT/F	RT/F	1	1.5
Fast discharge, slow chemical desorption	RT/2F	RT/F	2	1
Fast discharge, slow electrochemical desorption	2RT/3F	RT/F	2	1.5
Coupled discharge-chemical desorption control	2RT/F	3RT/F	1	0.67
Coupled discharge-electrochemical desorption control	2RT/F	2RT/F	1	1

*Assuming a cathodic transfer coefficient of 0.5

Most mechanistic studies of the evolution of hydrogen have been conducted on freshly polished and electrochemically cleaned electrode surfaces. The surface condition will clearly affect both the rate and, possibly, the mechanism of hydrogen evolution. Figure 2 shows the effect of the surface condition on the steady-state current for the reduction of H^+/H_2O on C-steel (Been et al. 2007). At potentials close to the corrosion potential (E_{CORR}) in anaerobic solutions (-750 mV_{SCE} to -800 mV_{SCE}), the rate of water reduction is approximately one order of magnitude higher on oxidized surfaces than on a surface electrochemically cleaned at a potential of -1300 mV_{SCE} and protected from oxidation by control of the potential away from the region in which the surface could oxidize. Catalysis of the HER is observed for surfaces either pre-oxidized *in situ* electrochemically or covered by a Fe₃O₄-containing millscale. It should be noted here that the results in Figure 2 only indicate that the rate of H^+/H_2O reduction is catalyzed by the presence of an oxidized surface layer. Surface layers will also affect the rate of hydrogen absorption, as discussed below.

2.1.2 Rate of Hydrogen Generation

Hydrogen is generated by the anaerobic corrosion of C-steel. Of the total amount of H₂ generated, only a small fraction is absorbed by the steel and can potentially degrade the container. However, the rate at which hydrogen is absorbed is related to the rate at which it is generated, so it is of interest to briefly review the rate of the anaerobic corrosion of C-steel under repository-relevant conditions.

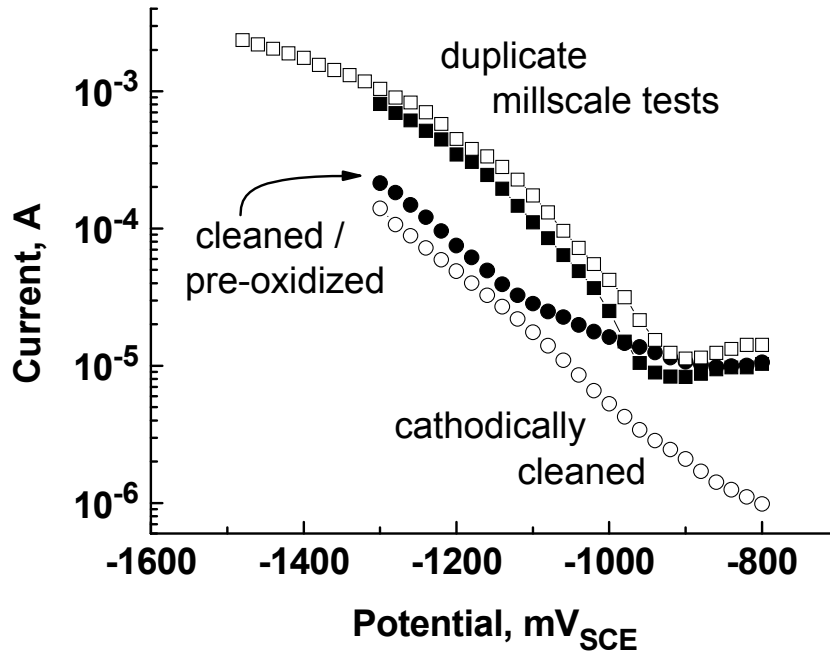


Figure 2: Steady-state Cathodic Polarization Curves for the Reduction of Water on Various Steel Surfaces in Dilute Synthetic Groundwater at ~pH 6.5 (Been et al. 2007).

King (2008) has recently reviewed the available literature on the anaerobic corrosion behaviour of C-steel. The aim of this review was to develop a justifiable (range of) anaerobic corrosion rate(s) for C-steel containers in a Nagra-style DGR in Opalinus Clay based on a critical review of studies performed for various national nuclear waste management programs. A significant difference was found between the results of studies in bulk groundwater or pore-water solutions and those conducted in the presence of compacted clay. Corrosion rates were lower in bulk solution (steady-state rates of the order of $0.1 \mu\text{m}\cdot\text{a}^{-1}$) than in compacted clay ($1\text{-}2 \mu\text{m}\cdot\text{a}^{-1}$ after 4 a exposure). Compact and protective Fe_3O_4 films were formed in bulk solution, whereas less-protective carbonate-containing films are found in compacted bentonite. The higher corrosion rate and the formation of a less-protective film in compacted bentonite is associated with the transport in, and interaction of Fe(II) with, the bentonite.

2.1.3 Fate of Generated Hydrogen in the Repository

Hydrogen generated by the reduction of H^+ or H_2O may undergo various fates in the repository. As discussed in more detail below, a fraction of the hydrogen will be absorbed by the container material and eventually diffuse into the internal void inside the UFC. This process will continue until such time that the chemical potential (as measured by either the activity of dissolved H_2 or the fugacity of gaseous H_2) inside the container is the same as that at the external wall. Permeation of hydrogen through the container wall and into the internal void has a number of implications for the performance of the UFC, as discussed in Section 5.

The largest fraction of the hydrogen generated by anaerobic corrosion will evolve from the container surface as either dissolved or gaseous H_2 . Because of the limited solubility of H_2 and because of the low permeability of the compacted bentonite surrounding the container, the flux of dissolved H_2 through the bentonite will be small. In Opalinus Clay of a similar hydraulic conductivity as compacted bentonite, the maximum flux of dissolved H_2 is equivalent to a C-steel corrosion rate of $0.003 \mu\text{m}\cdot\text{a}^{-1}$ (King 2008, Nagra 2004). In a saturated repository, therefore, the bentonite pore water will rapidly saturate with dissolved H_2 and a separate gas phase will be formed. The maximum H_2 pressure will be equivalent to the sum of the hydrostatic pressure at the repository depth and the breakthrough pressure in the bentonite, which in turn is approximately equal to the bentonite swelling pressure. Therefore, at a repository depth of 650 m with a bentonite dry density of $1.6 \text{ Mg}\cdot\text{m}^{-3}$, the maximum H_2 pressure would be of the order of 6-8 MPa (King and Kolar 2009).

The fugacity of the gaseous H_2 will depend not only on the amount of hydrogen generated by corrosion but also on the degree of saturation of the bentonite. If the repository only slowly saturates then there will be significant vapour-phase porosity for some time following the establishment of anaerobic conditions. Conversely, if the repository saturates quickly then the H_2 pressure will also develop quickly.

2.2 HYDROGEN ABSORPTION

Hydrogen can be absorbed by C-steel from both the gaseous and aqueous phases. Although there are similarities between the two processes, there are also significant differences and they are discussed separately in this section. In particular, we distinguish between the absorption of hydrogen from molecular H_2 in the gaseous phase (Section 2.2.3) and molecular hydrogen dissolved in solution (Section 2.2.2). In these mechanisms, the source of hydrogen in the metal is the hydrogen already present as H_2 . In the case of hydrogen absorption via electrochemical discharge (Section 2.2.1), the source of hydrogen in the metal is either H^+ or H_2O .

2.2.1 Hydrogen Absorption from the Discharge of Protons or Water

2.2.1.1 Hydrogen Absorption Reaction

The hydrogen absorption reaction (HAR) involves the absorption of adsorbed hydrogen (FeH_{ads}) by the matrix of the steel substrate. Figure 3 shows the various competing reactions involved in both the HER and HAR. In general, any process that either increases the surface coverage of FeH_{ads} (e.g., faster discharge (rate constant k_1) or slower chemical (k_2) or electrochemical (k'_2) desorption) or which increases the rate of the absorption process (k_3) (or slows the rate of desorption, k_3) will increase the rate or extent of hydrogen absorption. (It has also been suggested that the absorption of hydrogen proceeds directly from the discharge of H^+ (without going through an adsorbed FeH_{ads} intermediate species), but this mechanism is no longer favoured and seems highly unlikely in neutral and alkaline solutions (Flis 1991).)

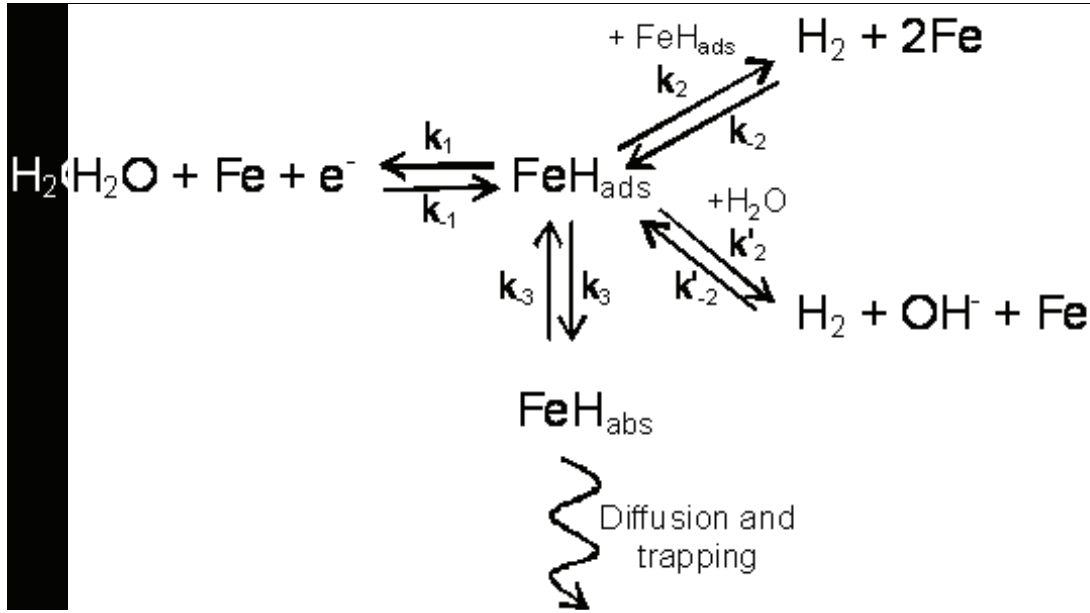


Figure 3: Mechanism of Possible Hydrogen Evolution Reaction Pathways and of the Hydrogen Absorption Reaction.

There are relatively few direct measurements of the hydrogen absorption efficiency as expressed by the ratio of the amount of FeH_{ads} formed to the amount of H absorbed as FeH_{abs} , although it would be possible to estimate this ratio from the many H permeation studies published in the literature. Various factors are known to either promote or inhibit H absorption, as discussed in more detail below. Based on the few reported measurements of the H uptake efficiency, however, it would seem that the efficiency is low. Gajek and Zakroczymski (2005) reported a value of between 0.0002 and 0.016 during aggressive cathodic charging (at a current density of $7.5 \text{ mA}\cdot\text{cm}^{-2}$) under film-free conditions at pH 2.6. In general, this ratio would be expected to increase with decreasing current density, but to decrease with increasing pH.

2.2.1.2 Promoters and Inhibitors of Hydrogen Absorption

A number of species are known to promote the absorption of hydrogen by steel, most notably elements from Groups VA (P, As, Sb, Bi) and VIA (S, Se, Te) of the periodic table. Of these species, the only one that may possibly exist in the repository environment is S. Flis (1991) presents compelling evidence that the active component is the molecular form of the hydride of these elements, i.e., H_2S in the case of sulphur. The enhancement of hydrogen absorption in environments containing $\text{H}_2\text{S}/\text{HS}^-/\text{S}^{2-}$ diminishes with increasing pH above pH 7, which corresponds to the pK of the $\text{H}_2\text{S}/\text{HS}^-$ dissociation reaction and, hence, decreasing fraction of the molecular species in solution. Interestingly, the point of zero charge of Fe_3O_4 is also pH 7 (Kosmulski 2002) which implies that, although the anionic HS^- species would become more predominant in solution with increasing pH, the increasingly negative surface charge would suppress adsorption of HS^- .

Various mechanisms have been proposed to explain the enhancement of hydrogen absorption by hydrogen sulphide and hydrides of other Group VA/VIA elements, including (Flis 1991):

- poisoning of the hydrogen recombination reaction (rate constant k_2 , Figure 3), which would result in an increase in the surface coverage by FeH_{ads} ,
- the adsorbed sulphide occupies surface sites reducing the surface concentration of FeH_{ads} and reducing the probability of two FeH_{ads} species combining to form H_2 ,
- a reduction in the Fe-H_{ads} bond energy, which would promote the adsorption of adsorbed hydrogen (k_3),
- a reduction in the Fe-Fe bond energy, thereby promoting the absorption of hydrogen via the chemisorption of H_2S , and/or
- the dissociative chemisorption of H_2S leading to an increase in $[\text{FeH}_{\text{ads}}]$.

Any mechanism that results in an increase in $[\text{FeH}_{\text{ads}}]$ would only result in an increase in hydrogen absorption if the subsequent chemical and electrochemical desorption steps (rate constants k_2 and k'_2 in Figure 3) are fast. If these latter reactions are slow, then the $[\text{FeH}_{\text{ads}}]$ will be high anyway and increasing the concentration would have minimal impact on H absorption. Furthermore, promotion of hydrogen absorption by chemisorption of H_2S is only likely on clean Fe surfaces, i.e., not on oxide-covered surfaces.

Other promoters of H absorption include: thiosulphate ($\text{S}_2\text{O}_3^{2-}$) and, in acid solution, sulphite (SO_3^{2-}) (Abd Elhamid et al. 2001), $\text{Ca}(\text{OH})_2$ surface films (due to decrease in k_3 in Figure 3) (Lillard et al. 2000), and cement mortar (Lillard and Scully 1996).

Other species inhibit the adsorption of hydrogen. On clean Fe surfaces, various S- and N-containing organic molecules that strongly adsorb on metal surfaces act as inhibitors of hydrogen absorption and may act in a number of ways, including:

- formation of a compact and continuous surface film on the surface on which H_2O or H^+ is discharged but which then acts as a barrier to hydrogen absorption,
- formation of a partial surface film which physically blocks part of the surface, thus diminishing (but not completely preventing) hydrogen absorption,
- altering the HER mechanism, promoting the recombination of adsorbed hydrogen, and/or
- decreasing the Fe-H_{ads} bond strength, thus also promoting hydrogen recombination.

Another important inhibitive species in the context of C-steel UFC in a DGR is Cl^- . Chloride ions have been reported to inhibit H entry in alkaline solutions (pH 13) at high cathodic polarization levels but to have no effect at low overpotentials (Allam et al. 1997). Conversely, Lillard and Scully (1996) report no effect of Cl^- on H pick up.

2.2.1.3 Effect of Surface Films

Oxides and other types of corrosion product film will also inhibit the absorption of hydrogen. Thus, although adsorbed H_2S will promote hydrogen uptake, the mackinawite (FeS) film formed as a consequence of the presence of sulphide in solution inhibits hydrogen adsorption by one or more of the mechanisms above. The formation of a protective sulphide film causes the H permeation currents in long-term tests to decrease with time.

The effect of corrosion product films may be a result of several factors:

- porous or defected insulating films may block the surface resulting in a decrease in the rate of H^+ or H_2O reduction and, consequently, of the surface coverage by H_{ads} ,
- continuous surface films may act as a diffusion barrier or exhibit slow rates of H absorption at the electrolyte/film interface or of desorption at the oxide/metal interface, and
- the rate of H^+/H_2O reduction on continuous conducting films may be slower than on film-free surfaces, or the rate of FeH_{ads} combination faster.

Cheng et al. (2000) report variable effects of a millscale surface film on the permeation of hydrogen through API (American Petroleum Institute) X-65 linepipe steel. (The millscale comprised a defected porous layer with an average thickness of 40 μm and consisting of a mixture of maghemite (γ - $FeOOH$), Fe_3O_4 , and possibly $FeCO_3$.) In some experiments, the flux of hydrogen was more than a factor of 10 lower than for a polished sample in the same environment, whereas in other tests the reduction in the permeation current was only a factor of 2. It was unclear from the results whether the millscale inhibited hydrogen permeation because it acted as an additional diffusion barrier or because it resulted in a lower absorbed hydrogen concentration.

Scully and Moran (1988a) studied the effects of strain and surface films on the uptake of H. Removal of surface films was found to enhance H uptake by increasing the surface coverage of FeH_{ads} and, possibly, increasing the absorption rate constant (k_3 in Figure 3).

Others reporting an inhibiting effect of surface films on H uptake include Lillard and Scully (1996) and Flis and Zakroczymski (1992).

In contrast, Tsuru et al. (2005) found enhanced H entry in the presence of a Fe_3O_4 film under wet-dry atmospheric corrosion conditions. This observation was explained by a change in rate-determining step from the electron transfer step (rate constants k_1/k_{-1} in Figure 3) on bare Fe to the desorption step (rate constants k_2/k_{-2}) on oxide-covered surfaces. The slow desorption step resulted in a higher surface coverage by FeH_{ads} and, consequently, a higher rate of H absorption.

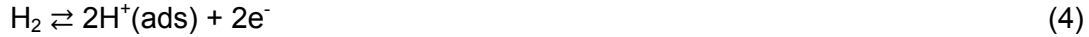
2.2.1.4 Hydrogen Absorption and Localized Corrosion

For some materials, there exists a close relationship between localized corrosion and hydrogen absorption. Crevices and pits can represent regions in which the rate of hydrogen absorption is rapid, both because of the locally acidic conditions (which increases the rate of H^+ discharge) and because the surfaces are film free (which enhances the fraction of adsorbed hydrogen that is absorbed by the material). In addition, depending upon the local geometry and distribution of anodic and cathodic sites, the potential within the occluded region may also favour H^+ discharge.

It is considered unlikely that significant hydrogen absorption will be associated with localized corrosion of the container. Localized corrosion is only likely during the initial aerobic phase due to the presence of O_2 or during the aerobic-anaerobic transition during which $Fe(III)$ reduction is the predominant cathodic process (King 2007). Evidence from corrosion experiments in compacted bentonite suggests that corrosion will tend to be uniform in nature, with limited spatial separation of anodic and cathodic processes (JNC 2000; Johnson and King 2003, 2008; King 2007).

2.2.2 Absorption from Molecular Hydrogen in Aqueous Solution

On some metallic surfaces (e.g., Pt), dissolved H_2 and adsorbed H^+ (or H_2O in neutral and alkaline solution) can be in equilibrium



Discharge of the adsorbed H^+ can then lead to the absorption of H atoms from the original dissolved H_2 molecule.

Although there may be a significant concentration of dissolved H_2 in the repository because of the build up of a gaseous H_2 pressure of up to 8 MPa, Reaction (4) is unlikely to be reversible on Fe or oxide-covered steel surfaces. Therefore, this pathway for the absorption of hydrogen is not considered further here.

2.2.3 Hydrogen Absorption from the Gaseous Phase

Hydrogen absorption from the gas phase involves three processes (Figure 4):

1. Physical adsorption (also referred to as physisorption)
2. Dissociative chemical adsorption (also referred to as chemisorption)
3. Hydrogen entry (or absorption)

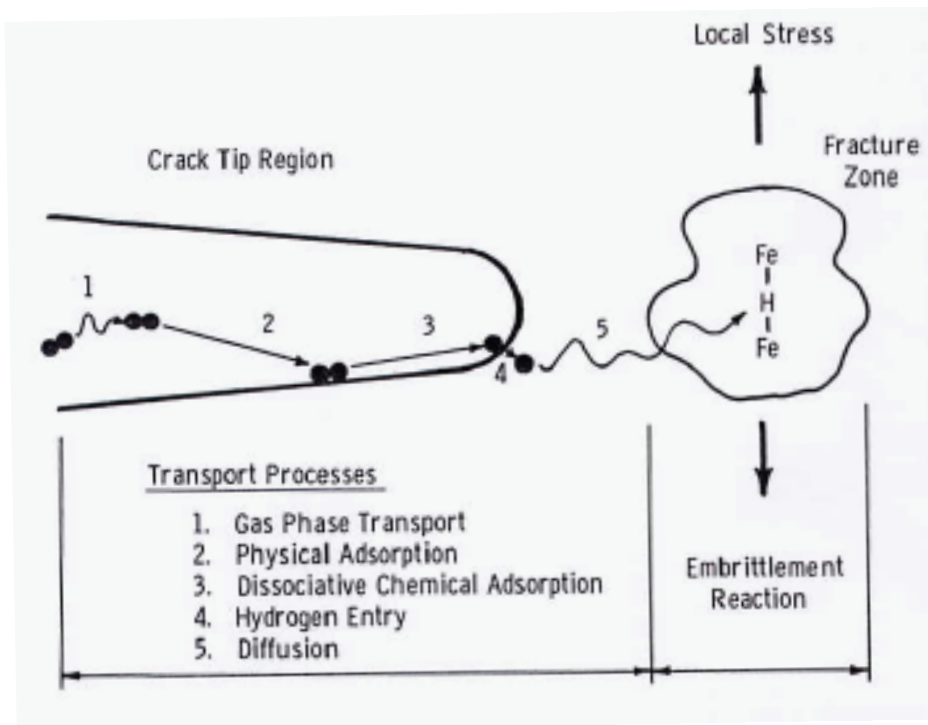


Figure 4: Processes Involved in the Absorption of Hydrogen from the Gas Phase and the Subsequent Embrittlement Reaction (Wei and Gao 1985).

Physisorption is the result of Van der Waal's forces between the adsorbate (H_2) and adsorbent (the steel, or more properly, the oxide-covered steel). The reaction is generally fast and, hence, at or close to equilibrium and is accompanied by an enthalpy change of $<20 \text{ kJ}\cdot\text{mol}^{-1}$ (Pasco and Ficalora 1985). For pure Fe, the sticking probability (i.e., the probability that a H_2 molecule contacting the surface will become physisorbed) is typically of the order of ~ 0.1 (Wedler 1985), with little or no data for steels or oxide-covered steels.

The chemisorption step is typically slow and rate determining. Pasco and Ficalora (1985) have suggested the following mechanism:



The nature of the final step and of the anionic adsorbed H species appears unusual, but Pasco and Ficalora (1985) indicate that the nature of the electron-transfer reactions has been confirmed by surface potential measurements. In contrast, and perhaps more conventionally, Marcus and Oudar (1985) refer to adsorbed H atoms resulting from the interaction of Fe surfaces with gaseous H_2 . The assumption by Pasco and Ficalora (1985) that the final form of adsorbed (and of absorbed) hydrogen is as the negatively charged anion H^- is based on the application of Pauling's electronegativity principle of covalent bonding, which would dictate that H would be present in the Fe lattice as an anion (since Fe is more electropositive than H). However, based on the band model for metals, hydrogen would exist as a cation in the Fe lattice with the electron interacting with the band structure of the metal. Using the band model, the chemisorption of hydrogen from the gaseous form would simply involve Reactions (5a) and (5b). Here, we shall use the band model for metals.

3. HYDROGEN TRANSPORT AND TRAPPING

Hydrogen absorbed by the C-steel may exist in different forms (Flis 1991):

- as an interstitial species dissolved in the matrix in solid solution,
- associated with structural defects, such as dislocations, and
- as gaseous H_2 accumulated in fissures, voids, or blisters.

These different forms exhibit different mobilities and affect the mechanical and physical properties of the material to different degrees. The amount of hydrogen associated with structural defects and present as gaseous H_2 depends on the properties and composition of the material. The amount of dissolved (lattice) hydrogen depends on the charging conditions and is, therefore, related to the external environmental conditions.

Interstitial (lattice) hydrogen dilates the Fe crystal lattice because the effective size of the hydrogen is greater than the free space at the interstitial site. Evidence suggests that the H occupies a tetrahedral site in the lattice (Hirth 1980). The extent to which the lattice is dilated by H, and hence the degree to which the strain field is increased, can be assessed from the partial molar volume of H. Hirth (1980) reports values for the partial molar volume of between $2.0 \text{ cm}^3\cdot\text{mol}^{-1}$ for pure Fe and $2.6 \text{ cm}^3\cdot\text{mol}^{-1}$ for Armco iron.

Lattice hydrogen exists as protons (H^+) but, as is common, is referred to here simply as H (Louthan 2008). Because of its small size, lattice H diffuses rapidly through crystal lattices and, because it dilates the lattice, tends to diffuse to areas of high stress, especially to the region of crack tips or other sharp defects where the hydrostatic stress can be very high (much greater than the yield stress).

Hydrogen is also very reactive and will interact with defects that cause distortion of the lattice. Dislocations, for example, attract (trap) hydrogen because of the dilation of the Fe lattice field in that region. Dislocations, and other types of trap site, are characterized by their binding energy. Trap sites with lower binding energy reversibly trap H, whilst those with higher binding energies lead to irreversibly trapped H. The hydrogen in the reversible trap sites is generally in equilibrium with the lattice hydrogen but, because the residence time in the trap is greater, the trapped H concentration is greater than the lattice H concentration.

Hydrogen will also react with itself to form H_2 within the crystal lattice. This precipitated H_2 acts in the same manner as gaseous H_2 and, if constrained at voids or micro-cracks, can exert significant pressures within the material.

In the absence of gaseous H_2 in voids and micro-cracks, the total H concentration in the steel (C_T) is equal to the sum of the concentrations of lattice H (C_0) and trapped H

$$C_T = C_0 + C_r + C_i \quad (6)$$

where C_r and C_i are the concentrations of reversibly and irreversibly trapped H, respectively. Because the reversibly trapped H is labile and can contribute to the diffusion of hydrogen in the lattice, the sum of the lattice and reversibly trapped H is termed “diffusible” H, although the use of this term in the literature is not consistent.

3.1 CONCENTRATION OF LATTICE HYDROGEN

3.1.1 Hydrogen Absorbed from the Aqueous Phase

Anaerobic corrosion is an important source of absorbed H for steel structures. The lattice hydrogen concentration is a function of the severity of the corrosive environment and generally increases with:

- decreasing pH,
- increasing temperature,
- the presence of H absorption promoters, such as H_2S ,
- the absence of surface films, and
- cathodic polarization (not a factor for UFC).

Significant H charging occurs in acidic sour (H_2S -containing) environments. In comparison the expected DGR environment is benign and expected lattice H concentrations will be low.

Absorbed H concentrations are typically determined from either permeation tests or by using thermal desorption, in which the amount of H_2 evolved from the sample is measured as a function of temperature. When determining C_0 , care must be taken to distinguish lattice H from reversibly trapped H and H_2 trapped in voids or defects created during charging.

There are relatively few measurements of c_0 under DGR-relevant conditions, partly because such conditions do not generally lead to H-related issues and partly because of the difficulty of measuring such small concentrations. Figure 5 shows the dependence of c_0 on pH for annealed C-steel (S content 0.004 wt.%) in a number of solutions saturated with 0.01 MPa H_2S (Yamakawa and Nishimura 1999). In the absence of CN^- (which is a strong promoter of H absorption), the lattice H concentration decreases with increasing pH. At the expected pore-water pH in compacted bentonite of \sim pH 8, the measured c_0 value is close to zero, but will be assumed to be of the order of 0.001-0.01 $cm^3 H_2/100 g Fe$ (9×10^{-4} to $9 \times 10^{-3} \mu g H_2/g Fe$). This is considered a conservative value for the DGR since the H_2S -purged test solutions contained $\sim 350 \mu g \cdot g^{-1}$ dissolved sulphide.

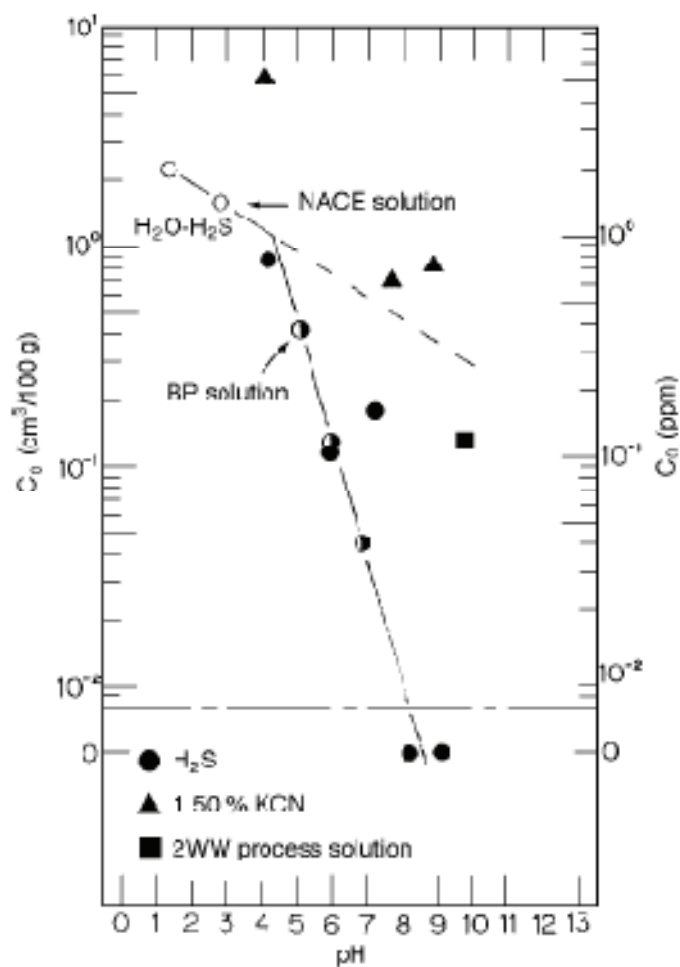


Figure 5: Dependence of the Lattice Hydrogen Concentration on Solution pH in the Presence of 0.01 MPa H_2S at 25°C (Yamakawa and Nishimura 1999). The BP solution is based on artificial seawater and the NACE solution contains acetic acid and NaCl.

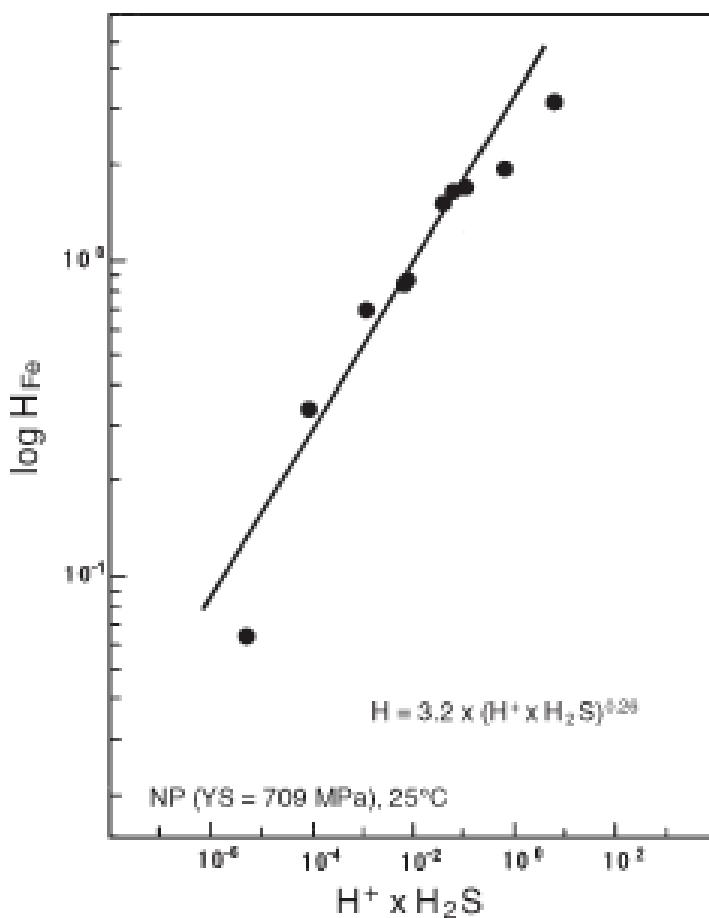


Figure 6: Dependence of the Lattice Hydrogen Concentration on pH and Dissolved Sulphide Concentration at 25°C (Asahi et al. 1994). The hydrogen concentration H_{Fe} is in units of $\mu\text{g}\cdot\text{g}^{-1}$ and the concentrations of H^+ and dissolved H_2S in $\text{mol}\cdot\text{dm}^{-3}$ and $\mu\text{g}\cdot\text{g}^{-1}$, respectively.

Figure 6 shows the relationship between the lattice H concentration and the solution pH and dissolved H_2S content for quench and tempered C-steel with a martensitic microstructure and a yield strength of 709 MPa and S content of 0.005 wt.%. At pH 8.5 and $1 \mu\text{g}\cdot\text{g}^{-1}$ H_2S , the predicted H concentration is $0.020 \mu\text{g}\cdot\text{g}^{-1}$ based on extrapolation of the data in Figure 6.

In the absence of H_2S , Griffiths and Turnbull (1995) suggest a value of $10^{-3} \mu\text{g}\cdot\text{g}^{-1}$ in neutral solution but in the presence of cathodic protection. Turnbull (2009) proposed a lattice H concentration of 1×10^{-4} to $2 \times 10^{-3} \mu\text{g}\cdot\text{g}^{-1}$ in near-neutral pH dilute groundwater solutions based on the total H concentrations reported by Cheng et al. (2000) and Asher and Singh (2008).

In summary, a reasonable estimate for the maximum H lattice concentration as a result of aqueous corrosion of the UFC in the DGR environment is $0.01 \mu\text{g}\cdot\text{g}^{-1}$.

3.1.2 Hydrogen Absorbed from the Gaseous Phase

Hydrogen forms a solid solution with Fe, with the dissolved hydrogen believed to occupy octahedral sites in the Fe lattice. The solubility of hydrogen in the face-centred cubic (fcc) austenite structure is significantly higher than that in the body-centred cubic (bcc) ferrite structure.

In contact with gaseous H_2 , the concentration S of hydrogen in the metal follows Sievert's law

$$S = S_0 \sqrt{p_{H_2}} \quad (7)$$

where p_{H_2} is the pressure of H_2 and S_0 is a constant. Hydrogen is only sparingly soluble in α -Fe, with a value of $\sim 0.001 \text{ cm}^3 \text{ H}_2/100 \text{ g Fe}$ ($9 \times 10^{-4} \text{ } \mu\text{g H}_2/\text{g Fe}$) at room temperature in contact with 0.1 MPa $H_2(g)$.

The solubility increases with increasing temperature, following an Arrhenius relationship of the form

$$S = S_1 \cdot \exp(-Q/RT) \quad (8)$$

where S_1 is a constant, R and T are the universal gas constant and the absolute temperature, respectively, and the heat of dissolution Q has a value of 27.2 kJ/mol (Oriani 1970).

The increase in solubility with increasing temperature accounts for the sensitivity of welds to H-induced damage. Hydrogen can be absorbed in molten steel during the welding process and then precipitate as H_2 as the weld metal solidifies. Common sources of hydrogen in welds are moisture in the welding consumables or inadequate removal of grease and organic residue prior to welding. However, proper specification of weld preparation procedures minimize the amount of H picked up during welding.

Although not as dramatic as the temperature change associated with welding, the UFC will also experience a temperature decrease as the used fuel decays. This temperature decrease will, in turn, result in a decrease in H solubility. However, these changes are relatively minor compared with the changes in temperature and H solubility during welding, and the rate of change of temperature will be so slow that excess H will simply dissolve out of the steel wall.

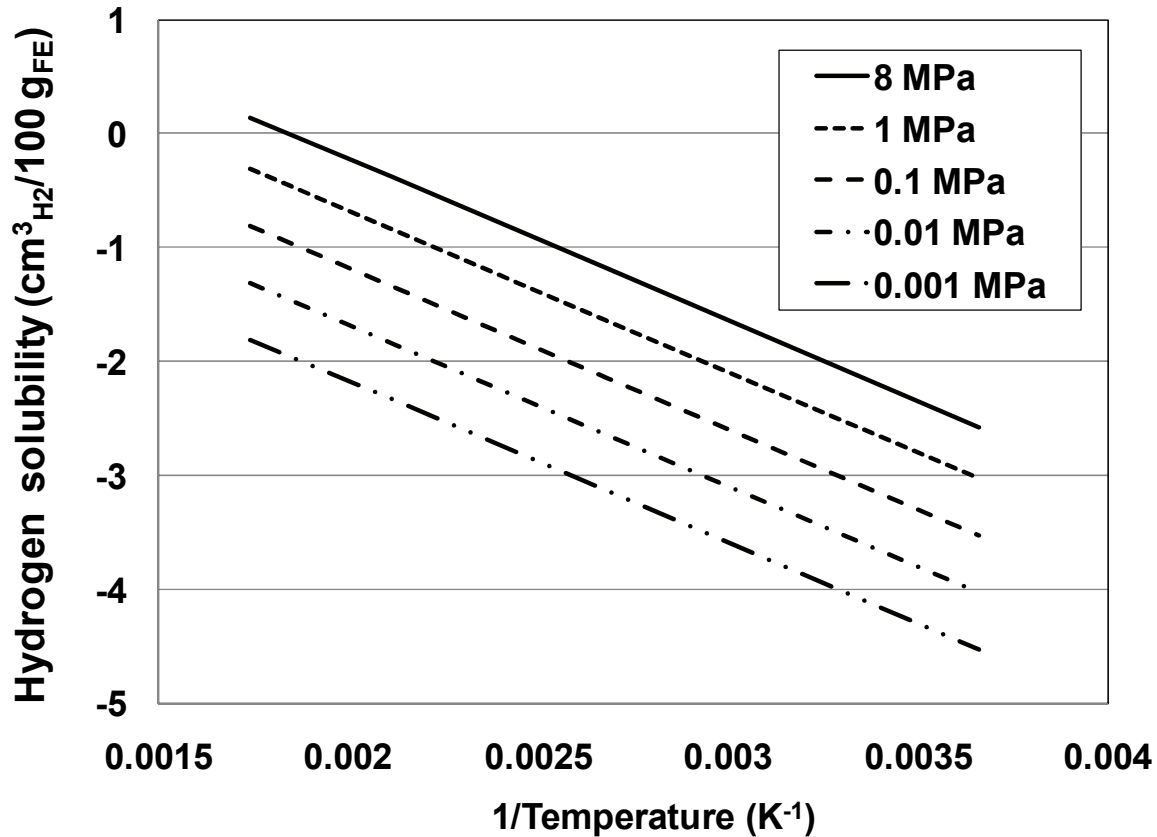


Figure 7: Temperature Dependence of the Solubility of Hydrogen in Iron as a Function of the Fugacity of Hydrogen Gas (after Oriani (1970)).

Figure 7 shows the dependence of the solubility of hydrogen in Fe on temperature and the H_2 fugacity, expressed in units of $cm^3 H_2/100 g Fe$ ($1 cm^3 H_2/100 g Fe$ is equivalent to $0.90 \mu g H_2/g Fe$) (Oriani 1970). The data are reliable for temperatures greater than $\sim 150^\circ C$, but become more uncertain at lower temperatures because of the low solubility and artifacts due to surface films. However, extrapolating the higher temperature data to a temperature of $20^\circ C$ indicates a solubility at $0.1 MPa H_2$ of $6.8 \times 10^{-4} cm^3 H_2/100 g Fe$, or approximately one H atom per 3×10^7 Fe atoms.

3.2 HYDROGEN TRANSPORT

The diffusivity of hydrogen in steel is a function of the crystal structure. Alpha-ferrite (bcc microstructure) exhibits a H diffusivity of $1.6 \times 10^{-5} cm^2 \cdot s^{-1}$ at $25^\circ C$ (Warren 1987), whereas the H diffusivity in austenite (fcc) is 4-5 orders of magnitude lower ($5.4 \times 10^{-10} cm^2 \cdot s^{-1}$). Steel (a bcc mixture of α -Fe and Fe_3C) has a H diffusivity of $3 \times 10^{-7} cm^2 \cdot s^{-1}$ (Warren 1987).

The diffusivity of hydrogen in steel follows an Arrhenius relationship, of the form

$$D = D_0 \cdot \exp(-\Delta E/RT) \tag{9}$$

where D_0 is a constant and ΔE is the activation energy for diffusion. Thus, the reported diffusivity of H in α -Fe is $1.5 \times 10^{-5} \text{ cm}^2 \cdot \text{s}^{-1}$, $3.5 \times 10^{-5} \text{ cm}^2 \cdot \text{s}^{-1}$, and $6.7 \times 10^{-5} \text{ cm}^2 \cdot \text{s}^{-1}$ at temperatures of 20°C , 100°C , and 200°C , respectively (Warren 1987), equivalent to an activation energy of 9.6 kJ/mol . For Fe and steel, Hirth (1980) recommends a value of

$$D = 0.002 \cdot \exp(-6880/RT) \text{ cm}^2 \cdot \text{s}^{-1} \quad (10)$$

Revie et al. (1993a) report a higher value for the activation energy of the diffusion of H in pipeline steels of 21 kJ mol^{-1} .

The reported values of D for steel at room temperature vary by several orders of magnitude because of variability in the degree of trapping in different materials. Figure 8 shows the variability of D based on compilations of Völkl and Alefeld (1978) (as reported by Hirth 1980) and Boellinghaus et al. (1995) (as reported by Turnbull 2009). The spread in reported values, especially at around room temperature, is a result of the different extent of trapping in the different samples used by various researchers. (Figure 8(b) also illustrates the dependence of D on microstructure, with higher diffusivity in austenite and δ -ferrite than in the ferrite-pearlite microstructure.)

The apparent diffusivity D_{app} is related to the lattice diffusivity D_0 by (Oriani 1970)

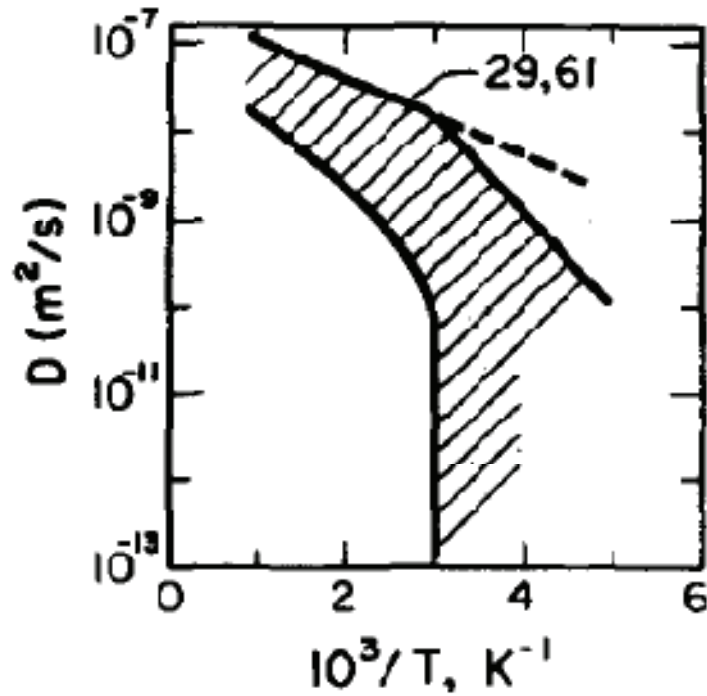
$$D_{app} = D_0 \left(\frac{c_0}{c_0 + c_t(1 - \theta_t)} \right) \quad (11)$$

where c_t and θ_t are the concentration of trapped H and the fractional occupancy of trap sites, respectively. Trap sites, in the form of dislocations, can be introduced by cold work. Huang and Shaw (1995) reported a 5-fold decrease in D_{app} after 40% cold work, but no further decrease on increasing deformation (Figure 9). Particles and non-metallic inclusions also act as H trapping sites and the apparent diffusivity decreases with increasing fraction of particle formers (Figure 10) (Scully and Moran 1988b).

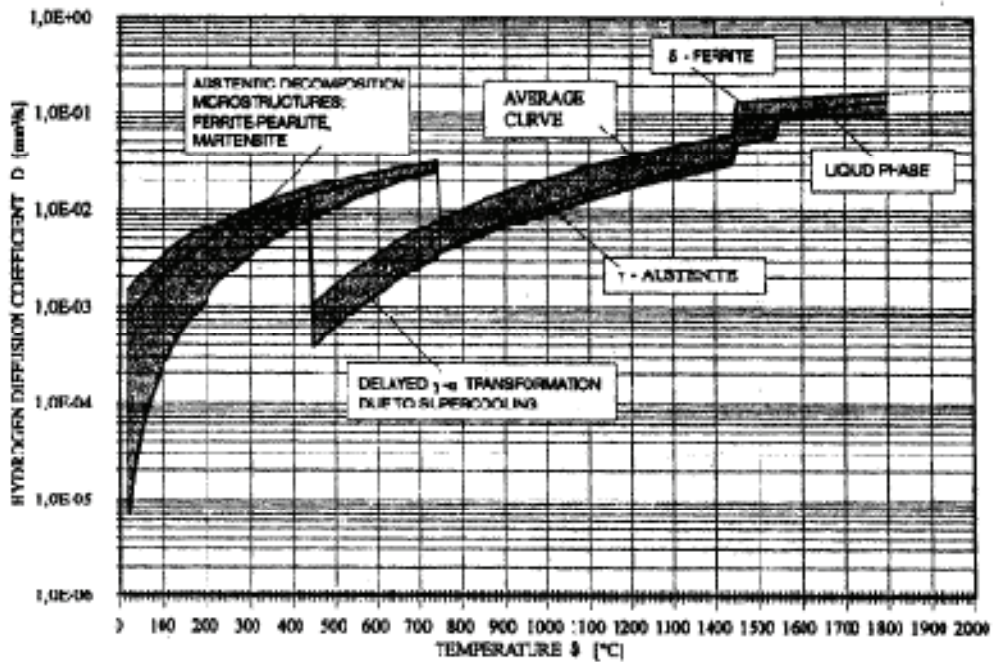
Tensile stress also increases the diffusivity of H in steel (Quan 1997); being one of the factors that lead to the concentration of hydrogen in a stress field (the other being the increased solubility, Section 3.3.2). Quan (1997) found that both the lattice and apparent diffusivities were proportional to the stress gradient ($d\sigma/dx$)

$$D_{app} = D_{app0} \exp \left(k_{app} \frac{d\sigma}{dx} \right) \quad (12)$$

where D_{app0} and k_{app} are fitting constants. Figure 11 shows the stress gradient dependence of D_{app} for a high-strength low alloy steel, but such high stress gradients are unlikely for lower-strength C-steels.



(a) Völkl and Alefeld (1978) (after Hirth 1980)



(b) Boellinghaus et al. (1995) (after Turnbull 2009)

Figure 8: Compilations of the Reported Diffusivity of Hydrogen in Iron and Steels.

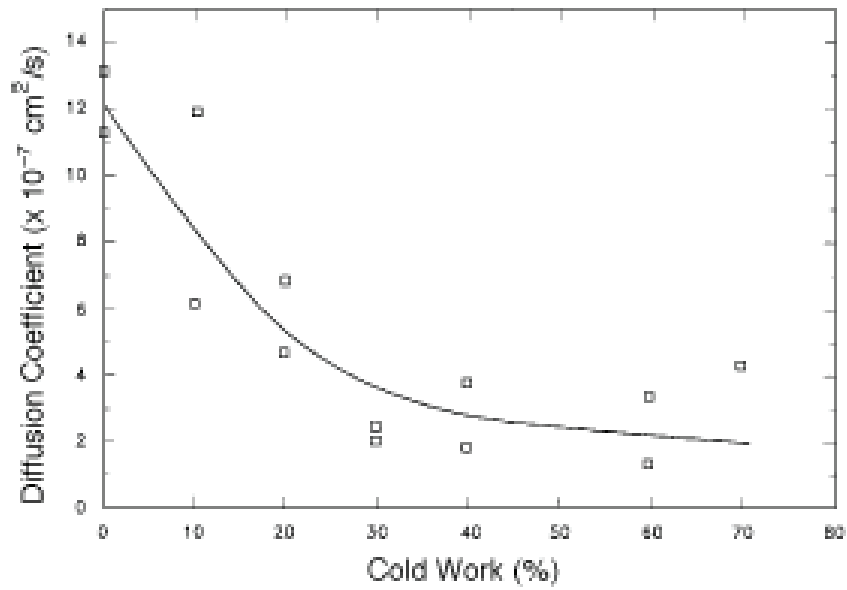


Figure 9: Relationship Between Cold Work and the Apparent Diffusivity of Hydrogen in 1020 Carbon Steel at 25°C (Huang and Shaw 1995).

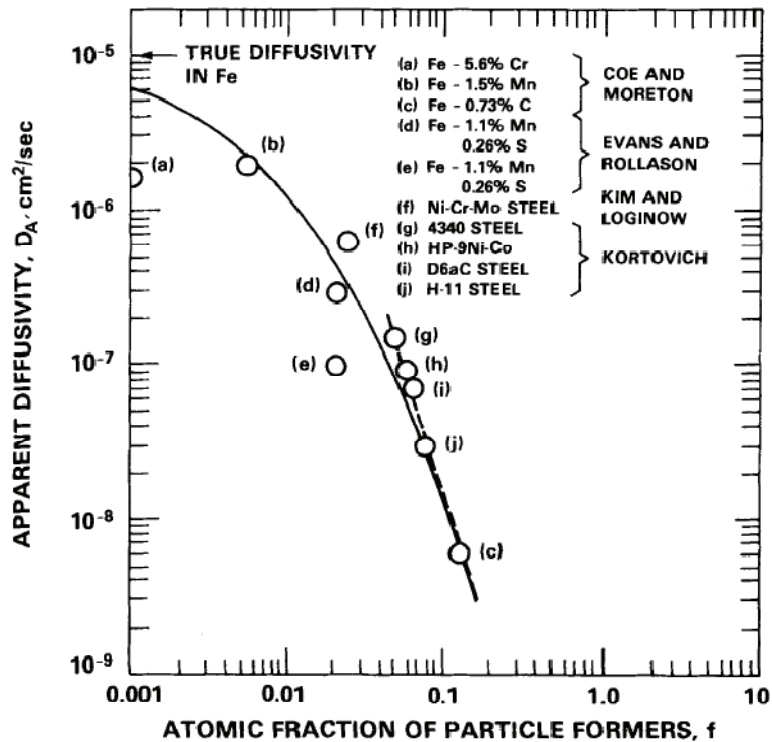


Figure 10: Dependence of the Apparent Diffusivity on the Fraction of Particle Formers in the Steel (Scully and Moran 1988b).

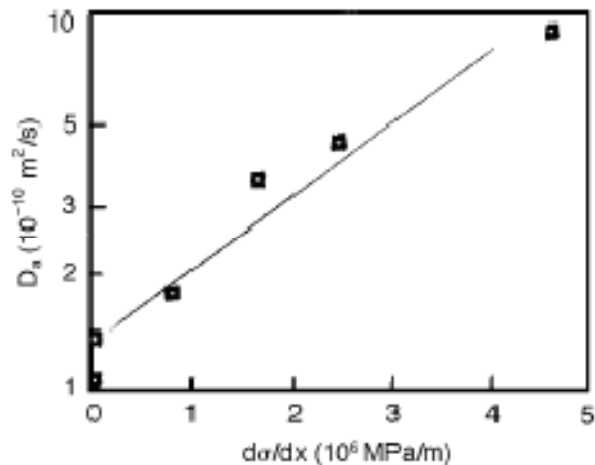


Figure 11: Effect of Stress Gradient on the Diffusivity of Hydrogen in a High-strength Low-alloy Steel. Diffusion in the same direction as the stress gradient.

3.3 TRAPPING AND INTERACTIONS WITH THE MATERIAL

3.3.1 Types and Number of Traps

Traps are locations in the metal that serve to locally concentrate hydrogen, leading to high local concentrations and the possible initiation of hydrogen damage. Once initiated as a crack or void, the flaw can grow to critical dimensions leading to unstable fast fracture. Alternatively, the growth of initiated flaws can lead to the linking of sub-critical cracks and again the possibility of failure.

In addition to accumulating H and acting as crack initiation sites, traps can (Scully 2004):

- provide a reservoir of H that can re-partition to the region of highest hydrostatic stress at the crack tip
- decrease the effective diffusivity (Section 3.2)
- increase the total H concentration
- create additional trap sites under the influence of self-induced or external stress

Traps can be categorized as being:

- Attractive – H is attracted to the trap site due to a gradient in stress or temperature
- Physical – a metallurgical or microstructural feature
- Mixed attractive-physical

The different types of physical trap sites in steel include:

- Dislocations
- Interfaces between inclusions and the steel matrix
- Voids
- Micro-cracks

The reaction between H and a trap site X can be described by (Hirth 1980):



where H_x represents the trapped species. At equilibrium, the distribution between the trapped (concentration c_x) and lattice H (c_0) is given by:

$$\frac{c_x}{(1-c_x)} \cong c_0 \exp\left(\frac{E_B}{RT}\right) \quad (14)$$

where E_B is the trap binding energy.

The binding energy required to remove hydrogen is typically determined using thermal desorption spectroscopy (in which the amount of H leaving the specimen is measured as the temperature is ramped). Depending upon the temperature of the system, traps of lower energy may reversibly trap hydrogen, since the activation barrier to overcome the trap is small. Deeper or stronger trap sites are more likely to irreversibly trap hydrogen which is only released at higher temperatures. For the moderate service temperatures for the UFC, occupancy of the deeper irreversible traps will be favoured over occupancy of the reversible traps. Table 2 lists a number of trap types, their characteristic binding energies, their typical density (Hirth 1980), and whether they act as reversible or irreversible trapping sites (Craig 2005). Similar data have been compiled by other authors, including Oriani (1970).

Table 2: Characteristics of Trap Sites in Iron and Steel (Hirth 1980, Craig 2005).*

Trap type	Binding energy ($E_B/\text{kJ}\cdot\text{mol}^{-1}$)	Trap density (cm^{-3})	Degree of reversibility
Perfect lattice	0	8.5×10^{22}	-
Elastic dislocation**	$20.2 \cdot (b/r)$	4×10^{14} to 4×10^{20}	Reversible
H ₂ vapour phase or in void	28.6	Dependent on steel properties	-
Dislocation core (screw)	20-30	10^{13} to 10^{19}	Reversible
Dislocation core (mixed)	58.6	4×10^{13} to 4×10^{19}	-
Grain boundary	~58.6	10^{13} to 10^{17}	Reversible/ irreversible
AlN particle interface	65	5×10^{18}	-
Free surface	70.7	10^{15}	-
Fe ₃ C interface	≥84	5×10^{18}	Irreversible
TiC interface	94.6	5×10^{18}	Irreversible
Roughened free surface	95.5	10^{15}	Irreversible

* Reference state is H in a perfect lattice

** Binding energy is inversely proportional to the distance from the dislocation, **b** is Burgers vector

Various factors affect the number of trap sites within a material. Cold work, otherwise known as strain hardening or work hardening, introduces dislocations near the surface of the material, resulting in high near-surface H concentrations. Cold-worked material, therefore, tends to undergo H cracking near the surface. Figure 12 shows the dependence of the number of trap sites on the degree of cold work for an initially hot-rolled type 1020 steel (Huang and Shaw 1995).

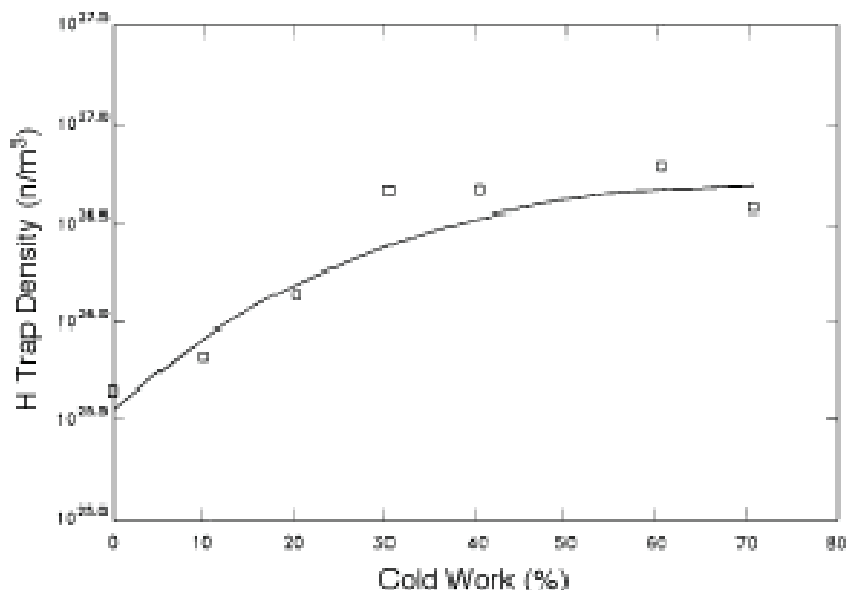


Figure 12: Effect of Cold Work on the Density of Trap Sites (Huang and Shaw 1995).

The microstructure also influences the trapping characteristics of the steel (Park et al. 2008). Park et al. (2008) studied the effect of various microstructures produced by thermomechanical controlled processing (TMCP) on the trapping characteristics of an X-65 grade linepipe steel (0.05 wt.% C, 0.002 wt.% S). The trapping efficiency increased in the order degenerated pearlite < ferrite/bainite < acicular ferrite, with the total H concentration increasing by a factor of ~2 and the effective diffusivity decreasing by the same proportion over this range of microstructures.

It is widely known that MnS inclusions act as both traps and as crack initiation sites. The shape of the MnS inclusions plays a critical role in the severity of trapping, with elongated inclusions better trap sites than spherical inclusions. Calcium is added to steels to control the shape and limit the formation of elongated inclusions. Lowering the overall S content also aids in this respect since the aspect ratio of the inclusion (length/thickness, L/T) increases with total S content (Figure 13).

Certain traps, particularly voids associated with inclusions, can act as so-called dynamic or non-saturable traps as they increase in size as H is trapped and the pressure of precipitated H₂ increases (Turnbull 2009)

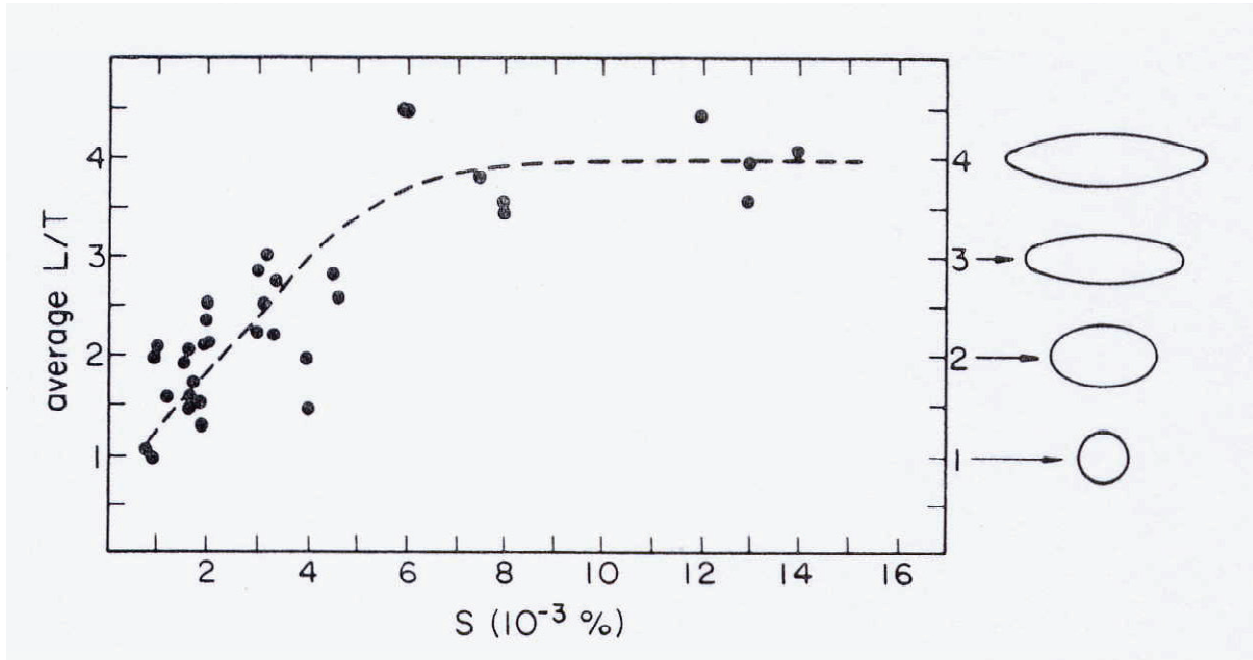


Figure 13: Dependence of the Aspect Ratio of MnS Inclusions on Total Sulphur Content (Bernstein and Pressouyre 1985).

Yu et al. (1997) report accumulation factors (the ratio of the trapped to lattice H concentration) for various types of inclusion and particle. Manganese sulphide inclusions exhibited accumulation factors of 10-17, whereas TiN, TiO, Al₂O₃, and CaO·Al₂O₃+CaS particles showed accumulation factors that ranged from 8 to 20.

3.3.2 Interaction of Hydrogen with the Stress Field

Thermodynamically, the presence of a tensile stress leads to a decrease in the chemical potential of lattice hydrogen under elastic conditions (and an increase in chemical potential under compressive loading). Therefore, the solubility of lattice hydrogen increases under tensile stress, according to:

$$c_{\sigma} = c_{\sigma=0} \exp\left(\frac{\sigma \bar{V}_H}{3RT}\right) \quad (15)$$

where c_{σ} and $c_{\sigma=0}$ are the lattice hydrogen concentrations at the location of hydrostatic stress and no stress, respectively, σ is the tensile stress, and \bar{V}_H is the partial molar volume of hydrogen in the metal. Equation (15) applies equally to stresses at surface cracks and defects, as well as to internal stresses associated with dislocations and inclusions.

The decrease in chemical potential at locations of higher stress will cause hydrogen to diffuse preferentially down the chemical potential gradient to these locations. As a consequence, hydrogen accumulates in these regions.

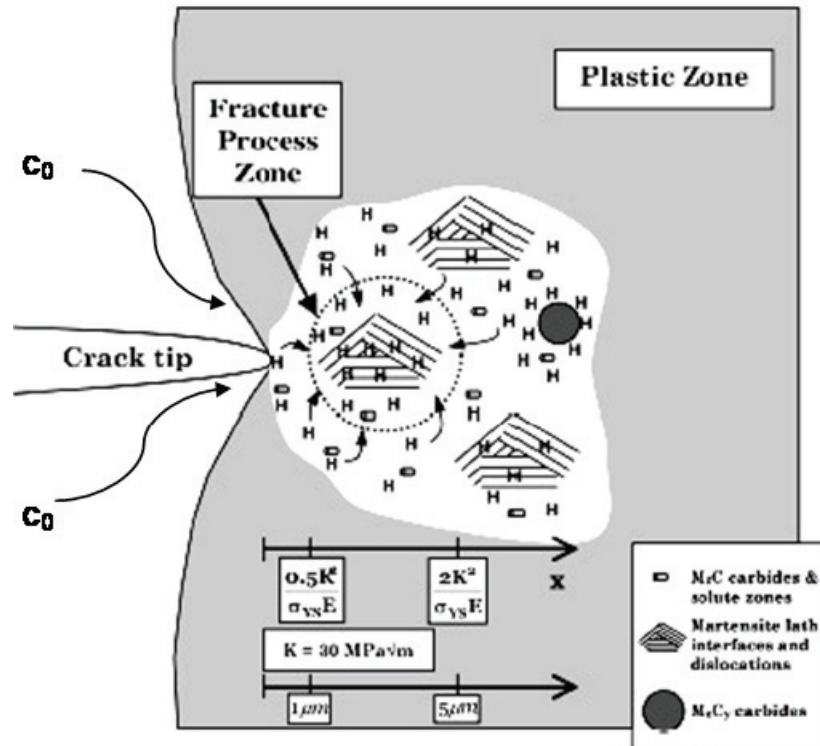


Figure 14: Schematic Illustration of the Processes Occurring in the Fracture Process Zone (Scully 2004).

Figure 14 illustrates the various processes occurring in the fracture process zone (FPZ) ahead of the crack tip (Scully 2004). (This illustration was developed for high-strength steels, but can be used also for C-steels.) The FPZ is that part of the plastic zone ahead of the crack tip in which the hydrostatic stress is a maximum. In addition to the enhanced diffusion of lattice H (concentration c_0) to the crack tip and the trapping of that H by dislocations, inclusions, and other types of trap, the re-distribution of H can also occur under the influence of a stress gradient.

The fact that H is concentrated at the crack tip has been demonstrated both experimentally and theoretically. Razzini et al. (1999) have used photoelectrochemical techniques to image the distribution of lattice H around cracks in C-steel. Although the technique is not quantitative, it clearly shows the higher concentrations in the fracture process zone ahead of the crack tip (Figure 15). It is interesting to note the relative distribution of H (based on the degree of brightness of the image) corresponds to the distribution of stress ahead of the crack tip.

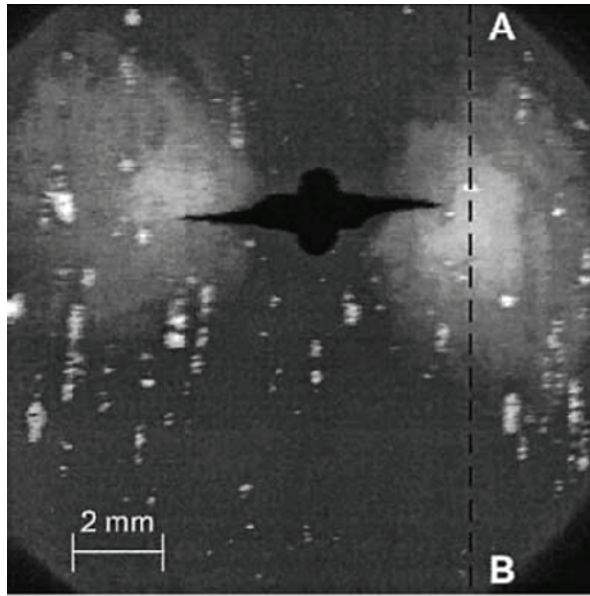


Figure 15: Photoelectrochemical Image of Hydrogen Concentrating at the Locations of Highest Stress in the Fracture Process Zone Ahead of the Crack Tip (Razzini et al. 1999).

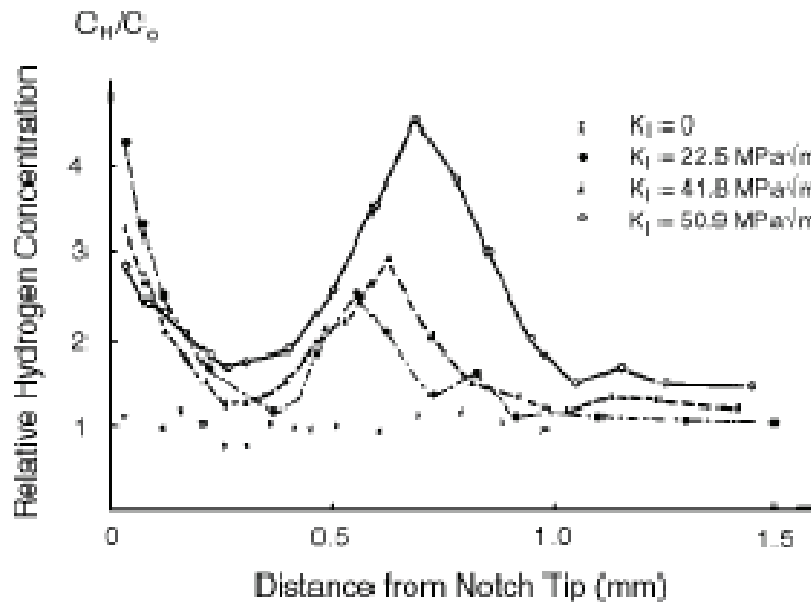


Figure 16: Measured Accumulation of Hydrogen Ahead of a Notch in Carbon Steel as a Function of Stress Intensity Factor (Yu et al. 1997).

Yu et al. (1997) have used an ion microprobe to map the relative concentration of H ahead of a notch in wedge open-loaded (WOL) C-steel samples. Figure 16 shows the concentration of H (c_H) relative to the bulk lattice concentration (c_0) as a function of distance from the notch for different stress intensity factors. There are two points of interest from the figure: first, there is no preferential accumulation of H in the absence of a stress ($K_I = 0$) and, second, in the presence of stress, the maximum H concentration is located at the point of highest hydrostatic stress a few hundreds μm ahead of the notch.

Models have also been developed that can account for the accumulation of H in the FPZ (Gangloff 2009, Lufrano and Sofronis 1998). The concentration of H that accumulates in the FPZ is given by (Gangloff 2009):

$$c_H = \frac{c_0 \exp\left(\frac{E_B}{RT}\right) \cdot \exp\left(\frac{\sigma_H \bar{V}_H}{RT}\right)}{\left[1 + c_0 \exp\left(\frac{E_B}{RT}\right) \cdot \exp\left(\frac{\sigma_H \bar{V}_H}{RT}\right)\right]} \quad (16)$$

where σ_H is the hydrostatic stress in the FPZ, and the other symbols have been defined above.

Equation (16) can be used to define the conditions under which H can be redistributed from trap sites to the lattice (Scully 2004), thus promoting crack growth. Partitioning of the H from the trap to the lattice is possible if $\sigma_H \bar{V}_H > E_B$, with the repartition probability (P_σ) defined by:

$$P_\sigma = \frac{\exp\left(\frac{\sigma_H \bar{V}_H}{RT}\right)}{\left[\exp\left(\frac{E_B}{RT}\right) + \exp\left(\frac{\sigma_H \bar{V}_H}{RT}\right)\right]} \quad (17)$$

Figure 17 shows the H repartition probability for a carbon steel with a yield strength of 483 MPa as a function of trap binding energy for various assumed hydrostatic stresses between 2.5 times and 8 times the yield strength (Scully 2004). Also shown on the figure are the typical binding energies for various reversible and irreversible types of trap. Even for the highest assumed hydrostatic stress level (3860 MPa), the probability that H will repartition from even the weakest trap site (Fe/Fe₃C interface) is <50%. At lower stress levels, the repartition probability is small, especially for dislocations, voids, and grain boundaries. Unlike high-strength steels, therefore, trap sites do not act as a "reservoir" of H that can be released under the action of an applied or residual stress and support crack growth.

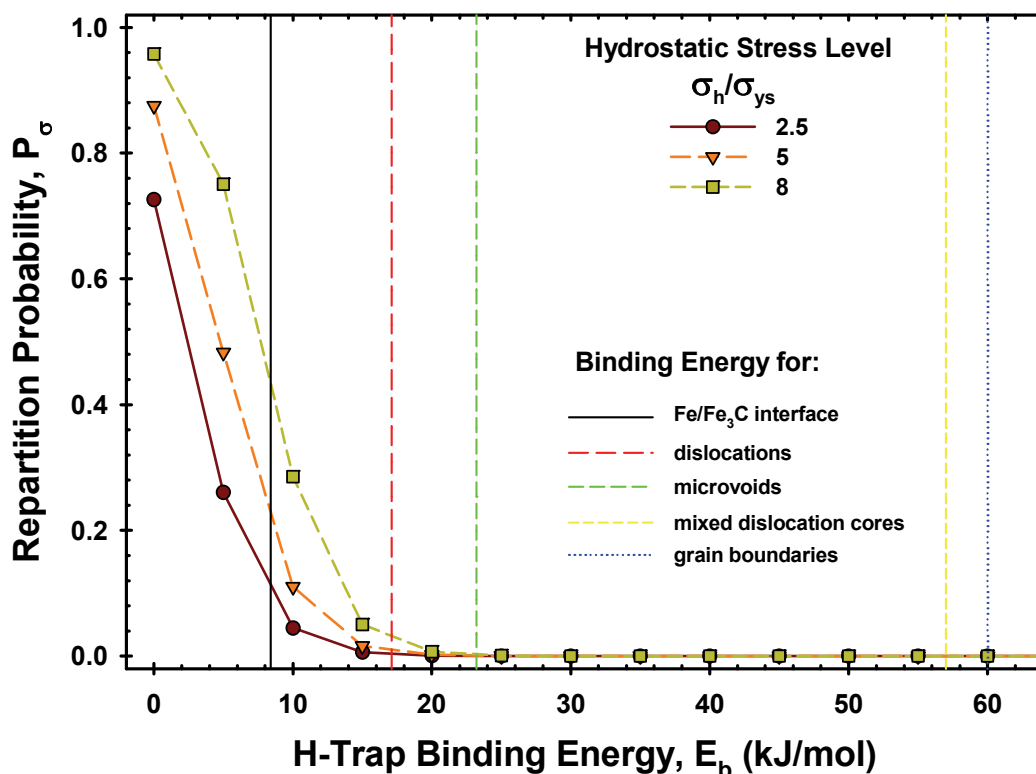


Figure 17: Predicted Hydrogen Repartition Probability for a Carbon Steel with a Yield Strength of 483 MPa as a Function of Trap Binding Energy (Scully 2004).

4. HYDROGEN DEGRADATION MODES AND MECHANISMS

4.1 DEGRADATION MODES

As noted above, absorbed hydrogen exists in three forms: as dissolved hydrogen in solid solution in the steel (also referred to as lattice hydrogen), as H associated with trap sites such as dislocations and interfaces, and as precipitated molecular hydrogen. These forms of hydrogen lead to distinct forms of hydrogen degradation. Lattice hydrogen interacts with dislocations and affects the plastic properties of the material and causes cracking. Molecular hydrogen results in the development of micro-cracks and other discontinuities, leading to deformation and changes to the plasticity of the material. A critical hydrogen concentration exists above which micro-cracks and voids nucleate as a result of H diffusion to regions of elevated stress.

A confusing range of terminology is used to describe the various forms of hydrogen damage. Some terms, such as hydrogen-induced cracking (HIC), refer to the mechanism of failure whereas others, such as blister formation, refer to the phenomenology (or mode) of failure. In this section, the focus will be on classification of the modes of failure, with some discussion of mechanism where necessary. Mechanistic descriptions will be discussed in more detail in Section 4.2.

For carbon and mild steels, the modes of hydrogen degradation are (ASM 1987):

- hydrogen embrittlement
- blister formation
- hydrogen attack

A number of other effects of H on C-steels have also been reported (Section 4.1.4).

4.1.1 Hydrogen Embrittlement

Hydrogen embrittlement (HE) is defined as the deterioration in the mechanical properties of the material, such as the tensile strength, elongation to failure, and fracture toughness. Hirth and Johnson (1976) distinguished three forms of hydrogen embrittlement:

- delayed failure
- reduced plasticity
- brittleness in contact with gaseous hydrogen

These various forms of hydrogen embrittlement can be reversible if the source of hydrogen is removed or irreversible if micro-cracks develop during exposure.

Hydrogen embrittlement is more likely in steels with higher strength (tensile strength >830 MPa or hardness >22 HRC, Warren 1987) and at higher applied or residual stress (for those forms of HE that require a pre-existing source of tensile stress). Severe cold working also increases the probability of HE.

Hydrogen embrittlement is caused by lattice hydrogen interacting with the steel. The elastic properties are not affected but the lattice H greatly affects the plastic properties of the steel, particularly the capacity for plastic flow in the presence of stress or a stress raiser.

The HE of plastically deformed steel is most evident at temperatures in the range -20°C to +40°C and at slow (tensile or bending) strain rates (Warren 1987). Under these conditions, which correspond to those expected in the DGR after a period of several thousands of years, hydrogen is able to diffuse to the location of plastic strain quickly enough to maintain a sufficient flux of H. Conversely, HE is rarely observed at temperatures below -100°C, because the diffusivity of H is too low, or at temperatures greater than +125°C, because the higher diffusivity prevents the concentration of H in regions of plastic strain. Similarly, HE is not observed at high strain rates, for example, under impact loading, because H cannot diffuse to the region of changing plastic strain sufficiently quickly.

4.1.1.1 Delayed Failure

Delayed failure is characterized by brittle cracks in H-containing material subject to stresses below the yield stress. As the name suggests, delayed fracture follows an induction time and exhibits a critical stress level. The severity of delayed fracture increases with increasing hydrogen content, increasing overall stress, and with the presence of local stress concentrators.

Terms used to describe delayed failure include HIC, stress-oriented hydrogen induced cracking (SOHIC), stepwise cracking (SWC), hydrogen stress cracking (HSC), and, in sulphide environments, sulphide stress cracking (SSC) (Table 3). The source of H is typically electrolysis (or cathodic protection), corrosion, or absorption of H or H₂O during thermal treatment or welding.

4.1.1.1.1 Hydrogen-induced cracking

Hydrogen-induced cracking is caused by the precipitation of molecular H₂ at voids or micro-cracks in the steel (Craig 2005). As the internal pressure increases, these voids and micro-cracks can grow and initiate further cracking. No pre-existing source of applied or residual stress is required for HIC. (Some authors include blister formation as a form of HIC since it also involves internal pressurization by H₂ but here it is treated separately.) Cracking occurs in low-strength steels and typically is orientated parallel to the plate rolling direction. The rate of crack growth depends on the supply of H and is, therefore, dependent on the diffusivity of H and the lattice H concentration, with a critical value of c_0 below which cracking is not observed. HIC is associated with lower temperatures, with a maximum sensitivity at ~20°C (Turnbull 2009).

The incidence of HIC is strongly correlated with the microstructural properties of the steel, in particular the density, shape, and orientation of MnS inclusions (Domizzi et al. 2001, Elboudjaini et al. 2003, Revie et al. 1993b). Although reducing the overall S content is beneficial, the major factor is the shape of the inclusion, with elongated inclusions primarily responsible for HIC. A banded microstructure (e.g., ferrite-pearlite banding) is particularly susceptible (Elboudjaini et al. 2003, Revie et al. 1993b), although if the banding microhardness is <300 Hv the influence of banding is minimal (Domizzi et al. 2001).

4.1.1.1.2 Hydrogen stress cracking/sulphide stress cracking

Both HSC and SSC result from the interaction of lattice H and the subsequent reduction in ductility. Under an applied or residual stress, the material cannot accommodate the required strain and a crack initiates. This form of cracking is typically associated with either higher-strength materials (lower limit HRC 34, equivalent to a tensile strength of 1030 MPa) or severe charging conditions (H₂S-containing, low pH solutions; the presence of cathodic polarization).

As with other forms of delayed failure, these forms of cracking are dependent on the microstructure (Koh et al. 2004). Ferrite-bainite and ferrite-pearlite microstructures are more susceptible than acicular ferrite as a result of more facile crack initiation at cementite at grain boundaries or hard martensite phases.

Table 3: Forms of Delayed Cracking of Carbon Steels (based on NACE 2001).

Form of Cracking	Stress Condition	Mechanism	Comments
Hydrogen-induced cracking (HIC)	No externally applied stress	Cracking due to pressurization by H ₂ at trap sites	Lattice H diffuses to trap sites and precipitates as molecular H ₂ . Cracks form in plane.
Hydrogen stress cracking (HSC)	Applied and/or residual tensile stress	Crack formation due to embrittlement by lattice H	Term generally used for cracking that occurs in absence of H ₂ S and generally for metals galvanically coupled to more active material
Stepwise cracking (SWC)	No externally applied stress	Cracking due to pressurization by H ₂ at trap sites	SWC is a specific form of HIC and describes the crack appearance rather than a separate form of cracking. Individual HIC cracks link due to interaction of stress fields at crack tips. Typically associated with low-strength steel plate.
Stress-oriented hydrogen-induced cracking (SOHIC)	Applied and/or residual tensile stress	Crack formation due to embrittlement by lattice H or pressurization by H ₂	Related to both SSC and HIC/SWC. Staggered small cracks aligned approximately perpendicular to principal tensile stress, resulting in "ladderlike" appearance.
Sulphide stress cracking (SSC)	Applied and/or residual tensile stress	Crack formation due to embrittlement by lattice H	Specifically refers to cracking in sulphide environments. Lattice H reduces ductility and increases susceptibility to crack formation in presence of a tensile stress. Particularly affects high-strength grades and hard weld zones.

4.1.1.1.3 Stress-oriented hydrogen induced cracking

Stress-oriented hydrogen induced cracking manifests itself as a "ladder-like" array of cracks orientated in the rolling direction, inter-connected by cracks in the perpendicular direction. This form of cracking may not lead to a loss of containment, but it does reduce the structural strength of the material. There is some disagreement about the basic mechanism, with some authors suggesting that the in-plane cracks are a result of internal pressurization by H₂ (Pargeter 2007, Turnbull 2009) and others suggesting a role for embrittlement by interstitial H (Hay 2003). If internal pressurization (i.e., HIC) was responsible, then HIC-resistant steels would also be resistant to SOHIC, but this does not seem to be the case (Pargeter 2007). Regardless, an applied or residual tensile stress is a pre-requisite for SOHIC.

The applied stress may play a number of roles in the cracking mechanism, including:

- formation of the inter-linking cracks normal to the in-plane cracks,
- increasing the hydrogen solubility in strained material,
- localization of H at inclusions, defects, and dislocations, and
- facilitating void growth.

As with HIC, the rate of crack growth depends on the flux of H, with SOHIC associated with severe charging conditions and high stresses (Pargeter 2007). The threshold H concentration is stress-dependent (Turnbull 2009). Microstructurally, the factors associated with HIC (such as elongated inclusions and banded microstructures) are also associated with SOHIC. Locally hard spots in welds also promote SOHIC (Hay 2003).

4.1.1.2 Reduced Plasticity

Reduced plasticity is characterized by a decrease in the elongation and reduction-in-area (necking) under tensile loading (Craig 2005). The effect is most noticeable at slow strain rate.

4.1.1.3 Brittleness

Brittleness as defined by Hirth and Johnson (1976) occurs in plastically strained materials in gaseous H₂ atmospheres and, unlike delayed failure, exhibits neither an induction time nor a critical stress level.

Somerday (2007) summarizes the tensile properties of smooth and notched C-steel samples exposed to air and 6.9 MPa H₂ at room temperature. Whilst there is little effect on either the yield or tensile strength, the % elongation of smooth samples and the percentage reduction-in-area (%RA) of both smooth and notched samples decreases significantly (average decrease in %RA of 37% and 71% for smooth and notched samples, respectively). The fracture toughness also decreases significantly, with K_{IH} in 6.9 MPa H₂ approximately 40% lower than the K_{IC} in air or N₂. Figure 18 shows the dependence of the fracture toughness on H₂ pressure for two low-strength C-steels (yield strength 280-375 MPa). It is interesting to note that the fracture toughness reaches a minimum at a H₂ pressure approximately equal to the maximum expected in the repository (~8 MPa).

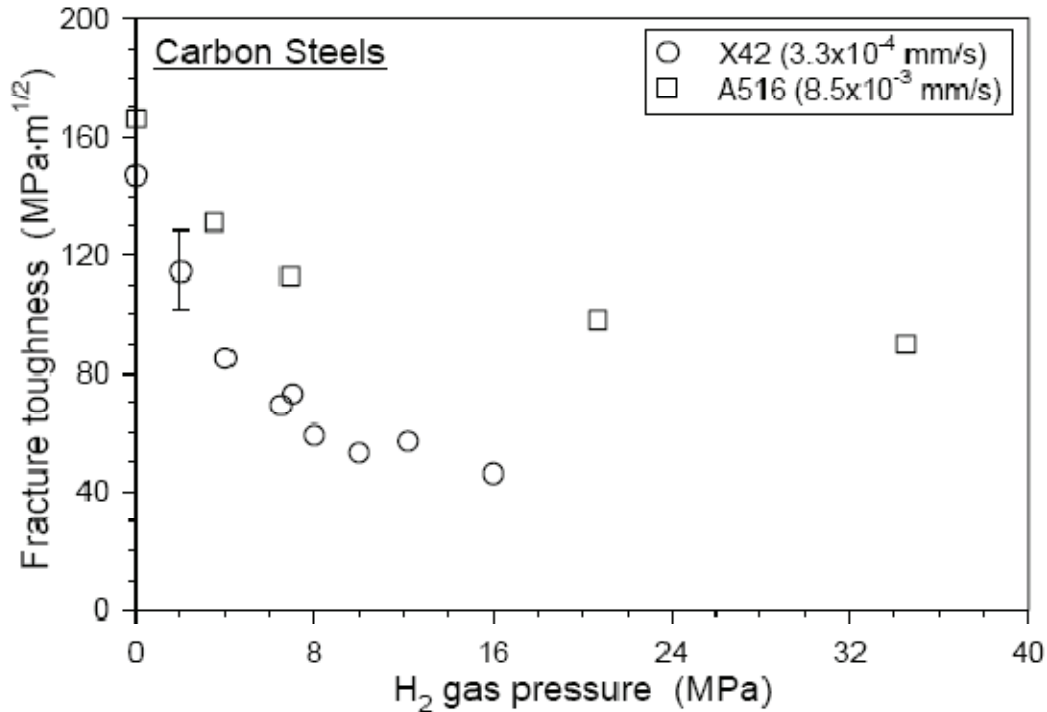


Figure 18: Dependence of the Fracture Toughness of Two Carbon Steels on the Hydrogen Gas pressure (Somerdav 2007).

4.1.1.4 Hydrogen Embrittlement of Welds

Welds can be particularly susceptible to HE because of (i) the effects of temperature changes on the solubility of H, (ii) the formation of susceptible microstructures, and (iii) the presence of residual stress and/or stress raisers. These factors can lead to the spontaneous cracking of the weld metal and/or the heat-affected zone (HAZ) due to the presence of the hard brittle martensite phase. Martensite has a body-centred tetragonal crystal structure and a much lower solubility for H than the fcc austenite, from which it forms as the material cools. Susceptible welds are typically those from material with a C content of 0.25-0.35 wt.% (Warren 1987).

The sources of H in the weld include moisture on coated electrodes (for this reason it is good practice to dry the welding electrodes prior to use), grease and fluxes, and a high-humidity atmosphere. All of these factors, however, are controllable. Other contributing factors are insufficient pre-heat (<93°C) and the failure to stress relieve by post-weld heat treatment.

Somerdav (2007) has summarized information on the tensile properties and fracture toughness of welded C-steel in the presence of 6.9 MPa H₂. The reduction in ductility (%RA) observed for the base metal was also determined in welded samples. The least-ductile welds were electric resistance, gas tungsten arc, and gas metal arc welds. In terms of the resistance to cracking, the weld fusion zone exhibited a similar fracture toughness to the base metal, but the heat-affected zone was significantly less-resistant to cracking.

4.1.2 Blister Formation

Blister formation results from the accumulation of gaseous H₂ at voids, laminations, micro-cracks, inclusion interfaces, or other defects resulting in the formation of large discontinuities or “blisters” within the material. Blister formation is more likely to occur at low applied stress and in materials of lower strength (yield strength of <480-550 MPa) or hardness (<22 HRC) (Warren 1987), but it does not cause embrittlement of the material as such. An applied stress is not required for blister formation but, if present, external stress affects the growth and stepwise-interlinking of blisters (Iino 1985). As with other forms of H damage, the presence of sulphide inclusions is deleterious, both as trap sites that can concentrate H and as sites at which blisters can nucleate.

For a steel surface in contact with gaseous H₂, the pressure of gas in the blister cannot exceed that in the external environment (Louthan 2008). The effective fugacity of hydrogen generated electrolytically can be much higher because of the higher concentration of adsorbed H (H_{ads}) so that corrosion, especially in sour systems, is a more likely cause of blister formation than exposure to gaseous H₂.

Blisters in themselves are not necessarily of concern as they do not lead to a through-wall defect and loss of containment. However, cracks can initiate from blisters as the edges act as notches causing an increase in triaxial stress and the accumulation of lattice H.

4.1.3 Hydrogen Attack

Hydrogen attack involves the conversion of C in the steel to methane (CH₄) in a process known as decarburisation involving the reaction of lattice H with cementite (Fe₃C) according to:



The resultant gas exerts an internal pressure, leading to voids, fissures, cracks, or flaking and a consequent loss of ductility and strength. This reaction is thermally activated and becomes increasingly severe with increasing temperature. Based on experience from industrial processes, the rate of this reaction is negligible for C-steel below a temperature of ~250 °C (Figure 19). As shown in the figure, the threshold temperature for H attack decreases with increasing exposure time because of the kinetics of the reaction. After 10,000 hrs exposure (1.1 a), the threshold temperature at a H₂ pressure of 8 MPa is 260°C with no attack, regardless of the exposure period, at a temperature of 253°C.

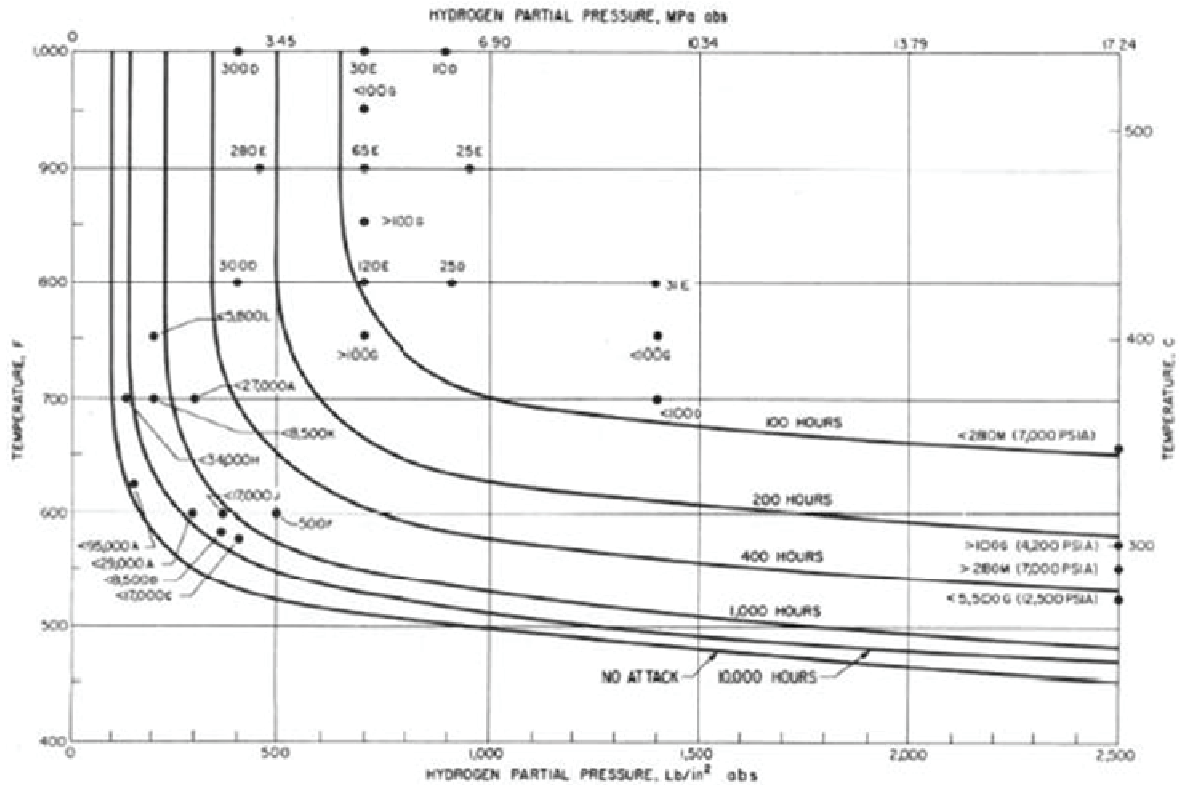


Figure 19: Nelson Curves for Carbon Steel as a Function of Exposure Time. The maximum H₂ pressure in the repository of 8 MPa is equivalent to a pressure of 1160 lb/in² (Nelson 1977).

4.1.4 Miscellaneous Effects of Hydrogen on Steels and Their Oxides

Hydrogen can impact other properties of C-steel that may be relevant to the long-term performance of the UFC. Absorbed H is known to promote the anodic dissolution of C-steel, but extreme charging conditions are generally used to demonstrate the effect. For example, Figure 20 shows the enhanced dissolution for a pipeline steel (yield strength 359 MPa) following 24 h cathodic charging at a current density of 3 mA·cm⁻² in a 1 mol·dm⁻³ H₂SO₄ solution containing 250 µg·g⁻¹ As₂O₃ (a H absorption promoter) (Gu et al. 1999). These charging conditions would lead to a lattice H concentrations of 10's µg·g⁻¹ (two to three orders of magnitude higher than that expected for a UFC in the DGR) and would cause significant lattice dilation, as well as possible blister formation and micro-crack initiation. The effect of less-aggressive charging conditions on H-enhanced anodic dissolution is unknown and, probably, immeasurable.

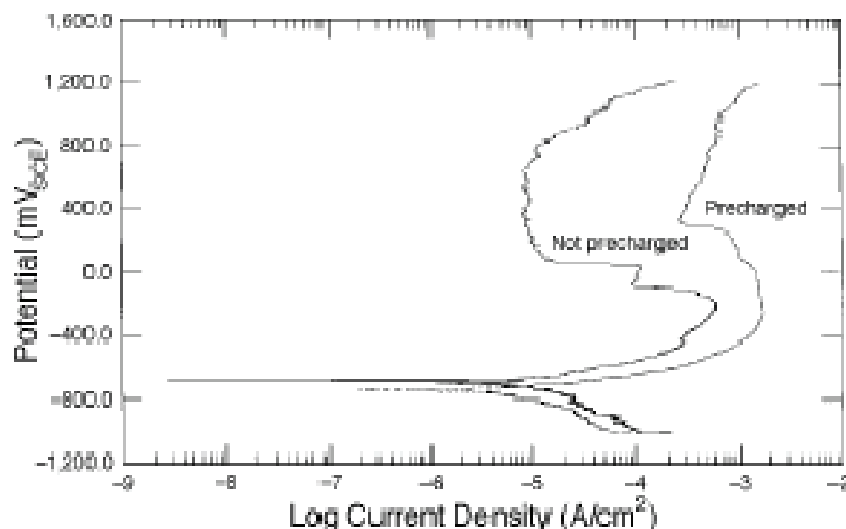


Figure 20: Enhanced Anodic Dissolution of Carbon Steel in $0.005 \text{ mol}\cdot\text{dm}^{-3}$ NaHCO_3 Solution Following Hydrogen Cathodic Pre-charging for 24 Hours in $1 \text{ mol}\cdot\text{dm}^{-3}$ $\text{H}_2\text{SO}_4 + 250 \mu\text{g}\cdot\text{g}^{-1}$ As_2O_3 Solution (Gu et al. 1999).

Hydrogen is also reported to destabilize passive films on Fe. Hydrogen leads to an increase in photocurrent as well as changes in other photoelectrochemical characteristics of the film (Zeng et al. 2004). Electrochemically, the Fe surface changes from passive to active-passive in moderately alkaline solutions in the presence of H charging (Yu et al. 2001, 2002). The magnitude of these effects increases with increasing cathodic charging current density. As noted above, however, these studies are typically carried out with charging current densities of $0.1 \text{ mA}\cdot\text{cm}^{-2}$ to $>1 \text{ mA}\cdot\text{cm}^{-2}$ and the relevance of the observations to less-aggressive charging conditions is unclear.

Finally, Oriani and Josephic (1981) showed that gaseous H_2 causes an increase in the room temperature creep rate of a spheroidized C-steel. The authors explained the observations in terms of the effect of H on the movement of dislocations and the softening effect of an increased number of micro-voids due to the presence of H.

It is also well known that H affects the corrosion fatigue properties of C-steel (Gangloff 2009). However, since the UFC will not experience cyclic loads, this effect is not considered further here.

4.2 DEGRADATION MECHANISMS

A number of different mechanisms have been proposed to account for the effect of hydrogen on materials in general. These mechanisms are discussed in more detail below and include: (i) the development of internal pressure, (ii) decohesion, (iii) hydrogen enhanced local plasticity (HELP), (iv) adsorption induced dislocation emission, and (v) hydride formation. Except for the

latter mechanism (iron does not form hydrides), each of these mechanisms has been proposed to account for hydrogen degradation in iron and steels. No single mechanism can account for all modes of hydrogen damage and, indeed, more than one mechanism may be operative in some forms of failure.

4.2.1 Internal Pressure

The development of an internal pressure due to the precipitation of molecular H₂ is one of the oldest mechanistic explanations for hydrogen damage (Craig 2005). Atomic hydrogen diffuses to locations such as voids or interfaces between inclusions or particles and the matrix and combines to form H₂. An increasing pressure develops as the concentration of hydrogen increases. Eventually the pressure increase is sufficient to either initiate a crack or to increase the volume of the void.

Based on the Griffith model for brittle fracture, the critical stress (σ_{crit}) for the growth of an elliptical crack of length a under plane stress conditions is

$$\sigma_{crit} = \left(\frac{2E\gamma}{\pi a} \right)^{1/2} \quad (19)$$

where E is Young's modulus and γ is the surface energy of the crack. If we consider the crack to represent an interface between an inclusion or particle at which a blister could initiate, the critical pressure for blister formation (P_{crit}) is given by (Subramanyan 1981)

$$P_{crit} = \sigma_{crit} - \sigma_{\perp} \quad (20)$$

where σ_{\perp} is the applied stress perpendicular to the length direction. In the absence of an external stress, the critical H concentration for blister formation (c_{crit}) is

$$P_{crit} = \left(\frac{2E\gamma}{\pi a} \right)^{1/2} \quad (21)$$

which can be related to the critical lattice H concentration using Sievert's law (Equations (7) and (8)).

Internal pressurization is clearly a plausible explanation for blister formation and HIC, but cannot explain other forms of cracking or changes in mechanical properties.

4.2.2 Decohesion

In the decohesion (or hydrogen enhanced decohesion (HEDE)) mechanism, hydrogen accumulates under an external stress to such a degree that the interatomic force between adjacent Fe atoms in the lattice is lowered sufficiently that cracks may form (Birnbaum 1991). The applied stress not only serves to concentrate the lattice H but also overcomes the lowered Fe-Fe bond energy. Fracture may occur transgranularly along cleavage planes or intergranularly, depending upon the location of H accumulation.

The decohesion mechanism is more important for high-strength materials because a high stress is required (Gerberich et al. 1993, Turnbull 2009). Other contributing factors are high H concentrations, sharp crack tips, and high applied or residual stresses. In addition to lattice H, trapped H can also re-partition to the crack tip if the hydrostatic stress is sufficient to overcome the binding energy of the trap. Although re-partitioning is feasible for high-strength steels, the analysis in Section 3.3.2 suggests that it does not occur for low-strength C-steels.

4.2.3 Hydrogen Enhanced Local Plasticity

In the hydrogen-enhanced local plasticity (HELP) mechanism, hydrogen enhances dislocation motion and the formation of dislocations at surfaces or crack tips, resulting in localized softening (plasticity) of the material (Craig 2005). Much of the evidence for HELP is based on examination of fracture surfaces. Whilst the concept of enhanced plasticity contributing to apparently brittle fracture appears contradictory, the distribution of H ahead of the crack is non-uniform (Birnbaum 1991). This leads to highly localized plastic deformation and an apparently brittle fracture surface. Although there is local plastic deformation, the overall ductility and %RA are significantly reduced.

The HELP mechanism requires an applied or residual stress to promote H transport and solubility ahead of the crack tip. The interaction of H with dislocations causes dislocation motion, resulting in a decrease in the flow stress and the occurrence of slip at stresses below those required in the absence of H (Birnbaum 1991). The dislocation velocity is proposed to increase with increasing H₂ pressure (Turnbull 2009).

4.2.4 Adsorption Induced Dislocation Emission

In the adsorption-induced dislocation emission (AIDE) mechanism, hydrogen absorbed in the first few atomic layers weakens the Fe-Fe interaction and facilitates the emission of dislocations at the crack tip. The fracture surface shows evidence of small voids at particles interconnected by a seemingly macroscopic brittle crack.

The AIDE mechanism shares similarities with the HELP mechanism, in that both are based on fractographic evidence for the presence of ductile features in an overall brittle fracture. However, the mechanisms differ in that (a) the AIDE mechanism involves the creation of dislocations rather than their movement (Turnbull 2009) and (b) AIDE involves surface concentration of H whereas the HELP mechanism also considers the effects on dislocation movement of H in the bulk of the material (Birnbaum 1991).

4.3 THRESHOLD OR CRITICAL CONDITIONS FOR HYDROGEN DAMAGE

Many forms of hydrogen degradation exhibit a threshold or critical condition below which damage is not observed. Generally, these critical conditions take the form of either a critical H concentration (c_{crit}), for blister formation or HIC, or a critical stress intensity factor (K_{IH}) for crack growth.

4.3.1 Critical Hydrogen Concentration

The concept of a critical H concentration is useful since it is then possible to compare c_{crit} with the concentration of lattice hydrogen in order to predict whether the material will be susceptible to a given form of damage in a given environment. It is important to note that the susceptibility to damage is related to the concentration of lattice hydrogen, rather than the total H concentration in the steel, the latter including the amounts of atomic or molecular H associated with dislocations, voids, blisters, etc.

The value of c_{crit} is a function of a number of variables, including:

- temperature,
- the number, size, shape, and distribution of inclusions,
- the degree of cold work (dislocations),
- the strength of the material,
- microstructure, and
- in the case of forms of HE that require an applied or residual stress, the stress level.

In general, the susceptibility to H damage increases with increasing lattice H concentration and with increasing strength of the material. Figure 21 delineates HE immune and “cracking” zones (as well as a region of blister formation) as a function of the yield strength of the steel and the diffusible (lattice) hydrogen concentration (Okada 1977). Data for both a “mild” and a “severe” notch (the meaning of which was not defined by Okada (1977)) are given, which clearly shows the stress-concentrating effect of notches or discontinuities on the surface. The figure also shows the approximate concentrations of lattice H generated in different environments, including liquid NH_3 and H_2S , both of which represent extreme service conditions. The environmental condition of most interest for a DGR is that labelled “natural environment” in Figure 21 and which represents near-neutral pH conditions. Under these relatively benign environmental conditions, Figure 21 indicates a lattice H concentration of $\sim 0.05 \mu\text{g}\cdot\text{g}^{-1}$ ($0.6 \text{ cm}^3 \text{ H}_2/100 \text{ g Fe}$), although in the text Okada (1977) suggests a concentration as low as 10^{-5} to $10^{-3} \mu\text{g}\cdot\text{g}^{-1}$. Under such conditions, steels with yield strengths of less than 1000 MPa would be immune to HE involving delayed failure.

Figure 21 also provides guidance on the critical lattice H concentration for blister formation. As noted above, blister formation is limited to lower strength materials in which the development of an internal H_2 pressure can exceed the yield strength. However, the critical lattice H concentrations are of the order of $10\text{-}100 \mu\text{g}\cdot\text{g}^{-1}$ ($11\text{-}110 \text{ cm}^3 \text{ H}_2/100 \text{ g Fe}$). Okada (1977) also describes a “peculiar” form of cracking that occurs in lower-strength materials, again at high lattice H concentrations, and which appears to be a form of delamination due to the development of internal H_2 pressure.

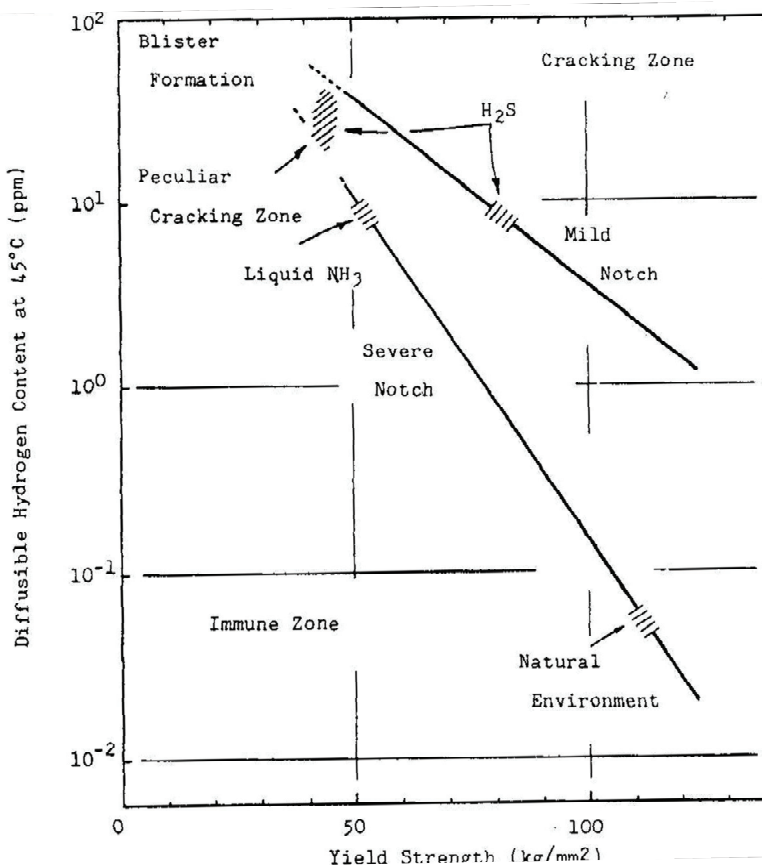


Figure 21: Zones of Susceptibility and Immunity to Cracking and Blister Formation as a Function of the Steel Yield Strength and Diffusible (Lattice) Hydrogen Concentration (Okada 1977). A yield strength of 100 kg/mm² is equivalent to 981 MPa and a diffusible H concentration of 1 ppm ($\mu\text{g}\cdot\text{g}^{-1}$) is equivalent to 1.12 cm³ H₂/100 g Fe.

Other measurements of c_{crit} for blister formation, HIC, SSC, and HE are given in Table 4. There is a wide range of c_{crit} values and, in some cases, it is not clear whether the authors are reporting lattice H concentrations or whether the reported threshold "diffusible" H concentration also includes reversibly trapped H.

A number of studies have included tests at different temperatures (Table 4 and Figure 22). In all cases, the value of c_{crit} increases with increasing temperature regardless of whether the form of damage is blister formation (Beck et al. 1966) or SSC (Asahi et al. 1994).

Table 4: Critical Hydrogen Concentrations for Various Forms of Hydrogen Damage.

Table 4(a): Blister formation

Form of H damage	Material	Composition (wt.%)	Temperature (°C)	Yield strength (MPa)	C _{crit} (µg·g ⁻¹)	Reference
Blister	Armco iron	Unknown	19	Unknown	0.031	Beck et al. (1966)
			26	Unknown	0.036	
			43	Unknown	0.047	
			66	Unknown	0.056	
			80	Unknown	0.100	
Blister	API X46	0.10C, 0.034S	RT?	310*	0.36	Maccagno et al. (1998)
	API X46	0.11C, 0.035S		310*	0.13	
	API X46	0.09C, 0.014S		310*	0.89	
	API X52	0.20C, 0.013S		359*	0.99	
	API X56	0.09C, 0.018S		386*	1.2	
	API X70	0.07C, 0.008S		483*	0.18	
Blister	API C90	0.26C, 0.002S, 1.06Cr, 0.26 Mo	RT?	668	8.5	Chu et al. (1999a)
	API C90	0.026C, 0.003S, 0.98Cr, 0.32Mo		658	9.4	
	API C90	0.23C, 0.013S, 0.95Cr, 0.21Mo		708	5.8	
	API C90	0.26C, 0.010S, 0.91Cr, 0.44Mo		672	5.0	
Blister	API C90	0.23C, 0.013S, 0.95Cr, 0.21Mo	RT?	658	1.8	Yu et al. (1997)
	API C90	0.26C, 0.010S, 0.91Cr, 0.44Mo		706	4.3	
Blister	API C90	0.26C, 0.002S, 1.06Cr, 0.26Mo	RT?	673	8.4	Chu et al. (1999b)
	"A"	0.72C, 0.010S		796**	0.7	
	"B"	0.74C, 0.014S, 0.09V		942**	2.1	

* Specified minimum yield stress (SMYS)

** Based on the UTS and an assumed Y/T ratio of 0.9

Table 4: Critical Hydrogen Concentrations for Various Forms of Hydrogen Damage.

Table 4(b): HIC

Form of H damage	Material	Composition (wt.%)	Temperature (°C)	Yield strength (MPa)	C _{crit} (µg·g ⁻¹)	Reference
	API X56	0.13C, 0.0084S, 1.09Mn		386*	0.8	
	API X42	0.22C, 0.0054S, 0.77Mn		290*	0.7	
	API X52/56	0.16C, 0.001S, 0.85Mn		359/386*	0.8	
HIC	API X52/56	0.10C, 0.0013S, 0.84Mn	25	359/386*	>1.8	Revie et al. (1993b)
	API X52	0.080C, 0.0016S, 0.80Mn		359*	>1.8	
	API X52	0.065C, 0.0054S, 1.08Mn		359*	<0.1	
	Seamless	0.20C, 0.0088S, 0.96Mn		Unknown	1.8	
	Seamless	0.095C, 0.0018S, 0.73Mn		Unknown	0.2	
HIC	API X70	0.03C, 0.25Cr	RT?	483*	1.63	Kim et al. (2008)
	API X70	0.05C, 0.25Cr		483*	1.3-1.8	
HIC	"B"	0.74C, 0.014S, 0.09V	RT?	942**	0.24	Chu et al. (1999b)

* Specified minimum yield stress (SMYS)

** Based on the UTS and an assumed Y/T ratio of 0.9

Table 4: Critical Hydrogen Concentrations for Various Forms of Hydrogen Damage.

Table 4(c): SSC and HE

Form of H damage	Material	Composition (wt.%)	Temperature (°C)	Yield strength (MPa)	c_{crit} ($\mu\text{g}\cdot\text{g}^{-1}$)	Reference
SSC	API C90	0.26C, 0.002S, 1.06Cr, 0.26 Mo	RT?	668	0.82*	Chu et al. (1999a)
	API C90	0.026C, 0.003S, 0.98Cr, 0.32Mo		658	2.0*	
	API C90	0.23C, 0.013S, 0.95Cr, 0.21Mo		708	3.1*	
	API C90	0.26C, 0.010S, 0.91Cr, 0.44Mo		672	3.3*	
SSC	"NS"	0.24C, 0.002S, 0.56Cr, 0.76Mo	25	705-1186	4.0**	Asahi et al. (1994)
			50		7.2**	
			80		7.2**	
SSC	"NP"	0.16C, 0.005S	25	641-1098	5.9**	Asahi et al. (1994)
			50		13.5**	
			80		25.0**	
HE	Unknown	Unknown	45	959 ^{\$}	3.8	Okada (1977)
				856 ^{\$}	7.8	
				757 ^{\$}	10.8	
				686 ^{\$}	17.7	
HE	"A"	0.72C, 0.010S	RT?	796 ^{\$\$}	0.09	Chu et al. (1999b)
	"B"	0.74C, 0.014S, 0.09V		942 ^{\$\$}	0.26	

* Critical stress is a function of the diffusible H concentration, c_{crit} defined for critical stress equal to the nominal yield stress for C90 of 621 MPa

** c_{crit} is a function of the actual yield stress and has been defined here for nominal yield stresses of 1000 MPa and 800 MPa for the "NS" and "NP" grades, respectively

^{\$} Based on a conversion of Vickers hardness to UTS and an assumed Y/T ratio of 0.9

^{\$\$} Based on the UTS and an assumed Y/T ratio of 0.9

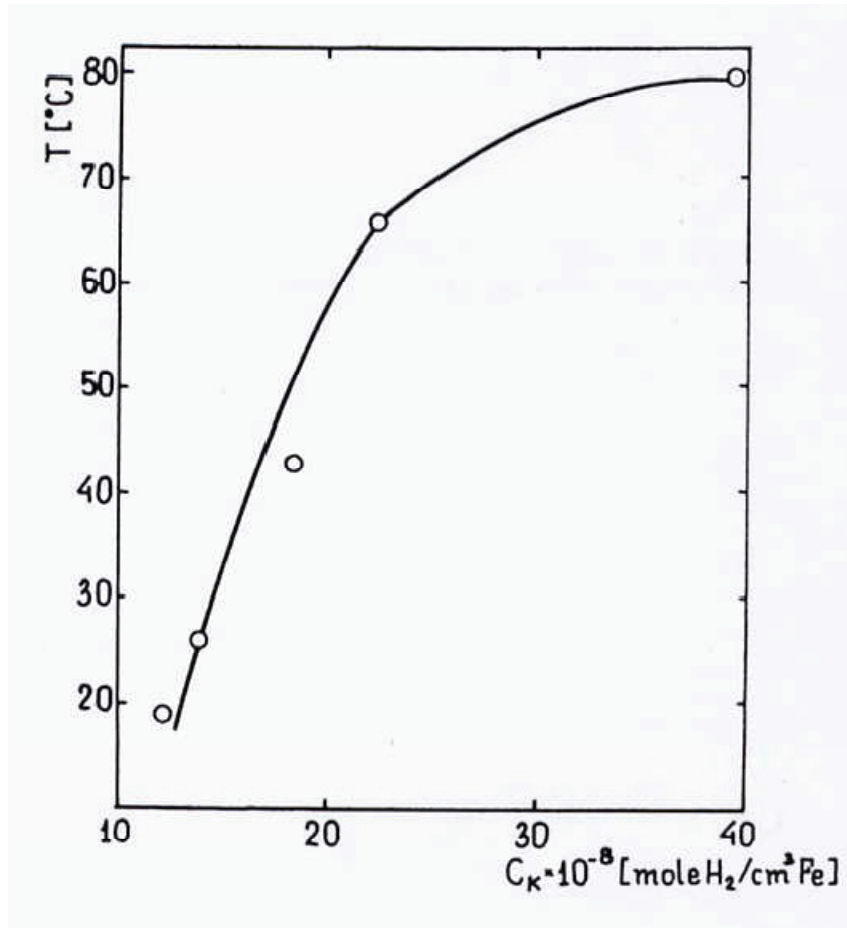


Figure 22: Temperature Dependence of the Critical Hydrogen Concentration (C_K) for Blister Formation on Armco Iron (Beck et al. 1966). A H concentration of $10^{-8} \text{ mol H}_2 \cdot \text{cm}^{-3} \text{ Fe}$ corresponds to $0.0025 \mu\text{g} \cdot \text{g}^{-1}$.

Because SSC requires an applied or residual stress (Table 3), the critical H concentration is a function of stress (Table 4(c)). Chu et al. (1999a) report the dependence of the critical stress (σ_{crit}) as a function of the diffusible H concentration for various API C90 alloys, e.g.,

$$\sigma_{\text{crit}}/\sigma_{\text{NYS}} = 1.13 - 0.11 \cdot \ln c_0 \quad (22)$$

for an alloy designated SM95 (0.26 wt.% C, 0.010 wt.% S, 0.91 wt.% Cr, 0.44 wt.% Mo), where σ_{NYS} is the nominal yield stress and c_0 is in units of $\mu\text{g} \cdot \text{g}^{-1}$. The c_{crit} values reported in Table 4(c) are calculated on the basis of $\sigma_{\text{crit}}/\sigma_{\text{NYS}} = 1$. Asahi et al. (1994) report the dependence of c_{crit} (in $\mu\text{g} \cdot \text{g}^{-1}$) on the actual yield stress (σ_{YS} in MPa) for a quench and tempered C-Mn steel and Cr-, Mo-microalloyed C-Mn steel with differing tempering temperatures, which produced variation in the yield stress. The stress-dependence reported for the C-Mn steel at 25°C was

$$\log c_{\text{crit}} = 4.01 - 0.00405 \sigma_{\text{YS}} \quad (23)$$

Similar expressions were provided for temperatures of 50°C and 80°C and at all three temperatures for the Cr-, Mo-microalloyed C-Mn steel.

4.3.2 Threshold Stress Intensity Factor

The threshold stress intensity factor for H-enhanced crack growth (K_{IH}) has been reported by a number of authors. K_{IH} is a function of:

- yield strength (Figure 23),
- severity of electrochemical (Figure 23) or gaseous H_2 (Figures 23 and 24) charging, and
- temperature (Figure 25).

The most susceptible materials, therefore, are high-strength alloys exposed to either extreme cathodic charging conditions or high-pressure H_2 environments at ambient temperature.

Table 5 summarizes additional values of K_{IH} for various materials in a number of environments. Additional values can be found in the compilations of Gangloff and Turnbull (1986) and Gangloff (1986).

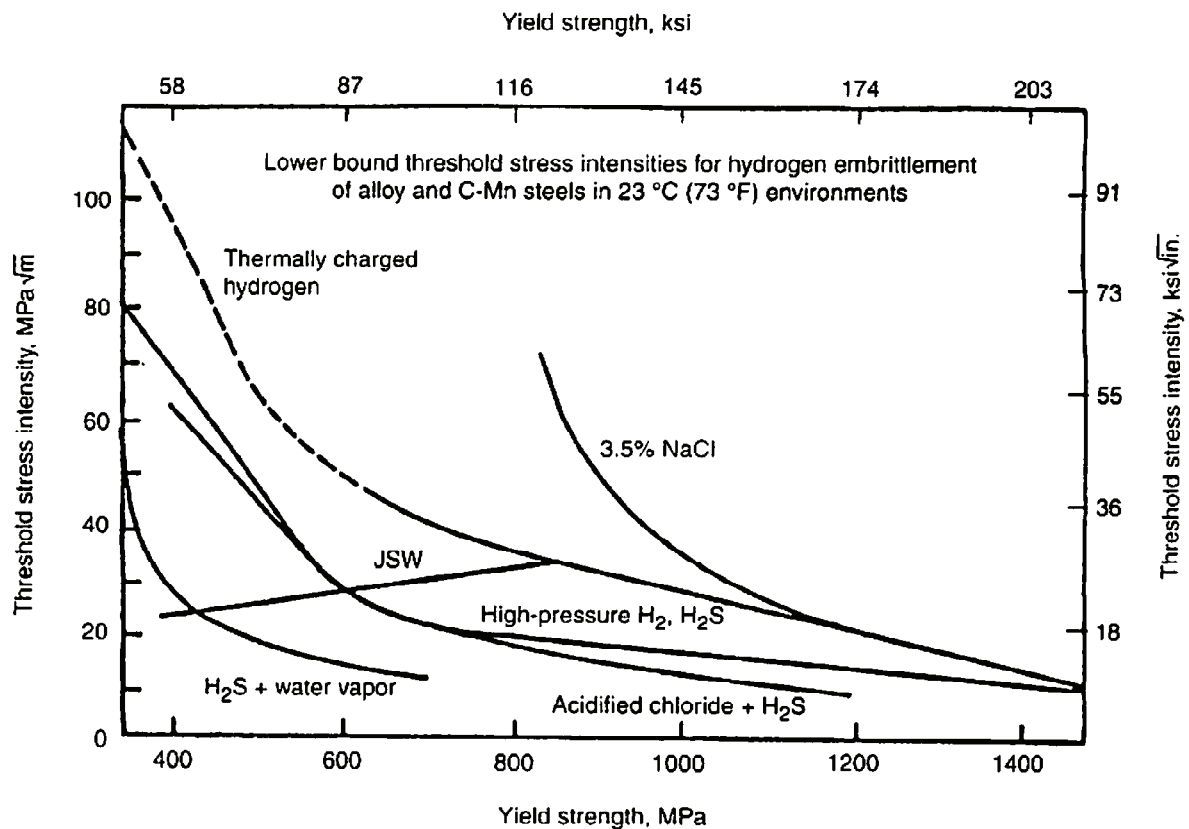


Figure 23: Dependence of the Threshold Stress Intensity Factor for Hydrogen Embrittlement of Alloy and C-Mn Steels at 23°C (Gangloff 2009).

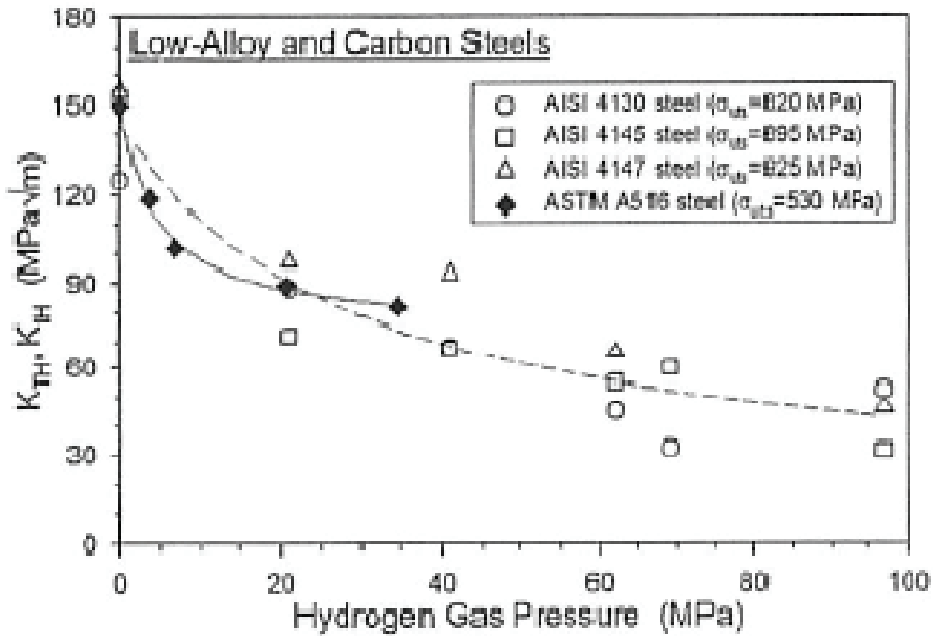


Figure 24: Dependence of the Threshold Stress Intensity Factor for Crack Growth (K_{IH}) for ASTM A516 Carbon Steel and for Crack Arrest (K_{TH}) for Three Low-alloy Steels on Hydrogen Pressure (Gangloff 2009).

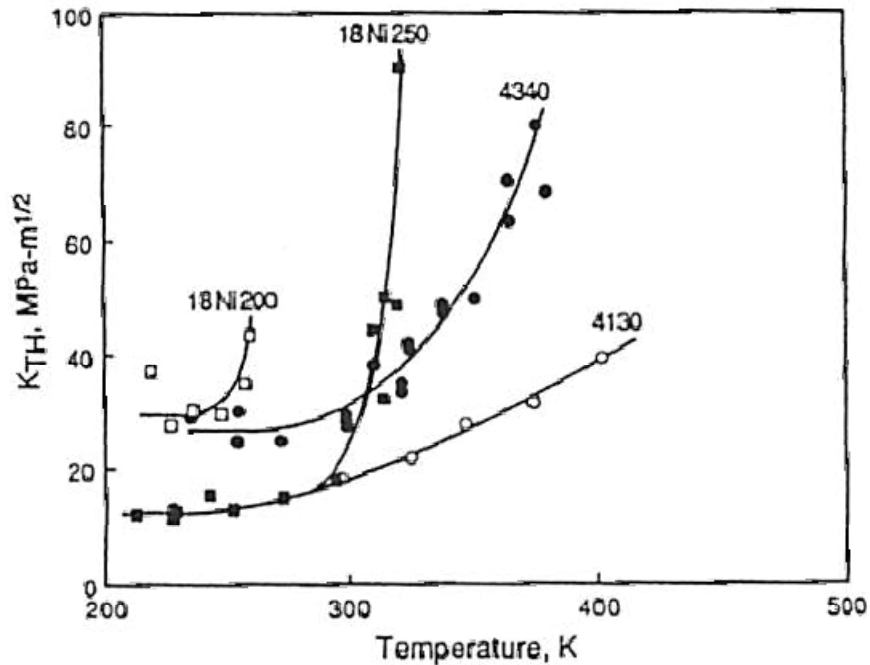


Figure 25: Temperature Dependence of the Threshold Stress Intensity Factor for Crack Arrest for Various High-strength Steels in Gaseous Hydrogen (Gangloff 2009).

Table 5: Critical Threshold Stress Intensity Factors for Hydrogen-assisted Cracking.

Material	Composition (wt.%)	Environment	Temperature (°C)	Yield strength (MPa)	K_{IH} (MPa·m ^{1/2})*	Reference
ASTM A516	Grade not given	69 MPa H2	13	290	82	Somerday (2007)
ASTM A106 Grade C	0.35C, 0.035S	97 MPa H2	13	345	55	Somerday (2007)
API C90	0.26C, 0.002S, 1.06Cr, 0.26Mo	Cathodic charging in H ₂ SO ₄ + As ₂ O ₃	RT?	658	46 – 12.5 ln c ₀	Yu et al. (1997)
"690"	0.15C, 0.001S, 0.49Cr, 0.45Mo	Biologically active sea water	RT?	690	43.1·e ^{-1.40c₀}	Robinson and Kilgallon (1994)
BS4360 Grade 50D, hardened	0.20C, 0.035S	Artificial sea water	RT?	355**	91.2e ^{-0.49c₀}	Lucas and Robinson (1986)

* c₀ in units of µg·g⁻¹

** specified minimum yield stress for Grade 50D, actual yield stress in hardened condition unknown

5. IMPLICATIONS FOR CARBON STEEL USED FUEL CONTAINERS

5.1 POSSIBLE DEGRADATION MODES FOR CARBON STEEL UFC

Based on the information presented above, the probability of failure of C-steel UFC by H-related mechanisms within the container design life appears to be low. This overall assessment is based primarily on the following factors:

- the absorbed hydrogen concentration will be low because the repository environment is relatively benign (maximum H₂ gas pressure of 8 MPa and the absence of rapid cathodic charging),
- the container will be fabricated from low-strength C-steel, which is less susceptible to H damage than higher-strength alloys,
- the applied (maximum 30-40 MPa) and residual ($<\sigma_{YS}$) stress are relatively low, and
- the container material and weld design can be optimized to minimize H effects.

5.1.1 UFC Susceptibility to Hydrogen-related Damage

The susceptibility of steels to H-related degradation increases with (i) increasing absorbed H concentration, (ii) increasing stress, and (iii) increasing strength of material.

Absorbed H concentration

Based on the evidence presented in Sections 2 and 3, the concentration of absorbed H is expected to be low because:

- the bentonite pore water pH will be neutral to moderately alkaline (pH 7-8.5) (Section 3.1.1),
- there is a general absence of H-absorption promoters (hydrides of Group VA and VIA elements) (Section 2.2.1.2),
- the interfacial concentration of H₂S, the only H-absorption promoting species likely to be present in the DGR, will be low ($<<1 \mu\text{g}\cdot\text{g}^{-1}$) because of the absence of microbial activity in the compacted bentonite surrounding the container and because of the likely precipitation as FeS of any sulphide produced elsewhere in the near-field,
- the absence of extensive localized corrosion during the aerobic period that could lead to local acidification in occluded regions and more-aggressive charging conditions (Section 2.2.1.4),
- the formation of surface oxides and mineralized films that will block H absorption (Section 2.2.1.3), and
- a maximum H₂ pressure of 8 MPa on the external and internal surfaces of the container (Section 3.1.2).

Of the two pathways for the absorption of H, i.e., via the cathodic reduction of H⁺/H₂ or via the dissociative adsorption of molecular H₂, that via H₂(g) may lead to the highest lattice H concentration (c_0) (see Section 5.2.1). Furthermore, as discussed by Turnbull (2009), both the external and internal surfaces of the container will be exposed to H₂(g), the inside of the container being exposed because of the diffusion of H through the container wall and recombination and evolution as H₂(g) into the interior void space.

Applied and Residual Stress

The magnitude of the applied and residual stresses will be limited because:

- the maximum applied stress resulting from the bentonite swelling pressure and hydrostatic (including possible glaciation loads) pressure is 40 MPa and is likely to be largely compressive in nature,
- the maximum level of residual stress will be of the order of 500-600 MPa (on the assumption that a low-strength grade is selected for the container material),
- non-thermal post-weld stress relief can be used to reduce the surface tensile residual stress on the final closure weld, and
- suitable container and closure weld design can be used to minimize the impact of stress raisers and other surface discontinuities.

One area of concern identified by Turnbull (2009) is the surface of the closure weld on the inner surface of the container. It is not possible to machine or modify the surface of this weld and heat treatment to relieve the residual stress and/or modify the weld microstructure is not feasible because of the thermal limits for the used nuclear fuel.

Material strength/hardness

The benefits of selecting a low-strength grade of C-steel for the container material include:

- minimizing the increase in H solubility due to high hydrostatic stress at the crack tip (Section 3.3.2),
- the absence of repartitioning of H from trap sites in the fracture process zone (Section 3.3.2), and
- maximum stress intensity factor for credible defect sizes below the threshold for H-related cracking (see below).

5.1.2 UFC Susceptibility to Specific Forms of H-related Damage

Various forms of H-related damage are discussed in Section 4.1. Here, the possibility of each of these forms of attack for the UFC is briefly described.

5.1.2.1 Hydrogen Embrittlement

A number of forms of delayed failure are described in Section 4.1.1.1, including hydrogen-induced cracking (HIC), hydrogen stress cracking (HSC)/sulphide stress cracking (SSC), and stress-oriented hydrogen induced cracking (SOHIC). Of these forms of cracking, HSC/SSC are unlikely to impact the container as they are generally associated with severe H charging environments and high-strength materials (Section 4.1.1.1.2). However, based purely on the strength of the material, HIC (and, in the presence of a sufficient applied stress, SOHIC) cannot be excluded since it primarily affects lower-strength steels (Section 4.1.1.1.1). The probability of HIC can be significantly reduced by reducing the number and shape of MnS inclusions.

Of the other forms of HE described in Section 4.1.1, the container material will be subject to reduced plasticity (decrease in the %RA), although the impacts of this can be managed to some

degree through appropriate container design (e.g., minimizing stress levels for the expected loads during service).

Exposure to gaseous H₂, both externally and internally, could lead to embrittlement of the container as described in Section 4.1.1.3. Based on Figure 18, the expected maximum H₂ pressure of 8 MPa is sufficient to reduce the fracture toughness by ~50% and the threshold stress intensity factor K_{IH} by ~20-30% (Figure 24).

5.1.2.2 Blister Formation

As with HIC, blister formation occurs primarily in lower-strength materials (Section 4.1.2) and, consequently, cannot be excluded as a possible damage mechanism for UFC. Blisters, by definition, occur primarily at or near the surface and, as such, do not pose a direct threat to the containment of the waste. In addition, the probability of blistering can be limited by the use of clean steels.

5.1.2.3 Hydrogen Attack

Based on the evidence presented in Figure 19, hydrogen attack is considered unlikely given a maximum UFC temperature of ~100°C.

5.1.2.4 Miscellaneous Forms of Hydrogen Damage

There is no evidence that enhanced anodic dissolution or reduction in the protectiveness of the corrosion product layer will occur at the rates of H absorption expected in the repository environment.

5.1.3 Possible Forms of Hydrogen-related Damage for C-steel UFC

In summary, the most likely forms of H-related damage for C-steel UFC in a DGR are:

- hydrogen-induced cracking (HIC) and, in the presence of sufficient applied stress, stress-oriented hydrogen induced cracking (SOHIC),
- blister formation, and
- cracking due to H absorbed from gaseous H₂.

However, it should be emphasized that, even for these forms of degradation, the probability of damage is considered low because of the relatively benign repository environment. The probability of damage can be reduced even further through appropriate selection of the material of construction and through appropriate design of the container and closure weld (Section 5.4).

5.2 PREDICTIONS OF UFC SUSCEPTIBILITY TO HYDROGEN DEGRADATION

As with other forms of localized attack, the prediction of the impact of H-related mechanisms on the lifetime of the UFC can be approached on the basis of either the susceptibility of the material or on the rate of degradation. The selection of which approach to take depends on the

nature of the corrosion mechanism and on the availability of robust modelling procedures and data on which to base a prediction. In the case of H-related damage, although models have been developed to predict the rate of crack growth (e.g., Boellinghaus and Hoffmeister 2000) these models have not been developed to that stage that reliable predictions are possible. For the forms of H-related damage of interest here, it is possible to define empirically-based threshold conditions (either a threshold concentration c_{crit} or threshold stress intensity factor K_{IH}). Therefore, it is recommended that prediction of the long-term behaviour of C-steel UFC be based on the susceptibility approach.

5.2.1 Prediction Based on the Threshold Concentration

Based on the concept of a threshold (or critical) concentration (c_{crit}), the condition for susceptibility is given by

$$c_0 \geq c_{\text{crit}} \quad (24)$$

Based on the discussion in Sections 3.1.1 and 3.1.2, the expected values of c_0 in the DGR environment are $0.01 \mu\text{g}\cdot\text{g}^{-1}$ as a result of cathodic charging and $0.0044 \mu\text{g}\cdot\text{g}^{-1}$ to $0.058 \mu\text{g}\cdot\text{g}^{-1}$ at 15°C and 100°C , respectively, as a result of exposure to 8 MPa H_2 . Here, a conservative estimate of $0.06 \mu\text{g}\cdot\text{g}^{-1}$ is assumed.

This value of c_0 is in good agreement with the estimates given by JNC (2000) of $0.1 \mu\text{g}\cdot\text{g}^{-1}$ due to cathodic charging in the presence of HS^- and $0.03 \mu\text{g}\cdot\text{g}^{-1}$ due to exposure to 10 MPa H_2 at 100°C . Turnbull (2009) also estimates a c_0 value of $0.03 \mu\text{g}\cdot\text{g}^{-1}$ due to exposure to 10 MPa H_2 at 90°C .

Figure 26 shows a compilation of values for the threshold concentration for various forms of H damage as a function of the yield strength based on the data in Figure 21 (and a similar figure used by JNC (2000)) and in Table 4. Also shown on the figure is the maximum c_0 value for the UFC of $0.06 \mu\text{g}\cdot\text{g}^{-1}$.

With two exceptions, the data show a consistent trend of decreasing susceptibility with decreasing yield strength. The two exceptions are the blister data from Maccagno et al. (1998) and the HIC data from Revie et al. (1993b). Both of these sets of data were measured using older ferrite-pearlite pipeline steels with banded microstructure and, in some cases, high MnS inclusion density. It has been suggested (J. Payer, private communication, 2008) that the JNC (2000) data may also refer to older ferrite-pearlite steels and that modern TMCP-produced steels with closer control of chemistry would be less susceptible. This, however, does not seem to be the case since the JNC (2000) curve shows a similar trend to the more-modern steels studied by Chu et al. (1999a) and Yu et al. (1997). It has also been suggested (A. Turnbull, private communication, 2009) that the JNC (2000) data are based on the total H concentration rather than on the lattice H concentration and cannot, therefore, be used with the threshold criterion for H damage defined by Equation (24). However, the JNC (2000) curve lies between the two curves given by Okada (1977) for a mild and a severe notch, and on which the JNC (2000) may have been based. The Okada (1977) data are based on the diffusible H concentration (assumed to be equivalent to the lattice H concentration).

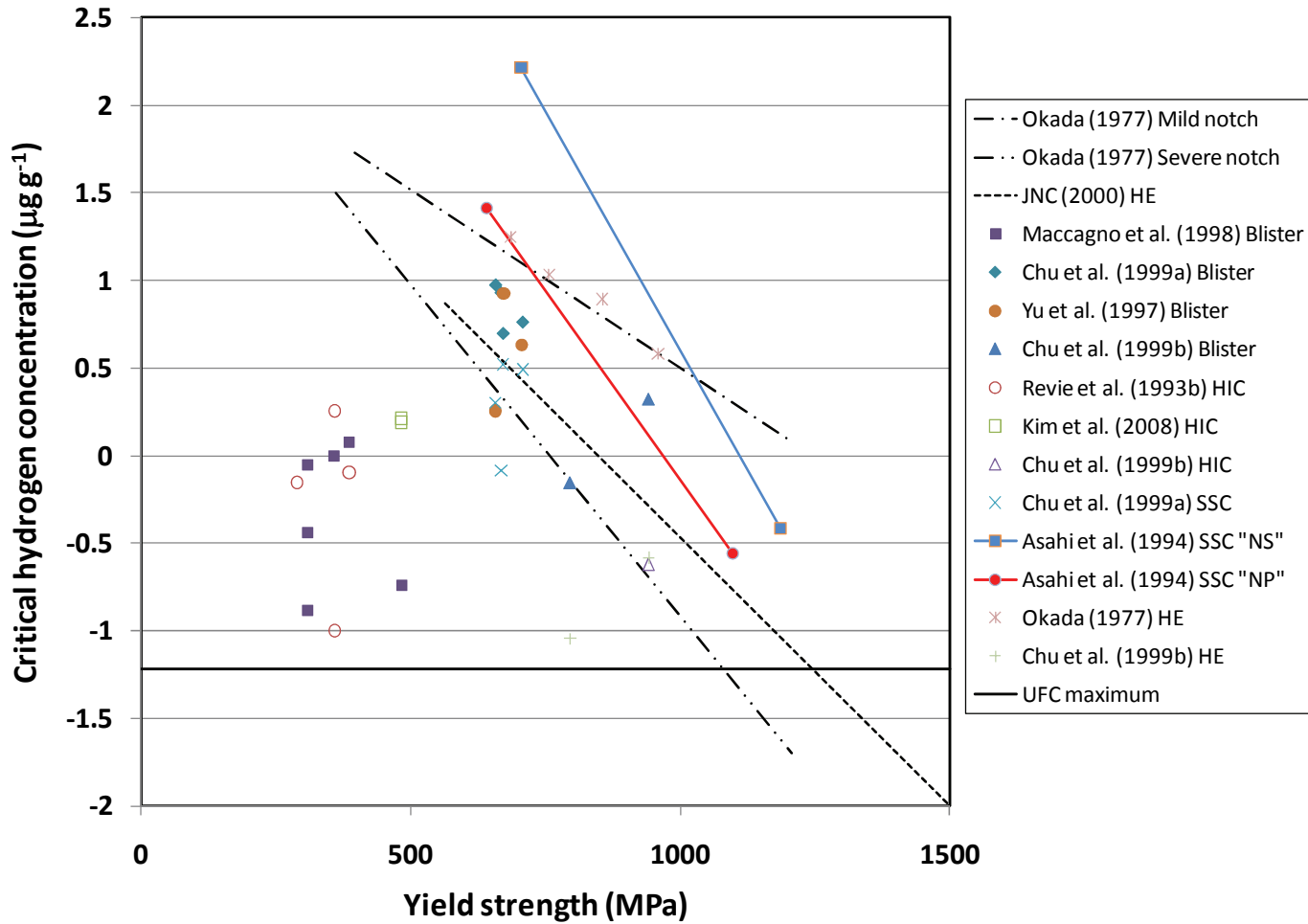


Figure 26: Compilation of Critical Lattice Hydrogen Concentrations for Various Forms of Hydrogen Damage as a Function of Yield Strength. All data for 25°C or room temperature, except for data of Okada (1977) at 45°C. Based on data in Table 4 and correlations given by Okada (1977) and JNC (2000).

The final piece of information required to make an assessment of the susceptibility to H damage based on Equation (24) is the yield strength of the container material. Although the grade and microstructural condition of the C-steel to be used for the UFC has not been defined, some guidance can be obtained from the Japanese and Swiss programs. JNC (2000) define a maximum hardness of 200 HV for the container material (including the weld), equivalent to a tensile strength of 635 MPa. JNC (2000) conservatively assumed a similar value for the yield strength. In the Nagra program, Johnson and King (2003), quoting an earlier design study, suggest a material with a yield strength of only 256 MPa. Turnbull (2009) has suggested a conservative value of 700 MPa for the yield stress of hardened material in the HAZ of the weld.

If we assume, for the current purposes, a maximum yield strength of 500-700 MPa, the data in Figure 26 (excluding those of Maccagno et al. (1998) and Revie et al. (1993b)) indicate a critical H concentration for H damage of $0.6-6 \mu\text{g}\cdot\text{g}^{-1}$, approximately 1-2 orders of magnitude higher than the maximum value of c_0 . On this basis, the UFC will be immune to H-related damage.

However, this analysis ignores the lower c_{crit} values of Maccagno et al. (1998) and Revie et al. (1993b). In order to provide assurance that the container material is less susceptible than the steels used in these two studies, it would be advisable to determine c_{crit} values for the actual material to be used for the UFC once it has been specified.

5.2.2 Prediction Based on the Threshold Stress Intensity Factor

The criterion for H-related crack initiation is

$$K_I \geq K_{IH} \quad (25)$$

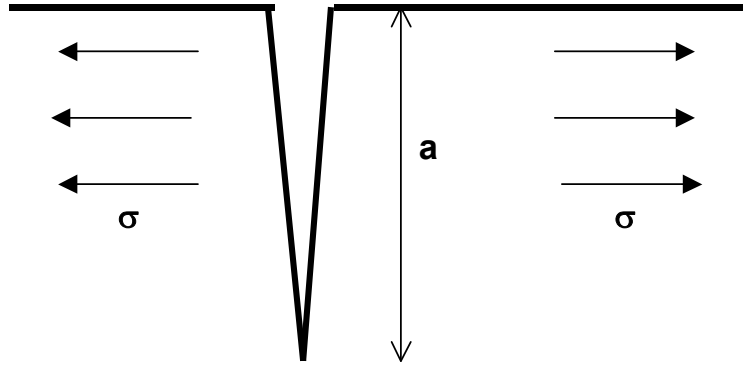
where K_I and K_{IH} are the stress intensity factor and the threshold for crack initiation.

A suitable value for K_{IH} can be obtained from the data in Table 5 and Figures 23 and 24. For exposure to 8 MPa $\text{H}_2(\text{g})$, Figure 24 suggests a value for K_{IH} for C-steel (ASTM A516) of approximately $100 \text{ MPa}\cdot\text{m}^{1/2}$. At higher p_{H_2} , the data in Table 5 suggest a value of 55-82 $\text{MPa}\cdot\text{m}^{1/2}$, again for C-steels. Based on cathodic charging of atomic H, the most relevant environment of those shown in Figure 23 is the 3.5 wt.% NaCl solution. For a strength level of 500-700 MPa, these data suggest a threshold stress intensity factor for crack growth of $>80 \text{ MPa}\cdot\text{m}^{1/2}$. Finally, based on the proposed maximum c_0 value of $0.06 \mu\text{g}\cdot\text{g}^{-1}$ (see above), the expressions for K_{IH} as a function of c_0 in Table 5 give threshold values of $81 \text{ MPa}\cdot\text{m}^{1/2}$, $40 \text{ MPa}\cdot\text{m}^{1/2}$, and $89 \text{ MPa}\cdot\text{m}^{1/2}$ from the studies of Yu et al. (1997), Robinson and Kilgallon (1994), and Lucas and Robinson (1986), respectively. Although there is some scatter in these data, a threshold stress intensity factor of $80 \text{ MPa}\cdot\text{m}^{1/2}$ will be assumed here as a best estimate.

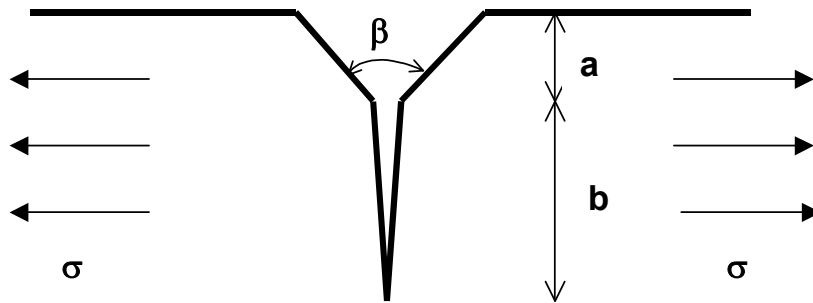
The value of K_I on the container depends on the nature and depth of the defect and the tensile stress. In assessing the effect of discontinuities on the stress corrosion cracking of copper containers, King (2004) considered both an edge crack (Figure 27(a)) and a combined notch and crack (Figure 27(b)). The stress intensity factor for the edge crack is given by (Murakami 1987):

$$K_I = 1.1215\sigma(\pi a)^{1/2} \quad (26)$$

where a is the crack depth and σ is the tensile stress.



(a) Edge crack of depth a in a semi-infinite plane subject to uniaxial tensile stress σ .



(b) Crack (of depth b) emanating from the base of a triangular notch (depth a , notch angle β) and subject to a uniaxial tensile stress σ .

Figure 27: Schematics of Crack-like Defects Used for the Analysis of the Maximum Stress Intensity Factor on Carbon Steel Used Fuel Containers (after King 2004).

Figure 28 shows the predicted value of K_I based on Equation (26) as a function of the crack depth a for three tensile stress values of 500 MPa, 600 MPa, and 700 MPa. These stresses are considered to cover the range of maximum yield strengths (and, therefore, the maximum tensile stress before yielding occurs) for both the body of the container and any hard spot in the closure weld. Also shown in the figure is the assumed value of K_{IH} . Based on this analysis, therefore, initiation of H-related cracking would only occur if the weld or container body contained a defect between 3.5 mm and 6.5 mm deep. Such a deep defect would almost certainly be detected by non-destructive examination of the container during fabrication and after the final closure weld.

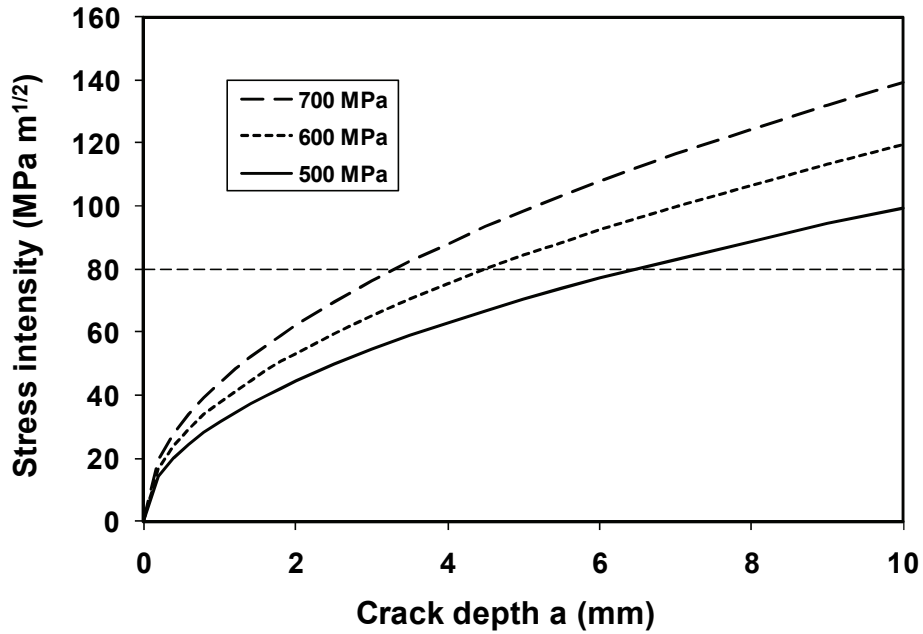


Figure 28: Predicted Dependence of the Stress Intensity Factor on the Depth of an Edge Crack Subject to Various Tensile Loads. Also shown on the figure is the assumed threshold stress intensity factor for the initiation of hydrogen cracking.

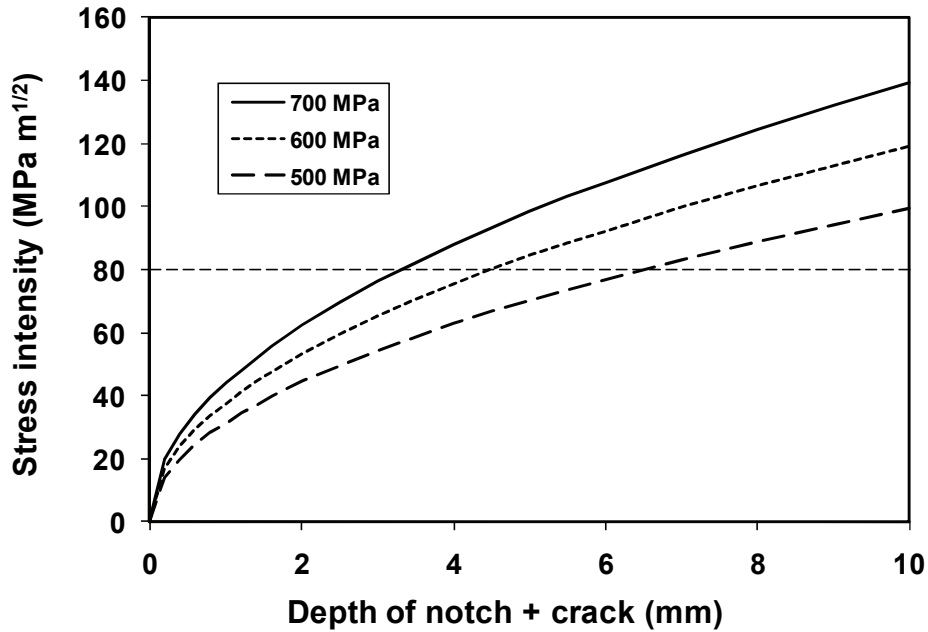


Figure 29: Predicted Dependence of the Stress Intensity Factor on the Combined Depth of a Crack in a Notch Subject to Various Tensile Loads. Also shown on the figure is the assumed threshold stress intensity factor for the initiation of hydrogen cracking.

Figure 29 shows a similar analysis for a crack in a notch. These K_I values were calculated for the worst case of a high crack: notch depth ratio (b/a) and for acute notch angles ($<90^\circ$). Nevertheless a similar range of defects depths is necessary to exceed the K_{IH} as for the edge crack.

5.2.3 Predicted Behaviour for UFC

Based on these analyses, therefore, it is considered unlikely that a C-steel UFC in the DGR will fail from a H-related mechanism because:

1. the lattice H concentration will not exceed the critical concentration for blister formation or HE for a low-strength C-steel, and
2. a defect (crack or notch) deep enough to cause crack growth is unlikely to pass the inspection procedure undetected.

5.3 PERIOD OF SUSCEPTIBILITY TO HYDROGEN EFFECTS

From a corrosion perspective, the repository environment will evolve from an initial aggressive phase to a period of long-term, relatively benign conditions. Thus, for processes such as stress corrosion cracking or localized corrosion, the period of greatest concern is the initial warm, aerobic phase during the evolution of the repository environment. In order to predict the period of greatest concern for H-related damage it is necessary to establish the likely time dependence of the factors that contribute to failure, namely: the lattice H concentration (c_0), the critical conditions for damage (c_{crit} and K_{IH}), and the applied or residual stress.

5.3.1 Time Dependence of Factors Related to Hydrogen Damage

5.3.1.1 Lattice H Concentration

The time dependence of c_0 will depend on the time-dependent (anaerobic) corrosion rate and the time-dependent H_2 gas pressure (both outside and inside the container).

Little, or no, H absorption is expected during the initial aerobic phase. Although the absorption of H during localized corrosion (supported by O_2 reduction) is important for some materials (e.g., during the crevice corrosion of susceptible Ti alloys), the extent of localized corrosion of C-steel in the repository environment is expected to be minimal. Any localized attack that does occur takes the form of surface roughening, rather than distinct pitting or crevice corrosion (Johnson and King 2003, 2008). Therefore, it is considered unlikely that locally acidic sites will persist, even if they form in the first place. In the absence of stable, acidified pits or crevices, it is unlikely that accelerated H absorption will occur.

Hydrogen absorption will commence, therefore, with the onset of anaerobic corrosion. The rate of H absorption will be determined by the corrosion rate and the H absorption ratio, which in turn will be affected by the presence of H absorption promoters (primarily H_2S in the repository environment) and inhibitors (e.g., surface films). The anaerobic corrosion rate will attain a steady-state value within a few months or years (King 2008). Film formation will occur immediately because of the restrictive mass-transport conditions within the repository. Although sulphide may be produced by sulphate-reducing bacteria in regions outside the compacted bentonite buffer immediately surrounding the container, the concentration of H_2S at the

container surface is unlikely to be significant as HS^- will precipitate with Fe(II) as it diffuses through the bentonite. Therefore, the lattice H resulting from the cathodic reduction of $\text{H}^+/\text{H}_2\text{O}$ will likely reach a steady state within a few years of the establishment of anaerobic conditions, a period possibly up to 100 a following repository closure.

The time dependence of the H_2 gas pressure on the outside of the container will depend on the time dependence of the degree of saturation of the bentonite. If we assume that the bentonite is fully saturated at all times and if we assume a 70-cm-thick layer of compacted bentonite with a total porosity of 40%, then the length of time required to generate sufficient H_2 to saturate the pore water at a corrosion rate of $1 \mu\text{m}\cdot\text{a}^{-1}$ is 25 a (assuming the pore solution is in equilibrium with $\text{H}_2(\text{g})$ at a pressure of 8 MPa). After this period, a separate H_2 gas phase with a pressure of 8 MPa would form at the container surface. At the other extreme, let us assume that the initial moisture in the bentonite is transported to the periphery of the buffer and that the inner 50 cm of bentonite is virtually dry indefinitely. Under these circumstances, it would take an estimated 5000 a to develop a H_2 pressure of 8 MPa within the unsaturated bentonite pores (assuming that the corrosion rate is not limited by the availability of H_2O). Therefore, it will take between 25 a and 5000 a for the maximum H_2 pressure to develop on the outside of the container.

Hydrogen will diffuse through the container wall and enter the interior void space surrounding the used fuel. This process will continue until the pressure inside the container is the same as that outside (assuming isothermal conditions). Turnbull (2009) has estimated that such a process will take between 100 a and 3500 a for a Nagra-design container, assuming a constant supply of H at the outer container surface.

In summary, the lattice H concentration near the outer surface of the container will reach the maximum value soon after the onset of anaerobic conditions, supported initially by the cathodic reduction of $\text{H}^+/\text{H}_2\text{O}$ and later by the development of a H_2 gas phase. Eventually the entire wall thickness of the container will attain a similar H concentration, with the inner surface finally saturating after a few thousand years.

5.3.1.2 Critical Conditions for Damage

Both c_{crit} and K_{IH} increase with increasing temperature (Figures 22 and 25, Table 4). Thus, the most susceptible period will be once the repository temperature has returned to ambient, a period of several tens of thousands of years post-closure. However, the container surface temperature will have fallen below 40-50°C after a few thousand years, approximately the same period for the complete saturation of the container wall with absorbed hydrogen (although significant H uptake will have occurred much earlier).

5.3.1.3 Applied and Residual Stress

There are several factors that contribute to the time dependence of the stress in the container wall.

First, the development of the external load depends on the time-dependence of the saturation of the repository and of the compacted bentonite and, ultimately, on the glaciation cycle. Saturation of the repository will depend on the permeability of the host rock, but may take from

several tens of years to several thousand years. Glaciation, and the development of high hydrostatic loads, occurs over periods of tens of thousands of years.

Some degree of residual stress will be present at all times, possibly relieved to some degree by non-thermal surface stress relief of the closure weld prior to container emplacement. As the container wall is reduced by corrosion, however, there will be re-distribution of the residual stress.

Finally, as the container wall is corroded the stress on the remaining wall will increase with time.

The net effect of all of these factors is that the stress on the container wall will generally increase over time.

5.3.2 Period of Susceptibility to Hydrogen Damage

In summary, the time-dependences of the processes contributing to the possibility of H damage are:

- the lattice H concentration will increase with time over a maximum period of several thousand years,
- the critical H concentration and threshold stress intensity factor for cracking will decrease with time as the temperature falls over a period of thousands to tens of thousands of years, and
- the applied stress will slowly increase with time due to saturation of the repository, thinning of the container wall by corrosion, and, eventually, glaciation events.

Taken together, these factors will result in an increase in susceptibility to H damage with time. Unlike other localized corrosion processes, therefore, H-related damage is characteristic of the long-term anaerobic period in the evolution of the repository environment. The period of greatest susceptibility is estimated to extend from 1000 a post-closure through to the end of the container design life.

5.4 MITIGATION OF HYDROGEN EFFECTS

Although the probability of H damage is deemed to be small, it is prudent to optimize the container design to reduce that probability even further. It is not deemed feasible, or necessary, to modify either the container environment or the level of applied stress, even if the latter were possible. Instead, the best strategy to avoid H-related failure is to specify a H-resistant steel and to optimize the container design and fabrication and sealing procedures.

5.4.1 Material Selection

There has been a lot of work on the development of steels resistant to various forms of cracking in sour (i.e., H₂S) service in the oil and gas industry. Although the conditions encountered downhole are generally more severe than those expected in the DGR, it is informative to consider the approaches to the development of resistant steels for these aggressive environments.

Resistance to H-related effects can be achieved by either reducing c_0 or increasing c_{crit} and/or K_{IH} (King 2007). Various alloying elements in low concentrations are found to lower c_0 in sour (i.e., H_2S -rich) environments, including:

- maximum 0.35 wt.% Cu (to stabilize protective iron sulphide films),
- 0.6-1.0 wt.% Co (also possibly through an effect on the iron sulphide film),
- Ni (to lower the corrosion rate and, possibly, inhibit H atom absorption), and
- 0.6 wt.% Cr (to reduce H absorption).

The alternative strategy is to increase the value of c_{crit} (Hay 2003) by:

- eliminating MnS inclusions of a certain (Type II) shape, Al_2O_3 particles, anomalous (heavily banded) microstructures, and other non-metallic inclusions (e.g., silicates, slag, Fe oxides, large Nb carbonitride particles),
- reducing the segregation of trace/impurity elements in the steel, and
- increasing the homogeneity of the microstructure.

Type II MnS inclusions are dendritic or rod-like in shape and serve to both trap H (as H_2) and locally raise the stress, thus increasing the H solubility. Elimination of Type II MnS inclusions can be achieved by:

- reducing the S content as much as possible (<0.003 wt.% and sometimes <0.001 wt.%)
- specifying a maximum Mn content of 1.00 wt.%, and preferably 0.80 wt.% max., and
- controlling the shape of the remaining MnS inclusions.

Shape control is achieved by adding elements that have a higher affinity for S than Mn, such as Ca (Hay 2003). In addition, CaS is spherical in shape (Type I) and non-deformable during processing. The optimum Ca:S ratio depends on the S content and whether the material is to be used as plate or as welded or seamless linepipe. For a S content of 0.003 wt.%, the Ca:S ratio should be in the range 1-3.5, with the upper end of the range decreasing with increasing S content.

Alumina particle stringers, or the voids associated with them, are also effective trap sites for H atoms (Hay 2003). The total Al content in the steel (including dissolved Al, aluminates, aluminum nitrides, and alumina particles) should not exceed 0.030 wt.%. The formation of alumina can be avoided by

- adding the minimum Al necessary when killing the steel,
- preventing oxidation of Al during casting, and
- preventing the incorporation of alumina particles as the steel solidifies.

Excessive banding in the microstructure (due to the formation of alternating ferrite and ferrite/pearlite bands) can be avoided by controlling the concentrations of C, Mn, and P. Microstructure control can be achieved if the C content is <0.10 wt.%, the P content is <0.015 wt.% (preferably <0.010 wt.%), and the maximum Mn content is 1.00 wt.%.

Reducing the C and Mn content to avoid excessive banding has the adverse effect of reducing the strength of the steel. Micro-alloying elements (such as Ti, Nb, and V) are therefore commonly added to increase the strength through the formation of Ti, Nb, or V carbides. These

elements are added to a maximum combined concentration of 0.12 wt.% to avoid the formation of small regions of high hardness in the HAZ of welds.

An alternative strategy for increasing the yield strength, obtaining resistance to H effects, and improving the toughness and weldability of linepipe steel is Thermo-Mechanical Controlled Processing (TMCP). The overall aim is to produce a steel with a uniform, clean, fine-grained, non-banded microstructure. In addition to chemical control, this process involves the careful control of temperature during the rolling process. Such steels tend to have a uniform ferrite-bainite microstructure, with no pearlite banding.

The recommended specification for HIC-resistant pressure vessel plate, similar to that from which a C-steel UFC might be manufactured, is (Hay 2003):

Processing:

- minimize use of scrap additions
- desulphurized, dephosphorized, and fully deoxidized (Al-Si killed)
- removal of oxide inclusions (35 ppm O max.)
- addition of Ca for sulphide shape control
- continuous casting
- normalized heat treatment

Chemical composition:

- C 0.18 wt.% max. (UTS ≤ 414 MPa), 0.21 wt.% max. (UTS > 414 MPa)
- Mn 1.30 wt.% max.
- Si 0.45 wt.% max.
- P 0.010 wt.% max.
- S 0.002 wt.% max.
- Cu 0.35 wt.% max.
- Ni 0.25 wt.% max.
- Cr 0.25 wt.% max.
- Mo 0.10 wt.% max.
- Total Al 0.040 wt.% max. (preferably <0.030 wt.% max.)
- Nb 0.015 wt.% max.
- V 0.015 wt.% max.
- Ti 0.020 wt.% max.
- B 0.0005 wt.% max.
- Ca 1.8-3.5 x %S
- Nb + V 0.020 wt.% max.

The carbon equivalent (CE), defined as

$$CE = C + \frac{Mn}{6} + \frac{(Cu+Ni)}{15} + \frac{(Cr+Mo+V)}{5} \quad (27)$$

should be limited to the range 0.40-0.47 (Hay 2003).

Microstructure:

The microstructure should be free of excessive ferrite/pearlite banding.

NACE Standard MR0175/ISO 15156-2 provides additional guidance on the selection of cracking-resistant carbon and low alloy steels for sour service. The severity of the environment is classified into four categories or regions based on the pH and H₂S content (Figure 30). It is interesting to note that the standard has no special material requirements for environments containing <0.3 kPa H₂S independent of pH (Region 0) and indicates that all but the most-susceptible materials should be immune to cracking. A partial pressure of 0.3 kPa H₂S is equivalent to a dissolved concentration of $\sim 3 \times 10^{-4} \text{ mol}\cdot\text{dm}^{-3}$ ($10 \mu\text{g}\cdot\text{g}^{-1}$). This concentration is at least an order of magnitude greater than that measured in the groundwater at the Forsmark site in Sweden and at Olkiluoto, Finland (King et al. 2009).

Based on experience in the oil and gas industries, pipeline steels with a specified minimum yield strength (SMYS) of up to 550 MPa exhibit good resistance to SSC in Region 1 (NACE 2003). Under the more-severe environmental conditions in Region 2, a maximum SMYS of 450 MPa is recommended for pipeline applications. For the severest environmental conditions (Region 3), the requirements include:

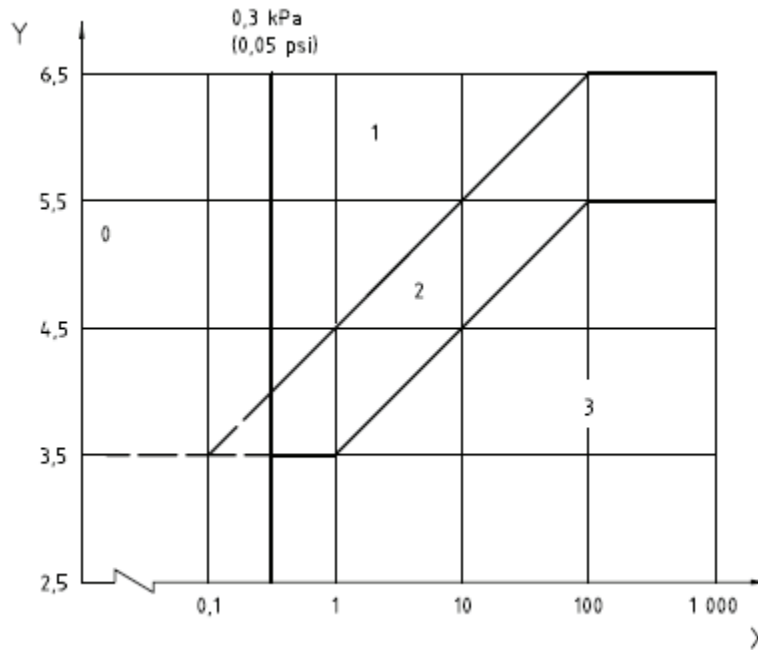


Figure 30: Regions of Susceptibility to Sulphide Stress Cracking (SSC) as a Function of H₂S Partial Pressure (X in kPa) and pH (Y) (NACE 2003).

- a maximum parent metal hardness of 22 HRC
- a maximum Ni content of 1 wt.%
- one of the following heat treatments:
 - hot rolled
 - annealed
 - normalized
 - normalized and tempered
 - normalized, austenized, quenched, and tempered,
 - austenized, quenched, and tempered

In addition there are requirements for the maximum hardness of the welds and on the need to thermally stress relieve excessive cold work. These requirements refer specifically to SSC and do not exclude the possibility that the steel could be susceptible to SOHIC or HIC/SWC.

5.4.2 Container Design and Manufacture

5.4.2.1 Closure Weld Design

The weld is typically more susceptible to H-related damage than the base material because of (i) high residual stresses, (ii) the presence of hard martensite phases, (iii) changes in H solubility accompanying solidification and microstructural phase changes, and (iv) stress concentration and/or intensification at discontinuities (e.g., cracks, voids, and weld beads).

Some or all of these factors can be eliminated by:

- appropriate weld design (e.g., use of integral backing to avoid poor quality surface finish on inside of closure weld, optimized joint design to impart compressive residual stress on inside of closure weld)
- post-weld surface preparation to remove or reduce stress raisers (e.g., machining of weld bead)
- use of low-H consumables to minimize hydrogen input
- control of time-temperature profile to minimize or avoid formation of susceptible microstructures (e.g., martensite)
- post-weld, non-thermal stress relief to impart compressive surface residual stress

Two major issues associated with the closure weld are the inability to thermally treat the weld and concern over the condition of the closure weld on the inside of the container and the potential for H-related cracking once a H₂ pressure has built up in the internal void space.

Post-weld heat treatment is used to both reduce the level of residual stress and to produce a non-susceptible microstructure. Although the former can be achieved, on the outer surface at least, by non-thermal stress relief techniques (such as laser peening or low-plasticity burnishing), it is not possible to alter the microstructure of the weld without thermal treatment.

Turnbull (2009) has raised the possibility of initiation of H-related cracking on the inner surface of the final closure weld. This region will be exposed to a maximum H₂ pressure of 8 MPa after a period of a few thousand years following closure of the repository. It is clearly impossible to machine or in any other way treat this weld once it has been made. However, it may be

possible through careful weld design to minimize the impact on the integrity of the container. For example, is it possible to design the weld with an integral backing strip so that the weld does not fully penetrate the lid? In addition, is it possible to design the weld joint or welding procedure so as to impart a compressive residual stress on the inner part of the weld?

5.4.2.2 Container Wall Thickness

The container wall thickness will be designed to withstand the external load and to provide a corrosion allowance. The corrosion allowance is typically based on the rate of uniform corrosion only. As the container wall thins, however, the stress in the container shell will increase. Since the threat from H-related failure continues throughout the design life, it is possible that the probability of failure will increase with time as both the stress and the solubility of H in the lattice increase. Therefore, an adequate wall thickness should be specified so that the increase in stress does not promote H-related failure within the container design life.

5.4.2.3 Miscellaneous Design Issues

Cold work is known to increase the number of dislocations (Figure 12) and to result in hardened microstructures. Therefore, all forms of cold work (or strain or age hardening) should be avoided, including the use of metal stamps for identification marks (which will also act as stress raisers) and excessive mechanical damage during container handling and emplacement. The acceptance criteria for container emplacement should include a maximum allowable amount of cold work as a result of mechanical damage during container fabrication, handling, and emplacement operations.

5.5 GAP ANALYSIS

Although the probability of H-related failure of a C-steel used fuel container in the expected DGR environment is considered to be small, there may be a need for selected further research to provide greater assurance, particularly since the threat continues throughout the container design life.

A pre-requisite for any further study is the closer specification of the container material. There is sufficient existing information on which to base a preliminary specification of the optimum material chemistry and microstructure for minimizing the effect of H (Section 5.4.1). The specification should also include the target yield and tensile strengths, as well as the maximum hardness of the container body and closure weld. The container material specification should take into account the effect on other corrosion and mechanical processes, such as the rate of uniform corrosion, the susceptibility to localized corrosion and stress corrosion cracking, and the creep properties.

Because of the enhanced susceptibility of the weld to H-related failure, a closure weld joint design and prototype welding procedure should also be defined at an early stage in any future program. One aim of the joint design program should be to minimize the level of tensile residual stress and stress-raising discontinuities on the inner surface of the container. Other aspects should include:

- control of the H input into the weld

- control of the hardness level
- definition of post-weld surface preparation and stress-relief procedures

One benefit of early development of a prototype weld design and procedure is that weld metal and HAZ material will be available for testing.

That testing program should include:

- determination of the lattice H concentration (c_0) under expected service conditions, including the effects of surface films, the possible presence of sulphide, and the effect of both cathodic charging and exposure to gaseous H_2 ,
- determination of the critical H concentration (c_{crit}) for various forms of degradation, but especially blister formation and HIC, and
- measurement of the threshold stress intensity factor for crack initiation (K_{IH}) in a range of service environments, but including exposure to both aqueous solutions and gaseous H_2 .

The need for the measurement of c_0 , c_{crit} , and K_{IH} for the actual container material (including weld metal and HAZ) in the expected DGR environment is deemed necessary because of the observation of blister formation and HIC for low-strength pipeline steels at critical H concentrations of $0.1-1 \mu\text{g}\cdot\text{g}^{-1}$ (Figure 26). Although these older steels may be more susceptible than the actual container material, these data points reduce the margin of safety based on a comparison of c_0 to c_{crit} . It would be prudent, therefore, to confirm the c_{crit} values for the actual container material.

Some studies are not considered necessary, for example:

- measurement of the diffusivity of H
- determination of the H absorption ratio
- measurement of the crack growth rate for various forms of H-assisted cracking

The diffusivity primarily determines the crack growth rate and the time for the development of the internal H_2 pressure. Since we are making long-term predictions based on susceptibility rather than the rate of crack growth and since the time to develop an internal H_2 pressure is short compared with the container design life, a more-accurate value for the diffusivity than is currently available is unnecessary. Similarly, the H absorption ratio is relatively unimportant, as illustrated by the following calculation. If we assume a steady-state corrosion rate of $1 \mu\text{m}\cdot\text{a}^{-1}$ and a total H concentration of $1 \mu\text{g}\cdot\text{g}^{-1}$, then the time required to saturate a 5-cm-thick container for a hydrogen absorption ratio of 0.01 (i.e., 1%) is only 140 a. This period is short in comparison with the container design life. For the time required to saturate the container wall with H to be significant in terms of the probability of H-related failure, the H absorption ratio would have to be (improbably) two or three orders of magnitude smaller.

6. SUMMARY AND CONCLUSIONS

Hydrogen affects the mechanical and corrosion properties of many materials including low-strength C-steels from which the used fuel containers will be manufactured. A review of the factors that will determine the susceptibility of UFC to H damage has been performed. Based on this review, the probability of H-related failure is deemed to be minimal, primarily because of:

1. the benign nature of the environment and the consequent low absorbed H concentration,
2. the moderate levels of applied and residual stress, and
3. the use of low-strength C-steel as the container material.

The various factors on which this conclusion is based and which have been reviewed here include:

- the mechanism and rate of H absorption due to the cathodic reduction of H^+ and/or H_2O , including the impact of species that either promote (e.g., H_2S) or inhibit (e.g., oxides and other surface films) H absorption,
- the mechanism of H absorption from the gas phase and the solubility of H in steel as a function of the H_2 pressure,
- an assessment of the maximum lattice H concentration for the expected repository environmental conditions,
- the diffusion of H in steel and the effects of trapping on the diffusivity,
- the nature of various attractive and physical trap sites in steel,
- the interaction of H with stress fields,
- the various modes of H damage, including hydrogen embrittlement (delayed failure, various forms of cracking (HIC, HSC, SSC, SWC, SOHIC), loss of ductility), blister formation, and hydrogen attack,
- the mechanisms proposed to account for the different forms of H damage, and
- threshold hydrogen concentrations and stress intensity factors for various forms of damage.

Based on these factors, the most likely forms of H damage are blister formation and hydrogen-induced cracking due to the accumulation of internal H_2 at inclusions, voids and micro-cracks within the material and cracking initiating on the inner surface of the closure weld. This latter failure mechanism is the result of the build up in H_2 pressure inside the container due to H diffusing through the container wall. The inner surface of the closure weld could be a particularly susceptible location for crack initiation as it is not possible to machine the weld surface or to mitigate residual tensile stress. However, for the reasons noted above, the probability of container failure by any of these mechanisms is considered to be small.

Appropriate selection of the container material and of the design of the container and closure weld could reduce the probability of failure due to H damage even further. Experience from the oil and gas industry can be used to specify a cracking-resistant material in terms of the chemical composition, cleanliness of the steel (i.e., the number and shape of inclusions), and preferred microstructure. If practical, the closure weld should be designed to avoid internal defects and tensile residual stress on the inner weld surface.

Although the probability of H-related failure is small, it is considered prudent to carry out a limited and targeted experimental program once the material and weld design have been specified. This experimental program should focus on the measurement of the lattice H concentration under repository conditions, the threshold H concentration for blister formation and HIC, and the stress intensity factor for crack initiation.

Of all the forms of localized corrosion to which the container could be subject, H-related damage is unique in that it is possible during the long-term anaerobic phase in the evolution of the repository environment. Other forms of localized corrosion, such as pitting or stress corrosion cracking, are limited to the early warm, aerobic period. In contrast, H effects are possible for much of the design life of the containers.

REFERENCES

- Abd Elhamid, M.H., B.G. Ateya, K.G. Weil, and H.W. Pickering. 2001. Effect of thiosulphate and sulfite on the permeation rate of hydrogen through iron. *Corrosion* 57, 428-432.
- Allam, A.M., B.G. Ateya, and H.W. Pickering. 1997. Effect of chloride ions on adsorption and permeation of hydrogen in iron. *Corrosion* 53, 284-289.
- Asahi, H., M. Ueno, and T. Yonezawa. 1994. Prediction of sulphide stress cracking in high-strength tubulars. *Corrosion* 50, 537-545.
- Asher, S. and P.M. Singh. 2008. Hydrogen production and permeation in near-neutral pH environments. *In Proc. CORROSION/2008, NACE International (Houston, TX), paper no. 08411.*
- ASM. 1987. Corrosion of carbon steels. *In Metals Handbook, Ninth edition, Volume 13, Corrosion. American Society for Metals International, Metals Park, OH, pp. 509-530.*
- Beck, W., J.O'M. Bockris, J. McBeen, and L. Nanis. 1966. Hydrogen permeation in metals as a function of stress, temperature and dissolved hydrogen concentration. *Proc. Roy. Soc.* 290A, 220-235.
- Been, J., H. Lu, F. King, T. Jack and R. Sutherby. 2007. The role of hydrogen in EAC of pipeline steels in near-neutral pH environments. *In Environment-Induced Cracking of Materials. Volume 2: Prediction, Industrial Developments and Evaluation, S.A. Shipilov, R.H. Jones, J.-M. Olive, and R.B. Rebak (eds.), Elsevier (Amsterdam), p. 255-266.*
- Bernstein, I.M. and G.M. Pressouyre. 1985. The role of traps in the microstructural control of hydrogen embrittlement of steels. *In Hydrogen Degradation of Ferrous Alloys, R.A. Oriani, J.P. Hirth, and M. Smialowski (eds.), Noyes Publications (Park Ridge, NJ), Chapter 25.*
- Birnbaum, H.K. 1991. Mechanisms of hydrogen-related fracture of metals. *In Environment-induced Cracking of Metals, R.P. Gangloff and M.B. Ives (eds.), NACE-10, NACE International (Houston, TX), pp. 21-29.*
- Bockris, J.O'M. and A.N. Reddy. 1970. *Modern Electrochemistry. Vol. 2. Plenum Press, New York.*
- Boellinghaus, T. and H. Hoffmeister. 2000. Numerical model for hydrogen-assisted cracking. *Corrosion* 56, 611-622
- Boellinghaus, T., H. Hoffmeister, and A. Dangeleit. 1995. *Welding in the World* 35, 83-96.
- Cheng, Y., L. Yang and F. King. 2000. Analysis of hydrogen permeation through pipeline steel in near-neutral pH SCC environments. *In Proc. International Pipeline Conf. 2000, Calgary, Alberta, Canada, 1-5 October 2000 (ASME International, New York, NY), pp. 1479-1485.*
- Chu, W.Y., L.J. Qiao, Y.B. Wang, and Y.H. Cheng. 1999a. Quantitative study for sulphide stress corrosion cracking of tubular steel. *Corrosion* 55, 667-673.

Chu, W.Y., J.X. Li, C.H. Huang, Y.B. Wang, and L.J. Qiao. 1999b. Hydrogen embrittlement of rail steels. *Corrosion* 55, 892-897.

Craig, B. 2005. Hydrogen damage. *In* *Metals Handbook*. Volume 13A Corrosion: Fundamentals, Testing, and Protection. ASM International (Metals Park, OH), pp. 367-380.

Domizzi, G., G. Anteri, and J. Ovejero-García. 2001. Influence of sulphur content and inclusion distribution on the hydrogen induced blister cracking in pressure vessel and pipeline steels. *Corros. Sci.* 43, 325-339.

Elboujdaini, M., R.W. Revie, and C. DeRushie. 2003. Effects of metallurgical parameters and non-metallic inclusions on behaviour for oil and gas industry steels on hydrogen induced cracking. *In* *Proc. CORROSION/2003*, NACE International (Houston, TX), paper no. 03528.

Flis, J. 1991. Corrosion of metals and hydrogen-related phenomena. *Materials Science Monographs*, Vol. 59 (Elsevier, Oxford).

Flis, J. and T. Zakroczymski. 1992. Enhanced hydrogen entry in iron at low cathodic polarizations in neutral and alkaline solutions. *Corrosion* 48, 530-539.

Gajek, A. and T. Zakroczymski. 2005. Long-lasting hydrogen evolution on and hydrogen entry into iron in an aqueous solution. *J. Electroanal. Chem.* 578, 171-182.

Gangloff, R.P. 1986. A review and analysis of the threshold for hydrogen environment embrittlement of steel. *In* *Corrosion Prevention and Control*, M. Levy and S. Isserow (eds.), U.S. Army Sagamore Materials Research Conference, 33 (Watertown, MA, US Laboratory Command), p. 64.

Gangloff, R.P. 2009. Science-based prognosis to manage structural alloy performance in hydrogen. *In* *Effects of Hydrogen on Materials*, *Proc. 2008 Int. Hydrogen Conf.*, B. Somerday, P. Sofronis, and R. Jones (eds.), ASM International (Materials Park, OH), pp. 1-21.

Gangloff, R.P. and A. Turnbull. 1986. Crack electrochemistry modeling and fracture mechanics measurement of the hydrogen embrittlement threshold in steel. *In* *Proc. Conf. Modeling Environmental Effects on Crack Growth Processes*, R.H. Jones and R.H. Gerberich (eds.), TMS-AIME (Warrendale, PA), p. 55.

Gerberich, W.W., P. Marsh, J. Hoehn, S. Venkataraman, and H. Huang. 1993. Hydrogen/plasticity interactions in stress corrosion cracking. *In* *Corrosion-Deformation Interactions*. CDI '92, T. Magnin (ed.), Les Editions de Physique, Les Ulis, France, pp. 325-343.

Griffiths, A.J. and A. Turnbull. 1995. On the effective diffusivity of hydrogen in low alloy steels. *Corros. Sci.* 37, 1879-1881.

Gu, B., J. Luo, and X. Mao. 1999. Hydrogen-facilitated anodic dissolution-type stress corrosion cracking of pipeline steels in near-neutral pH solution. *Corrosion* 55, 96-106.

Hay, M. 2003. Hydrogen-induced cracking in low strength steel. Short Course, COM'2003, Vancouver, August 2003.

Hirth, J.P. 1980. Effects of hydrogen on the properties of iron and steel. *Met. Trans. A* 11A, 861-890.

Hirth, J.P. and H.H. Johnson. 1976. Hydrogen problems in energy-related technology. *Corrosion* 32, 3-25.

Huang, H. and W.J.D. Shaw. 1995. Hydrogen embrittlement interactions in cold-worked steel. *Corrosion* 51, 30-36.

Iino, M. 1985. Hydrogen-induced blister cracking of linepipe steel. *In* Hydrogen Degradation of Ferrous Alloys, R.A. Oriani, J.P. Hirth, and M. Smialowski (eds.), Noyes Publications (Park Ridge, NJ), Chapter 28.

JNC. 2000. H12: Project to establish the scientific and technical basis for HLW disposal in Japan. Japan Nuclear Cycle Development Institute, Supporting Report 2, Repository Design and Engineering Technology.

Johnson, L.H. and F. King. 2003. Canister options for the disposal of spent fuel. Nagra Technical Report 02-11.

Johnson, L.H. and F. King. 2008. The effect of the evolution of environmental conditions on the corrosion evolutionary path in a repository for spent fuel and high-level waste in Opalinus Clay. *J. Nucl. Mater.* 379, 9-15.

Kim, W.K., S.U. Koh, B.Y. Yang, and K.Y. Kim. 2008. Effect of environmental and metallurgical factors on hydrogen induced cracking of HSLA steels. *Corros. Sci.* 50, 3336-3342.

King, F. 2004. The effect of discontinuities on the corrosion behaviour of copper containers. Swedish Nuclear Fuel and Waste Management Company Report, TR-04-05.

King, F. 2005. Overview of the corrosion behaviour of copper and steel used fuel containers in a deep geologic repository in the sedimentary rocks of the Michigan Basin, Ontario. Ontario Power Generation, Nuclear Waste Management Division Report 06819-REP-01300-10101-R00.

King, F. 2007. Overview of a carbon steel container corrosion model for a deep geological repository in sedimentary rock. Nuclear Waste Management Organization Technical Report, NWMO TR-2007-01, Toronto, Ontario.

King, F. 2008. Corrosion of carbon steel under anaerobic conditions in a repository for SF and HLW in Opalinus Clay. Nagra Technical Report 08-12. Nagra, Wettingen, Switzerland.

King, F. and M. Kolar. 2009. Theory manual for the steel corrosion model version 1.0. Nuclear Waste Management Organization Technical Report, NWMO TR-2009-07, Toronto, Ontario.

King, F., C. Lilja, K. Pedersen, P. Pitkänen, I. Puigdomenech, M. Snellman, and M. Vähänen. 2009. An update of the state-of-the-art report on the corrosion of copper under conditions in a deep geologic repository. Posiva/SKB Technical Report, in preparation.

Koh, S.U., J.S. Kim, B.Y. Yang, and K.Y. Kim. 2004. Effect of line pipe steel microstructure on susceptibility to sulphide stress cracking. *Corrosion* 60, 244-253.

- Kosmulski, M. 2002. The pH-dependent surface charging and the points of zero charge. *J. Colloid Interface Sci.* 253, 77-87.
- Lillard, R.S. and J.R. Scully. 1996. Hydrogen absorption in iron exposed to simulated concrete pore solutions. *Corrosion* 52, 125-137.
- Lillard, R.S., D.G. Enos, and J.R. Scully. 2000. Calcium hydroxide as a promoter of hydrogen absorption in 99.5% Fe and a fully pearlitic 0.8% C steel during electrochemical reduction of water. *Corrosion* 56, 1119-1132.
- Louthan Jr., M.R. 2008. Hydrogen embrittlement of metals: a primer for the failure analyst. Westinghouse Savannah River Corp. report, WSRC-STI-2008-00062.
- Lucas, K.A. and M.J. Robinson. 1986. The influence of lattice hydrogen content on the hydrogen-assisted cracking of high strength steel. *Corros. Sci.* 26, 705-717.
- Lufrano, J. and P. Sofronis. 1998. Enhanced hydrogen concentrations ahead of rounded notches and cracks – competition between plastic strain and hydrostatic stress. *Acta Metall.* 46, 1519-1526.
- Maccagno, T.M., K. Ikeda-Cameron, T. Jack, M. Wilmott, W.X. Chen, and D. Dorling. 1998. Hydrogen effects in gas transmission pipeline steels. *In Proc. International Pipeline Conf. 1998*, Vol. I, (ASME International, New York, NY), pp. 479-484.
- Marcus, P. and J. Oudar. 1985. Gas-iron surface equilibria. *In Hydrogen Degradation of Ferrous Alloys*, R.A. Oriani, J.P. Hirth, and M. Smialowski (eds.), Noyes Publications (Park Ridge, NJ), Chapter 3.
- Mazurek, M. 2004. Long-term used nuclear fuel waste management – geoscientific review of the sedimentary sequence in southern Ontario. Nuclear Waste Management Office Background Paper 6-12.
- Murakami Y. 1987. *Stress Intensity Factors Handbook*. Pergamon Press (Oxford, UK).
- NACE. 2001. Petroleum and natural gas industries – materials for use in H₂S-containing environments in oil and gas production. Part 1: General principles for selection of cracking-resistant materials. NACE International (Houston, TX)/International Standards Organization, NACE MR0175/ISO 15156-1.
- NACE. 2003. Petroleum and natural gas industries – materials for use in H₂S-containing environments in oil and gas production. Part 2: Cracking-resistant carbon and low alloy steels, and the use of cast irons.. NACE International (Houston, TX)/International Standards Organization, NACE MR0175/ISO 15156-2.
- Nagra. 2004. Effects of post-disposal gas generation in a repository for spent fuel, high-level waste and long-lived intermediate level waste sited in Opalinus Clay. National Cooperative for the Disposal of Radioactive Waste, Nagra Technical Report NTB 04-06.
- Nelson, G.A. 1977. Hydrogenation plant steels. *In Hydrogen Damage*, C. D. Beachem, Editor, American Society for Metals (Metals Park, OH), p. 377-394.

Okada, H. 1977. Stress corrosion cracking and hydrogen cracking of structural steels. *In Proc. Stress Corrosion Cracking and Hydrogen Embrittlement of Iron Base Alloys, NACE-5, NACE International (Houston, TX), pp.124-134.*

Oriani, R.A. 1970 The diffusion and trapping of hydrogen in steel. *Acta Metall.* 18, 147-157.

Oriani, R.A. and P.H. Josephic. 1981. The effects of hydrogen on the room-temperature creep of spheroidized 1040-steel. *Acta Metall.* 29, 669-674.

Pargeter, R.J. 2007. Susceptibility to SOHIC for linepipe and pressure vessel steels – review of current knowledge. *In Proc. CORROSION/2007, NACE International (Houston, TX), paper no. 07115.*

Park, G.T., S.U. Koh, H.G. Jung, and K.Y. Kim. 2008. Effect of microstructure on the hydrogen trapping efficiency and hydrogen induced cracking of linepipe steel. *Corros. Sci.* 50, 1865-1871.

Pasco, R.W. and P.J. Ficalora. 1985. Entry of hydrogen from the gas phase. *In Hydrogen Degradation of Ferrous Alloys, R.A. Oriani, J.P. Hirth, and M. Smialowski (eds.), Noyes Publications (Park Ridge, NJ), Chapter 10.*

Quan, G.F. 1997. Experimental study of hydrogen diffusion behaviors in stress fields. *Corrosion* 53, 99-102.

Razzini, G., M. Cabrini, S. Maffi, G. Mussati, and L. Peraldo Bicelli. 1999. Photoelectrochemical visualization in real-time of hydrogen distribution in plastic regions of low-carbon steel. *Corros. Sci.* 41, 203-208.

Revie, R.W., V.S. Sastri, M. Elboujdaini, R.R. Ramsingh, and Y. Lafrenière. 1993a. Hydrogen-induced cracking of line pipe steels used in sour service. *Corrosion* 49, 531-535.

Revie, R.W., V.S. Sastri, G.R. Hoey, R.R. Ramsingh, D.K. Mak, and M.T. Shehata. 1993b. Hydrogen-induced cracking of linepipe steels. Part 1 – threshold hydrogen concentration and pH. *Corrosion* 49, 17-23.

Robinson, M.J. and P.J. Kilgallon. 1994. Hydrogen embrittlement of cathodically protected high-strength, low-alloy steels exposed to sulfate-reducing bacteria. *Corrosion* 50, 626-635.

Scully, J.R. 2004. Hydrogen measurements in other alloy systems: implications towards pipeline steel. Presentation given at Environment-Induced Cracking of Materials-2, Banff, Alberta, September 19-23, 2004.

Scully, J.R. and P.J. Moran. 1988a. The influence of strain on hydrogen entry and transport in a high strength steel in sodium chloride solution. *J. Electrochem. Soc.* 135, 1337-1348.

Scully, J.R. and P.J. Moran. 1988b. The hydrogen embrittlement susceptibility of ferrous alloys: the influence of strain on hydrogen entry and transport.. *In Hydrogen Embrittlement: Prevention and Control. ASTM Special Technical Publication STP 962, L. Raymond (ed.), American Society for Testing and Materials, Philadelphia, PA, p. 387-402.*

Somerday, B.P. 2007. Technical reference on hydrogen compatibility of materials. Carbon steels: C-Mn alloys (code 1100). Sandia National Laboratories, Matls Tech Ref, available from <http://www.ca.sandia.gov/matlsTechRef/>.

Subramanyan, P.K. 1981. Electrochemical aspects of hydrogen in metals. *In* Comprehensive Treatise of Electrochemistry, Vol. 4 Electrochemical Materials Science, J.O'M. Bockris, B.E. Conway, E. Yeager, and R.E. White (eds.), Plenum Press (new York), chap. 8.

Tsuru, T., Y. Huang, Md. Rostom Ali, and A. Nishikata. 2005. Hydrogen entry into steel during atmospheric corrosion process. *Corros. Sci.* 47, 2431-2440.

Turnbull, A. 2009. A review of the possible effects of hydrogen on lifetime of carbon steel nuclear waste containers. National Cooperative for the Disposal of Radioactive Waste, Nagra Technical Report NTB 09-04, in preparation.

Völkl, J. and G. Alefeld. 1978. *In* Hydrogen in Metals, Topics in Applied Physics, G. Alefeld and J. Völkl (eds.), Vol. 28, pp. 321-348.

Warren, D. 1987. Hydrogen effects on steel. *Materials Performance*, pp. 38-48.

Wedler, G. 1985. Kinetics of adsorption of hydrogen onto iron alloys from the gas phase. *In* Hydrogen Degradation of Ferrous Alloys, R.A. Oriani, J.P. Hirth, and M. Smialowski (eds.), Noyes Publications (Park Ridge, NJ), Chapter 9.

Wei, R.P. and M. Gao. 1985. Chemistry, microstructure and crack growth response. *In* Hydrogen Degradation of Ferrous Alloys, R.A. Oriani, J.P. Hirth, and M. Smialowski (eds.), Noyes Publications (Park Ridge, NJ), Chapter 23.

Yamakawa, K. and R. Nishimura. 1999. Hydrogen permeation of carbon steel in weak alkaline solution containing hydrogen sulfide and cyanide ion. *Corrosion* 55, 24-30.

Yu, G.-H., Y.-H. Cheng, L. Chen, L.-J. Qiao, Y.-B. Wang, and W.-Y. Chu. 1997. Hydrogen accumulation and hydrogen-induced cracking of API C90 tubular steel. *Corrosion* 53, 762-769.

Yu, J.G., J.L. Luo, and P.R. Norton. 2001. Effects of hydrogen on the electronic properties and stability of the passive films on iron. *Appl. Surf. Sci.* 177, 129-138.

Yu, J.G., J.L. Luo, and P.R. Norton. 2002. Electrochemical investigation of the effects of hydrogen on the stability of the passive film on iron. *Electrochim. Acta* 47, 1527-1536.

Zeng, Y.M., J.L. Luo, and P.R. Norton. 2004. A study of semiconducting properties of hydrogen containing passive films. *Thin Solid Films* 460, 116-124.